

Foam films in the absence and presence of solid particles

Citation for published version (APA):

Hudales, J. B. M. (1989). *Foam films in the absence and presence of solid particles*. [Phd Thesis 1 (Research TU/e / Graduation TU/e), Chemical Engineering and Chemistry]. Technische Universiteit Eindhoven.
<https://doi.org/10.6100/IR321865>

DOI:

[10.6100/IR321865](https://doi.org/10.6100/IR321865)

Document status and date:

Published: 01/01/1989

Document Version:

Publisher's PDF, also known as Version of Record (includes final page, issue and volume numbers)

Please check the document version of this publication:

- A submitted manuscript is the version of the article upon submission and before peer-review. There can be important differences between the submitted version and the official published version of record. People interested in the research are advised to contact the author for the final version of the publication, or visit the DOI to the publisher's website.
- The final author version and the galley proof are versions of the publication after peer review.
- The final published version features the final layout of the paper including the volume, issue and page numbers.

[Link to publication](#)

General rights

Copyright and moral rights for the publications made accessible in the public portal are retained by the authors and/or other copyright owners and it is a condition of accessing publications that users recognise and abide by the legal requirements associated with these rights.

- Users may download and print one copy of any publication from the public portal for the purpose of private study or research.
- You may not further distribute the material or use it for any profit-making activity or commercial gain
- You may freely distribute the URL identifying the publication in the public portal.

If the publication is distributed under the terms of Article 25fa of the Dutch Copyright Act, indicated by the "Taverne" license above, please follow below link for the End User Agreement:

www.tue.nl/taverne

Take down policy

If you believe that this document breaches copyright please contact us at:

openaccess@tue.nl

providing details and we will investigate your claim.

**FOAM FILMS IN THE ABSENCE
AND PRESENCE
OF SOLID PARTICLES**

J.B.M. HUDALES

FOAM FILMS IN THE ABSENCE AND PRESENCE OF SOLID PARTICLES

PROEFSCHRIFT

ter verkrijging van de graad van doctor aan de Technische Universiteit Eindhoven, op gezag van de Rector Magnificus, prof. ir. M. Tels, voor een commissie aangewezen door het College van Dekanen in het openbaar te verdedigen op dinsdag 28 november 1989 te 16.00 uur

door

JOHANNES BERNARDUS MARIA HUDALES

geboren te Geleen

**Dit proefschrift is goedgekeurd door
de promotoren
prof. dr. H.N. Stein
en
prof. dr. A. Prins**

Voor Sylvia,
voor Mariska, Stefan en Wouter

CONTENTS

I	FOAMS, FREE LIQUID FILMS AND PLATEAU BORDERS	1
	Introduction	1
	Three important aspects of film and foam stability	3
	Force balance at the border/film transition	7
	Earlier work on the subject treated in this thesis	13
	References	23
II	PROFILE OF THE PLATEAU BORDER IN A VERTICAL FREE LIQUID FILM	27
	Abstract	27
	Introduction	27
	Experimental	28
	Results	32
	Discussion	42
	Conclusions	49
	Summary	50
	Acknowledgement	50
	Appendix	50
	References	57
III	MARGINAL REGENERATION OF A MOBILE VERTICAL FREE LIQUID FILM	61
	Abstract	61
	Introduction	61
	Experimental	62
	Results	66
	Discussion	70
	Conclusions	79
	Summary	80
	References	80
IV	THE INFLUENCE OF SOLID PARTICLES ON FOAM AND FILM DRAINAGE	83
	Abstract	83
	Introduction	83
	Experimental	84
	Results	87
	Discussion	95
	Conclusions	97
	Summary	97
	References	98
V	CONCLUSIONS	101
	References	103
	LIST OF SYMBOLS	105
	SUMMARY	109
	SAMENVATTING	111
	CURRICULUM VITAE	113

CHAPTER I

FOAMS, FREE LIQUID FILMS AND PLATEAU BORDERS

INTRODUCTION

Foams are generally divided into so-called "dilute foams", in which the gas bubbles retain their identity and are present as spheres, and "concentrated foams", in which the shape of a gas bubble is strongly distorted from spherical to polyhedral, by adjacent bubbles (1).

In this thesis, attention is focused on concentrated (polyhedral) foams. Here the gas bubbles are separated by thin liquid films (called "free liquid films"), which are limited and mutually connected by small liquid canals, the so-called Plateau borders.

The scientific study of foams and of free liquid films dates back to R. Boyle (1660); in a historical review compiled by Mysels and collaborators in 1959 (2), 324 references are mentioned. We will not repeat and update this review exhaustively; nevertheless, some particulars must be mentioned in order to set the scene for the research described in the present thesis.

Foams and free liquid films are essentially unstable. This is clearly seen, when one tries to form a foam or a free liquid film from pure liquids. However, dissolved substances may impart to foams and films a certain metastable resistance towards collapse. Especially surface active agents (e.g. soaps) are effective in this respect. In many cases foams are a nuisance rather than a desired phenomenon; in these cases the instability of a foam is less of a problem than their (limited) stability. Foam is, however, employed intentionally with the following objectives:

- a. Reduction of overall specific mass, e.g. in foamed concrete, with the aim of reducing the necessary amount or strength of supporting materials;
- b. Inhibition of gas convection: in fire extinction, and for reduction of heat transfer;
- c. Separation of mixtures of solid particles by selective adhesion to foam bubbles, through the hydrophobic (or hydrophilic) character of their surface. This is the essence of the unit operation, flotation, in chemical engineering.

It will be noticed, that many cases, in which foam is encountered, we are dealing with systems in which the foam contains solid particles as well as liquid (e.g., foamed concrete, flotation). In other cases, e.g. in foams formed from emulsions, we are dealing with the presence of liquid droplets dispersed in another liquid. This is not such a far-fetched situation as may seem at first view: many emulsifying agents, necessary to impart a certain stability to an emulsion, are also stabilizers for foam. Thus in the handling of emulsions, e.g. in liquid/liquid extraction or in emulsion polymerization, foam may readily be formed.

In spite of foam having long been investigated, there are still unsolved problems, even in foams formed from homogeneous solutions. This applies even more to foams, in which disperse phases are present.

Much work has been devoted to the study of separate films, in order to obtain insight in the behaviour of one important type of constituent of foam. The wish for surveyability of the system led many investigators to

study films free from influences by gravity. Because of the relevance of gravity to drainage and formation of liquid films and foams, however, the present investigation is devoted to foams and films in a gravity field.

THREE IMPORTANT ASPECTS OF FILM AND FOAM STABILITY

A foam, even if stabilized by a surfactant, should finally disappear being a metastable system, because the liquid films in it break down. In this breaking down of a film, two processes can be distinguished, while a third one is exclusively connected with foam behaviour:

a. Drainage

Drainage can be described as the gradual withdrawal of liquid from the film under the influence of gravity. Distinction should be made between drainage from films between rigid and mobile surfaces.

When the film surfaces are rigid, the flow of liquid between them under the influence of gravity can be calculated through (2):

$$v_v = \frac{\rho g}{2\eta} (y^2 - \delta_f y) \quad [I-1]$$

with: v_v = vertical velocity;

y = distance in a direction perpendicular to film surfaces, starting from the mid film plane;

δ_f = film thickness;

ρ = specific mass of liquid in the film;

g = acceleration due to gravity;

η = viscosity.

With the total volume transported downward through one horizontal section being given by:

$$Q_v = -y_f \int_{-y_f}^{y_f} v_v dy \quad [I-2]$$

with y_f half the film thickness ($= \frac{1}{2}\delta_f$), and

$$\left(\frac{\partial \delta_f}{\partial t}\right)_z = \left(\frac{\partial Q_v}{\partial z}\right)_t \quad [I-3]$$

we find for the thinning rate of the film at one particular height z :

$$\left(\frac{\partial \delta_f}{\partial t}\right)_z = -\frac{\rho g \delta_f^2}{4\eta} \left(\frac{\partial \delta_f}{\partial z}\right)_t \quad [I-4]$$

Two effects, however, limit the applicability of this equation:

1. The liquid in the film is not only subject to a pressure gradient in vertical direction, but also in the direction towards the most nearby Plateau border. The hydrostatic equilibrium pressure is thought to exist (see, however, Ch. II of this thesis), the pressure gradient towards the most nearby Plateau border may be considerable.
2. Many foams and films do not have completely rigid surfaces. Films with mobile surfaces drain much faster than predicted by eqn. [I-4]. This is ascribed to a process called marginal regeneration: in a liquid stretched between two Plateau borders, which have due to the hydrostatic equilibrium pressure at the level concerned curved surfaces (see fig. I-1), a thickness fluctuation is thought to originate (2), which leads to a force difference acting on the planes at A and B, even if the pressure difference between film and borders is not affected.

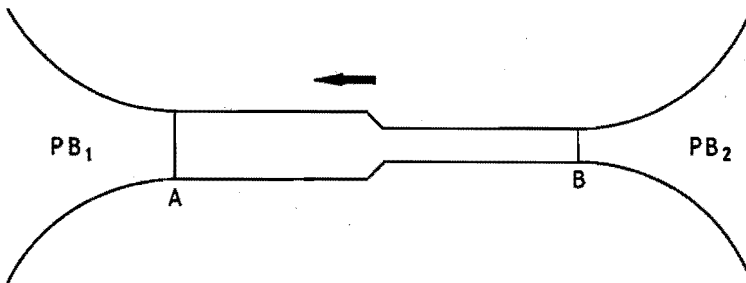


Fig. I-1. Fluctuation arising in a film stretched between two Plateau borders (PB_1 , PB_2). Top view of a horizontal cross section through an imaginary vertical film with borders.

This force difference on A and B causes the fluctuation to move in the direction of the thicker surface. This leads to consumption of thick film in PB_1 , and generation of thin film at PB_2 . The net effect is the exchange of a thick film element against a thin film element with about equal surface area.

A quantitative elaboration of this model and a comparison with experiments will be found in Ch. III of this thesis.

Drainage of films with rigid surfaces leads to films with a parabolic dependence of thickness with height (fig. I-2). The point, at which the parabolic profile starts, does, however, coincide with the suspension point A of the film, only in the first stages of drainage. In the later stages, at the top a "black" film (AB) is generated. The thickness of this film is so small, that light rays reflected from the back and front surface, respectively, show no interference colours.

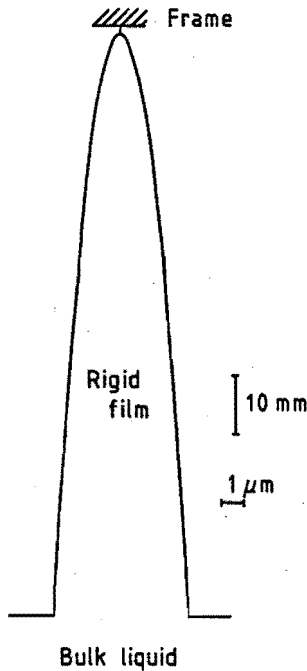


Fig. I-2. Profile expected for a film, by drainage, if the film has a rigid surface (1). Horizontal distances exaggerated with respect to vertical distances.

With mobile surfaces, a bell shaped profile is found. Examples of this will be met in Ch. III.

b. Rupture

Rupture of films is thought to be connected with surface waves in the film (3-7). As long as the films are thick, they have a pronounced stability against rupture, because every rupture process would be accompanied by flows in a direction of decreasing surface tension. Near an originating hole the surface is stretched, has therefore a smaller surface excess of surfactant, and consequently a higher surface tension than other surface elements of a film. Growth of such a potential hole would imply a flow from near this hole, towards film regions with a lower surface tension.

However, when two surfaces are close together, waves originating on one surface are accompanied by waves on the other. Two different types of waves appear to be stable (3):

1. The waves in the two surfaces are antisymmetrical ("bending" mode); they are not accompanied by changes in film thickness and cannot lead to rupture;
2. The waves in the two surfaces are symmetrical ("squeezing" mode). Such waves are accompanied by changes in film thickness, and may lead to film rupture through exponential growth of a thin region, once the latter becomes thinner than a certain critical thickness.

This mechanism will be referred to in Chapter IV of this thesis.

c. Disproportionation

A third aspect, called disproportionation (1), needs to be mentioned, which, however, only plays a role in foam stability, and not in film stability, because it concerns the pressure inside foam bubbles (However, in another meaning of the word, it is also of importance in the case of liquid films (3)):

According to the Laplace equation:

$$\Delta p_L = \gamma \left(\frac{1}{R_1} + \frac{1}{R_2} \right) = \frac{2\gamma}{r} \quad [I-5]$$

with Δp_L the pressure difference across a curved surface, γ the surface tension, R_1 and R_2 the principal radii of curvature in a point on the curved surface, which are equal in case of a spherical surface, and r the radius of this sphere. The Laplace pressure difference between the inside and outside of a small soap bubble is larger than that of a large bubble. So the pressure in the smaller one of two adjacent bubbles in a foam is larger than that in the larger one. Transport of air by diffusion through the separating liquid film will be in the direction of the larger bubble. In this way, large bubbles will grow at the expense of small bubbles. This diffusion-controlled mechanism plays a role in a dilute foam, when bubbles are merely spherical, but then the separating foam films are relatively thick. At later stages, when these films have drained, they also have become more or less plane, but because of their small thickness only a small pressure difference is necessary to obtain appreciable diffusion-controlled transport of air towards the larger bubble.

However, this mechanism is left out of consideration in the further discussion.

FORCE BALANCE AT THE BORDER/FILM TRANSITION

In Chapter II use will be made of a balance of pressure and surface tension forces at the border/film transition. Although this has been employed several times (8-11), a review of the most relevant points will be presented here for convenience.

a. Foams, in which the interaction between the surfaces can be neglected.

This is the case for relatively thick films ($\delta_f \geq 50$ nm). There exists a pressure difference between Plateau borders and the surrounding atmosphere:

$$p_b = p_a - \gamma_b \left(\frac{1}{R_1} + \frac{1}{R_2} \right) \quad [I-6]$$

with p_b the pressure in the border, p_a the pressure in the surrounding atmosphere, γ_b the surface tension in the border and R_1 and R_2 the principal radii of curvature of the border surface. In this thesis, the liquid films studied separately (i.e. not in foams) are surrounded by Plateau borders, in which one of the radii of curvature is very large: the liquid films are found in a straight-legged frame, see chapters II and III. Thus:

$$p_b = p_a - \frac{\gamma_b}{r} \quad [I-7]$$

In the film itself, however, the surfaces are not curved. Thus:

$$p_f = p_a \quad [I-8]$$

The pressure difference between border and film leads to a difference in pressure forces on a plane at the border/film transition (shaded area in fig. I-3). The pressure force exerted by the border on this plane is:

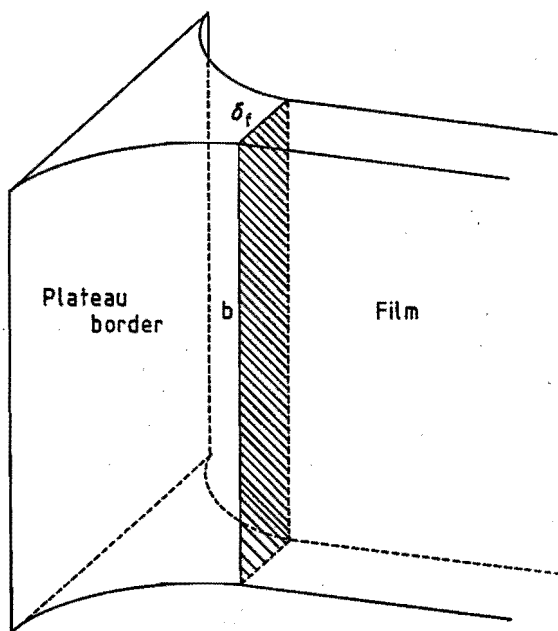


Fig. I-3. Plane at the Plateau border/film transition.

$$F_{P_b} = p_b b \delta_f = \left(p_a - \frac{\gamma_b}{r} \right) b \delta_f \quad [I-9]$$

while that exerted by the film is:

$$F_{P_f} = p_f b \delta_f = p_a b \delta_f \quad [I-10]$$

This difference is, however, accounted for by a difference in surface tension forces:

$$F_{\gamma_b} = 2\gamma_b b \quad [I-11]$$

$$F_{\gamma_f} = 2\gamma_f b$$

Thus, the force balance, per unit length in vertical direction, becomes:

$$\left(p_a - \frac{\gamma_b}{r} \right) \delta_f - 2\gamma_b = p_a \delta_f - 2\gamma_f \quad [I-12]$$

This enables us to calculate:

$$\gamma_f = \gamma_b \left(1 + \frac{\delta_f}{2r} \right) \quad [I-13]$$

from the film thickness δ_f and the radius of curvature r of the adjacent Plateau border.

With increasing height, the radius of curvature decreases (if in the border realisation of hydrostatic equilibrium is assumed). This, together with [I-13], will lead to a surface tension increasing with height in the film. In addition, a horizontal section through the film at greater height must support a larger weight of film, than a horizontal section at a lower height. This also leads to a surface tension increasing with height in the film.

This is illustrated in fig. I-4, where a film, again with horizontal distances exaggerated, is shown. All the weight of the liquid below the horizontal section ABCD must be supported by the surface tension along the lines AB and CD (12). This requires a surface tension increasing with

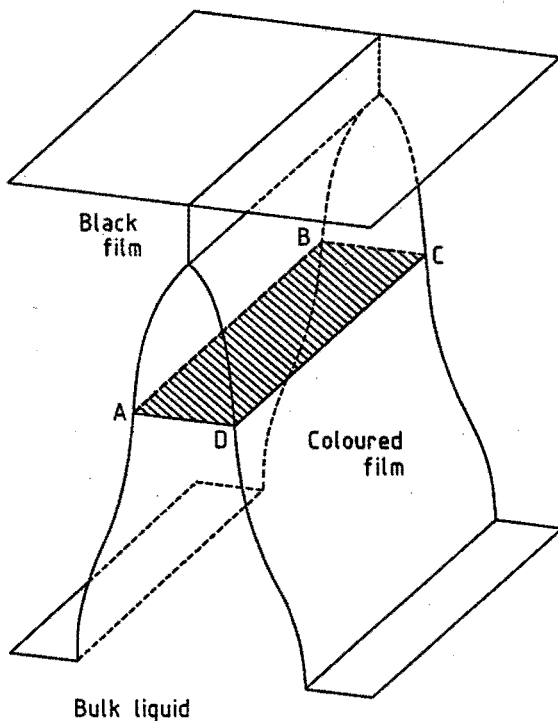


Fig. I-4. Film with lines AB and CD supporting the weight of the film below plane ABCD (Plateau borders are omitted).

height. A Marangoni flow in upward direction, however, is not generated, because the surface tension gradient is exactly balanced by the increasing weight of the film. This effect is absent in the Plateau border, because there the increasing weight of the border, with increasing height at a certain time, can be taken into account by a decreasing radius of curvature.

The differences between the surface tensions in border and film, encountered in the present thesis, remain, however, small (up to 0.7 % of the bulk surface tension value, see Ch. II).

b. Films, in which the interaction between the surfaces can no longer be neglected.

With films of thickness ≤ 50 nm, the interaction between the surfaces can no longer be neglected. This leads to a contact angle θ_f between border and film (9). The attraction energy, V_A , per unit surface between two film surfaces separated by a distance δ_f , caused by London-Van der Waals forces (13,14), amounts to:

$$V_A = - \frac{Af}{12\pi\delta_f^2} \quad [I-14]$$

where A is the Hamaker constant and f is a correction factor in order to account for the retardation effect (14); this effect is caused by the time necessary for propagation of the electromagnetic waves between the surfaces and thus becomes smaller with increasing film thickness. f is tabulated in (14) as a function of $p = 2\pi\delta_f/\lambda$, where λ is the wavelength connected with the motion of electrons in the atoms and is assumed to be of the order of 1000 Å. For film thicknesses larger than about 200 nm f can be approximated by (14):

$$f \approx 0.49 \frac{\lambda}{\pi\delta_f} \quad [I-15]$$

This makes V_A inversely proportional to the third power of the film thickness:

$$V_A = - 0.49 \frac{A\lambda}{12\pi^2\delta_f^3} \quad [I-16]$$

For $\delta_f < 200$ nm, this leads to a pressure increase in the film equal to:

$$\begin{aligned} P_A &= \frac{\partial V_A}{\partial \delta_f} = \frac{Af}{6\pi\delta_f^3} - \frac{A}{12\pi\delta_f^2} \frac{df}{d\delta_f} = \frac{A}{12\pi\delta_f^2} \left(\frac{2f}{p} \frac{p}{\delta_f} - \frac{df}{dp} \frac{dp}{d\delta_f} \right) \\ &= \frac{A}{6\lambda\delta_f^2} \left(\frac{2f}{p} - \frac{df}{dp} \right) \end{aligned} \quad [I-17]$$

From the tabulated values of f(p) in (14), it follows, that $df/dp \ll 2f/p$, and

we will omit this term. For larger thicknesses:

$$P_A = 0.1225 \frac{A\lambda}{\pi^2 \delta_f^4} \quad [I-18]$$

where [I-15] has been substituted into [I-14] before differentiation.

The repulsive pressure due to charges on the film surfaces and their counter-ions (if an ionogenic surfactant is used (15,16)), is given by (17,18):

$$P_R = - 2nkT (\cosh u - 1) \quad [I-19]$$

where n is the electrolyte concentration (in molecules/m³), k the Boltzmann constant, T the absolute temperature and u is the potential midway between the surfaces, given by:

$$u = 8 \exp(-\frac{1}{2}\kappa\delta_f) \quad [I-20]$$

where κ is the Debye-Hückel parameter, which is a function of the electrolyte concentration. Furthermore, it has been assumed in eqn. [I-20], that $\tanh(z_0 e_0 \psi_0 / 4kT) \approx 1$, where z_0 is the valence of the ions in the liquid, e_0 the elementary charge and ψ_0 the surface potential; Thus, the force balance, per unit length in vertical direction, requires (cf. [I-12]):

$$P_b \delta_f - 2\gamma_b \cos\theta_f = (p'_f + P_A + P_R) \delta_f - 2\gamma'_f \quad [I-21]$$

In this relation, primed quantities refer to values in the absence of interaction. We introduce, analogous to [I-13]:

$$\gamma'_f = \gamma_b + \frac{1}{2} (p'_f - p_b) \delta_f \quad [I-22]$$

and we obtain:

$$\gamma_b (1 - \cos\theta_f) = \frac{1}{2} (P_A + P_R) \delta_f \quad [I-23]$$

According to Gibbs' definition of surface tension (19,20):

$$\gamma = \left(\frac{\partial G}{\partial w} \right)_{T, P, n_i} \quad [I-24]$$

where G is the Gibbs free energy and w is the surface area. The term $\frac{1}{2}(P_A + P_R)\delta_f$ should be included in the surface tension of the film (9):

$$\gamma_f = \gamma_f' - \frac{1}{2} (P_A + P_R) \delta_f \quad [I-25]$$

These eqns. will be used in Ch. II to calculate the attractive and repulsive forces and the contact angle θ_f between the film and the Plateau border, mentioned in Table II-i.

EARLIER WORK ON THE SUBJECT TREATED IN THIS THESIS

Although we do not intend to review exhaustively all investigations up to the present, relating to foam stability, some of the papers of particular significance to our work must be mentioned.

Much previous work has been devoted to films, which are not subject to a hydrostatic pressure gradient (though there may be a suction from the border). This method was introby Scheludko and collaborators (21-23). A circular, plane-parallel, horizontal film is generated in the centre of a double-concave drop of liquid, and studied by microscopy. From the interference pattern in the border, the contact angle θ_f is calculated (8,21-26). In principle, from the data also the radius of curvature of the Plateau border surface, and consequently the hydrostatic pressure, might have been calculated (see Ch. II, Appendix). However, this appears not to have been done.

In interpreting drainage rates in these experiments (23), it is supposed, that the drainage is determined by the Reynolds relation between the flow rate, the radius of the circular film, and the pressure difference between film and border. However, then the influence of marginal regeneration, which at least for vertical films with mobile surfaces, is the predominant factor (2), is neglected. The Reynolds relation mentioned leads to lifetimes of the film at given film radius, which are contradicted by experiments (27-29). This led to the hypothesis, that in drainage, surface waves are determining factors as much as in the

case of film rupture (4-7).

Perhaps because of the difficulties in interpreting drainage rates observed by this method, most authors employing it focus attention on measurements of "equilibrium films" (thus called, because here drainage has come to a standstill, since a balance of forces is reached between hydrostatic pressure, London-Van der Waals attraction and electrostatic repulsion (10,11,30-33)). Interesting results are then obtained, both on the value of the Hamaker constant operative in the systems studied (10,11,31,32), its description by the Landau-Lifshitz theory (34), and the behaviour of attractive forces with distance (8).

However, the drainage of vertical films, and the role of marginal regeneration in this drainage, remained unsolved. This is the more to be regretted, because the foams and thin liquid films met in practical situations are always subject to a pressure gradient due to gravity. Frankel in ref. (2) already had derived an equation for it, which, however, was (as far as the present author knows) never compared with experiments. Prins & Van Voorst Vader (35) were interested in the limiting surface dilatational modulus, just permitting marginal regeneration according to Mysels' mechanism; this mechanism (see fig. I-1) is counteracted by surface tension differences generated by the compression of one part of the Plateau border, and expansion of the other. In the special case of films stabilized by a mixture of sodium dodecyl sulphate and n-dodecanol, they found good agreement between the experimentally measured modulus at the onset of marginal regeneration, at the transition of a rigid to a mobile film, on the one hand, and theoretical predictions on the other.

Vertical free liquid films

Because in this thesis the investigation of vertical free liquid films occupies an important space, a brief summary of the work done on this subject over the last three decades will be given below, without having the pretention of being complete. The same rough division as made below for vertical films can be made for horizontal films, and the latter will therefore be left out of consideration as much as possible. Some relevant aspects on these horizontal films have been mentioned previously.

Vertical free liquid films have been studied recently for a large variety of reasons, but these investigations can be roughly divided into three main subjects: a. equilibrium films; b. the mechanism of film rupture; and c. liquid flow in film and Plateau border.

a. Equilibrium films

Equilibrium or black films, the result of attracting Van der Waals forces counterbalancing electric double layer repulsion and steric hindrance, have been an important topic of investigation, because they can be used to confirm existing theories concerning colloidal stability (13). Before the very thin black films were reached, however, thicker coloured films were studied:

Soon after the publication of Mysels' book on soap films (2), several attempts were undertaken to verify Frankel's law for film formation, in which the film thickness is related to the rate of pull-out from the liquid. This is a special case of Frankel's equation for film drawn out from a Plateau border during marginal regeneration (Ch. III, eqn. [III-2]). Mysels & Cox (36) found good agreement with experimental results in the case of relatively fast film formation ($4 \mu\text{m/s}$ - 4mm/s), when film thickness did not reach values smaller than 100 nm. These speeds, however, are still very slow compared with the bulk liquid descent rate of about 30 mm/s applied in our experiments (Ch. III). Lyklema (37), being interested in thicknesses below 100 nm, measured thicknesses at film speeds down to 260 nm/s. He also found good agreement with Frankel's law down to about 110 nm for mobile films and down to about 80 nm for rigid films; below these thicknesses Van der Waals forces start to compress the film, while electrostatic repulsion is not important yet, because of the ionic strength ($\approx 0.1 \text{ M}$) used, which reduces the double layer thickness.

Experiments with an improved set-up (38) gave results for rigid films, which again agreed well with Frankel's law for films thicker than 80-100 nm, while mobile films showed complications below a rate of pullout of 11 $\mu\text{m/s}$, ascribed to the welt, formed between black and coloured film (2,39). For their measurements they used a window of very thin wire (12.5 μm diameter) stretched in a glass frame in order to reduce marginal

regeneration and thus the rate of thinning.

Lyklema & Mysels (40) created black rigid and mobile films from sodium dodecyl and tetradecyl sulfate, either with or without dodecyl and tetradecyl alcohol, respectively, at different ionic strengths, at frame velocities between 0.5 and 2 $\mu\text{m/s}$; at these velocities, film thickness appears to be independent of this velocity, as observed earlier (37,38). They found good qualitative agreement between experiment and the existing theories of Van der Waals attraction and electric double layer repulsion. Jones et al. (41) investigated the stability and other properties of the second or common black film about 440 nm thick from sodium dodecyl sulfate solutions in the presence of NaCl and several additives.

Duyvis and Overbeek (30,42) studied the existence of two types of equilibrium films, now called common and Newton black film, drawn horizontally from nonionic surfactant solutions at low electrolyte concentrations, and demonstrated in a large vertical film, that these two types are in equilibrium with each other. The two types of black film occur, because of two minima in the free energy vs. thickness curve: at the lowest thickness (common) steric hindrance counteracts Van der Waals attraction, while at larger thickness (Newton) electric repulsion, Van der Waals attraction and hydrostatic pressure are in equilibrium.

Clunie et al. (43) used new techniques, including X-ray scattering at small angles ($2\theta < 5^\circ$), radiotracer determination and film conductance, for the study of the structure of black films of cationic surfactant solutions; they obtained good agreement between the results, evidencing a sandwich structure of two surfactant monolayers enclosing an aqueous core. Later, thicknesses of black films formed by a nonionic surfactant solution were used to calculate Hamaker's constant for the calculation of the Van der Waals attraction (44). In these experiments, the glass frame containing the film was totally withdrawn from the surfactant solution. Ingram (45) studied the effect of salt addition on the film thickness of the common and Newton black film, stabilized with a nonionic and a cationic/anionic ($\text{C}_{10}^+\text{C}_{10}^-$) surfactant in the presence of inorganic electrolyte. The abrupt transition between the two film types was ascribed to a specific ion adsorption effect.

The effect of rapid temperature changes of the surrounding atmosphere on the thickness of an equilibrium film was studied by Prins & Van den Tempel (46), after preliminary experiments by Jones et al. (41). The resulting large decrease in film thickness is ascribed to evaporation and not to film expansion or contraction.

Addition of increasing amounts of urea or sucrose to an anionic surfactant solution increased the equilibrium film thickness and made the ion specificity disappear (47): due to accumulation of the organic substances in the Stern Layer of the surfactant monolayers, counterions are desorbed, as a result of which the double layer becomes more diffuse and the repulsion increases.

Ellipsometry as well as reflectometry were applied to a Newton black film by Den Engelsen & Frens (48) to investigate the composition of this film. A three-layer model, as proposed by Duyvis (29), was favoured over a one-layer model and the refractive indices of the film core and surface layers were determined, that for the surface being higher than that for the core.

Yamanaka (49) found for SDS as well as several nonionics, that the rate of growth of black film was proportional to the excess film tension $\Delta\gamma = 2\gamma - \gamma_f$, where γ is the surface tension of the solution and γ_f the film tension (44), over a wide range of electrolyte concentrations; $\Delta\gamma$ acted as the driving force for the growth of black films, so the reciprocal of the slope was thought to be a viscosity parameter. He also studied the relationship between the properties of the black film, the surface tension γ and the foam stability (50). Foam stability was found to be mainly determined by the rate of film thinning.

Donners (33) measured the light scattering ratio as a function of film thickness of a CTAB-solution.

A logical continuation of the studies on black films is the measurement of the contact angle θ_f between the black film and (lower) Plateau border, which appears due to the existence of interaction forces between the film surfaces and corresponds to a change in surface tension of the black film. This has already been predicted to exist in a (horizontal) liquid film

(51,52), and the contact angle has first been observed and measured for a small bubble on the surface of a surfactant solution (9,53). The first measurement of a contact angle for a vertical film in contact with the bulk was reported by Princen (54). He made use of the fact, that the prism-like top of the double meniscus deflects a horizontal light beam downward at a certain angle. However, observed fringes in the measured intensity profile could not be satisfactorily explained by simple geometrical optics. This was done two years later (55), making use of the curvature of the border (which, however, was not explicitly calculated) and of a Fourier analysis. An elaboration of this short communication showed, that contact angles larger than 2° can be most conveniently determined from the angular positions of the diffraction maxima and minima, while smaller angles are more readily derived from the ratio of the intensities at the first maximum and the deep minimum preceding it (56).

In the mean time, Prins (57) demonstrated a simple technique for contact angle measurement, based on the Wilhelmy plate technique for measuring surface tensions: instead of a metal plate, a soap film in a glass frame can be used to measure the surface tension. When the black film reaches the lower Plateau border, a sudden drop in the force exerted on the frame is measured. From this decrease the contact angle can be calculated. This method has been used by Yamanaka (49) to measure the excess surface tension $\Delta\gamma$.

However, Princen's method is more commonly used, e.g. by Mysels & Buchanan (58), who successfully applied the small angle technique to films drawn from anionic surfactant solutions in the presence of added electrolytes. Agterof (59) measured very small contact angles ($7-33'$) of SDS-solutions containing 1 M glycerol to prevent evaporation. He also combined contact angle measurements with thickness measurements for black films drawn from SDS- and CTAB-solutions in the presence of various counterion concentrations and 1 M glycerol; interaction free energies calculated from both experiments were compared. Results from the thickness measurements were in good agreement with the DLVO-theory, when a surface potential of 128 mV was assumed, independent of electrolyte concentration; contact angle experiments yielded reasonable agreement only at higher concentrations, while at

lower concentrations deviations were considerable.

De Feijter & Vrij (32) used the method for large angles in the case of SDS-solutions above the c.m.c., while for solutions below the c.m.c. Scheludko's expansion method for a microscopic horizontal film (8,24) was used, because of the lack of stability of large vertical films. The absolute value of the interaction free energy, which was calculated from these contact angles, was found to increase with increasing salt concentration and with decreasing temperature. From the latter variation the interaction entropy and interaction energy were calculated. Other results were interpreted in terms of a thermodynamic analysis published at the same time (31).

b. Mechanism of film rupture

The mechanism of film rupture has been studied, because film lifetime is a very important factor in foam stability. In all the experiments mentioned in this thesis the most important cause of film bursting, namely evaporation, is eliminated.

De Vries (1,60) studied spontaneous film rupture, taking place in the thinnest part of the film, as well as film rupture induced by an electric discharge, with a high speed camera; from the photographs the rate of hole expansion in the ruptured lamella was calculated. He theoretically calculated the activation energy necessary to induce a hole in a film of certain thickness, by means of the surface area increase. He discussed several mechanisms of film rupture, i.e. of unstable films from low-molecular solutions, surface tension depression and induced and spontaneous temperature fluctuations in the liquid (1,61).

Mysels and co-workers investigated the bursting of soap films in a series of four publications: McEntee & Mysels (62) took high speed flash photographs of bursting films, initiated by a perforating spark, in reflected light, and measured the rim velocity dependence on film thickness and composition for mobile and rigid films. These velocities are close to those required by conservation of momentum in the absence of an aureole; however, such an aureole of thickened film has been found to spread ahead of the narrow rim surrounding the growing hole. Several

aspects of the results mentioned above (62) are theoretically considered and treated hydrodynamically by Frankel & Mysels (63). Mysels & Stikeleather (64) introduced a photographic technique for the study of spontaneous bursting of soap films, based on a triggering of the submicrosecond flash photcamera by the burst itself. The proces of spontaneous bursting appears to be similar to initiated bursting, although the former always originates at the border. Frens et al. (65) measured the profile of the aureole, which priveded the basis for an interpretation in terms of surface tension changes accompanying the contraction of the film. Under the condition of a bursting film, the surface tension of a film drawn from an SDS-solution dropped from 38 to 14 mN/m.

Surface waves

Scheludko (66) was the first to propose a mechanism for film rupture, in which a deformation grows spontaneously, during which process the increase in free energy, caused by the increase in surface area, is more than compensated by the gain in Van der Waals energy due to disproportionation. The latter is caused by the tendency of molecules to be driven from the thinner to thicker parts of the film, because of the excess attractive Van der Waals forces in the thicker part. A critical thickness could be derived from the wavelength of this surface deformation through the condition of thermodynamic instability. Vrij (67) further developed this theory and tested it by the data obtained with microscopic, horizontal films, published by Scheludko and his collaborators (14,21,22,66,68). Vrij & Overbeek (3) took the interaction forces into account in this mechanism. Light scattering from the "rough" film surface is proposed as a powerful tool for investigating these molecular interactions.

Felderhof (69) derived the dispersion equations for two types of fluctuations in a film, the squeezing mode and the bending mode, for an inviscid fluid.

Lucassen et al. (70) analyzed the different modes of vibration in a thin liquid film in terms of symmetric and anti-symmetric modes. De symmetric or squeezing mode receives special attention, because it involves thickness fluctuations (71): if a very small fluctuation is

accompanied by a decrease in free energy (65), it will grow and may lead to film rupture. Joosten et al. (72) were the first to test the theory of surface waves on a vertical free liquid film through laser beat spectroscopy and found good qualitative agreement. Joosten (73) was the first to observe the bending mode by means of dynamic light scattering, from which data the film tension could be determined to amount to about twice the surface tension of the bulk solution. Experiments on the squeezing mode showed some quantitative discrepancies, which, however, could be explained. From these experiments it follows, that the ratio of surface tension and viscosity in the film equals that of the bulk solution. Combination of these results leads to the conclusion, that the viscosities are also equal.

Sharma and Ruckenstein went deeper into the subject of surface waves theoretically to predict film lifetimes (4), to introduce a new mechanism for film thinning, involving the enhancement of Reynold's velocity by thickness fluctuation (5), to predict the thinning velocity, critical thickness of rupture and lifetimes of tangentially immobile foam and emulsion films (6), and to study the effects of surfactants and surface waves on the thinning velocity (7).

c. Liquid flow in film and Plateau border

Actual flow in vertical films and Plateau borders, which means the behaviour of coloured films, has rarely been studied.

Flow properties of thick films were studied by Miles et al. (74), who designed an apparatus, in which films could be formed without enlarging the total surface area. They discovered the difference between rigid and mobile films and measured the transition temperature between the two film types.

Mysels et al. (2) have measured the profile of a rigid film, the descent constant for a mobile film and its dependence on the frame width, besides some experiments on the black film. A few years later, Mysels et al. (75) were the first to measure the elasticity of mobile and rigid films with essentially the same apparatus later used by Mysels & Cox (36). In order to measure film elasticity, the thickness of a stationary vertical film in a

frame was recorded, while the total surface area of film and bulk liquid was increased and decreased by withdrawing another film-carrying frame from the solution, respectively lowering it in the solution (cf. (74)). Simultaneously, surface tension was measured with a dynamometer, from which the film under observation was suspended. Elasticity of a rigid film was found to be ten times higher than of a mobile film. Purification by foaming was investigated by Razouk & Mysels (76), who measured its effect on surface tension, Marangoni effect and film elasticity.

Film stretching was also applied by Roberts et al. (77), by moving the upper horizontal glass barrier, after the film had been totally withdrawn from the solution. Film lifetime was increased by a factor 4 and film thinning was considerably retarded, when 5 μ l of a liquid crystalline phase, containing water, sodium caprylate and decanol, was placed on the movable bar. Experiments with a foam showed, that this film-stabilizing substance was concentrated in the Plateau borders, which might have been concluded from the film photographs as well, since the black film appeared only in the centre of the film.

Koczó & Rácz (78) studied flow in a single Plateau border between three films in a tripod frame. Liquid could be flown through this border and the film from a tube in contact with the border. The shape of the border and the cross-sectional area, determined by measuring the electrical resistance, were measured as a function of the flow rate. It was found, that the border dimensions and the flow rate at a given pressure drop were predominantly determined by the mobility of the surfaces.

In most of the investigations mentioned above, which dealt with film thickness determination, measurement of light reflectance was applied to do so. An exception is formed by Clunie et al. (43), who used X-ray scattering and radiotracer measurements, with which they were able to determine the total thickness of the film and the thickness of the surfactant monolayers; thus, they calculated the aqueous core thickness.

Highfield et al. (79) used critical reflection of neutrons to measure directly the thickness of the aqueous core of a vertical soap film, which was suspended in a 4-legged frame, thus only the top Plateau border

being adjacent to a glass wall.

Von Wandruszka & Winefordner (80) introduced a new technique, for which they dissolved the laser dye Rhodamine B in several surfactant solutions. The dye molecules are known to accumulate in the film surfaces, which leads to fluorescence, induced by laser light illumination, exhibiting interference. Polarization measurements showed, that in some surfactant monolayers the dye molecules have a very specific anisotropic orientation. Formulae are given for the film thickness at constructive interference fringes of known order for two different orientations of the film with regard to the excitation and fluorescence beams.

On reviewing this extensive number of investigations, it is striking, that three items have only insufficiently been investigated:

- a. The local pressure in a Plateau border near a vertical free liquid film;
- b. The mechanism of marginal regeneration;
- c. The influence of solid particles on film and foam stability.

All three subjects, however, are of paramount importance in practical situations involving foams: the first two determine the drainage, while many foams contain dispersed phases. In the present thesis material has been collected on these subjects, in the special case of 0.02 M CTAB solutions.

REFERENCES

1. De Vries, A.J., Ph.D. Thesis, Utrecht, 1957.
2. Mysels, K.J., Shinoda, K. & Frankel, S., "Soap films; studies of their thinning and a bibliography". Pergamon Press, 1959.
3. Vrij, A. & Overbeek, J.Th.G., *J. Am. Chem. Soc.* **90**: 3074-3078 (1968).
4. Sharma, A. & Ruckenstein, E., *Langmuir* **2**: 480-494 (1986).
5. Ruckenstein, E. & Sharma, A., *J. Colloid Interface Sci.* **119**: 1-13 (1987).
6. Sharma, A. & Ruckenstein, E., *J. Colloid Interface Sci.* **119**: 14-29 (1987).
7. Sharma, A. & Ruckenstein, E., *Colloid Polymer Sci.* **266**: 60-69 (1988).
8. Scheludko, A., Radoev, B. & Kolarov, T., *Trans. Far. Soc.* **64**: 2213-2220 (1968).
9. Huisman, F. & Mysels, K.J., *J. Phys. Chem.* **73**: 489-497 (1969).

10. De Feijter, J.A., Ph.D. Thesis, Utrecht, 1969.
11. De Feijter, J.A. & Vrij, A., *J. Electroanal. Chem.* **37**: 9-22 (1972).
12. Lucassen, J., in: "Surfactant Sci. Ser., Vol. 11: Anionic Surfactants; Physical Chemistry of Surfactant Action" (E.H. Lucassen-Reynders, Ed.), Ch. 6: 217-265. Marcel Dekker, 1981.
13. Verwey, E.J.W. & Overbeek, J.Th.G., "Theory of the Stability of Lyophobic Colloids", p. 101. Elsevier publ. Co., 1948.
14. J.Th.G. Overbeek, in: "Colloid Science" (H.R. Kruyt, Ed.) Vol. I, pp. 266-268. Elsevier Publ. Co., 1952.
15. Scheludko, A. & Exerowa, D., *Kolloid-Z.* **165**: 148-151 (1959).
16. Mysels, K.J. & Jones, M.N., *Disc. Far. Soc.* **42**: 42-50 (1966).
17. As ref. (13), pp. 90-97.
18. As ref. (14), pp. 252-256.
19. Gibbs, J.W., see: "Collected Works", Vol. 1, 304. Dover Publications, New York.
20. Somorjai, G.A., "Principles of Surface Chemistry", Ch. 2. Prentice-Hall, Inc., 1972.
21. Scheludko, A., *Kolloid-Z.* **155**: 39-44 (1957).
22. Scheludko, A. & Exerowa, D., *Kolloid-Z.* **168**: 24 (1960).
23. Scheludko, A., Platikanov, D. & Manev, E., *Disc. Far. Soc.* **40**: 253-265 (1965).
24. Kolarov, T., Scheludko, A. & Exerowa, D., *Trans. Far. Soc.* **64**: 2864-2873 (1968).
25. Haydon, D.A. & Taylor, J.L., *Nature* **217**: 739-740 (1968).
26. Requena, D.A., Billet, D.F. & Haydon, D.A., *Proc. Roy. Soc. London A* **347**: 141-159 (1975).
27. Rao, A.A., Wasan, D.T. & Manev, E.D., *Chem. Eng. Commun.* **15**: 63-81 (1982).
28. Radoev, B.P., Scheludko, A.D. & Manev, E.D., *J. Colloid Interface Sci.* **95**: 254-265 (1983).
29. Manev, E.D., Sazdanova, S.V. & Wasan, D.T., *J. Colloid Interface Sci.* **97**: 591-594 (1984).
30. Duyvis, E.M., Ph.D. Thesis, Utrecht, 1962.
31. De Feijter, J.A., Rijnbout, J.B. & Vrij, A., *J. Colloid Interface Sci.* **64**: 258-268 (1978).
32. De Feijter, J.A. & Vrij, A., *J. Colloid Interface Sci.* **64**: 269-277 (1978).
33. Donners, W.A.B., Ph.D. Thesis, Utrecht, 1976.

34. Dyaloshinskii, I.E., Lifshitz, E.M. & Pitaevskii, L.P., *Adv. Physics* 10: 165 (1961).
35. Prins, A. & Van Voorst Vader, F., in: "Berichte vom VI. Internationalen Kongress für Grenzflächenaktive Stoffe, Zürich", pp. 441-448. 1972.
36. Mysels, K.J. & Cox, M.C., *J. Colloid Sci.* 17: 136-145 (1962).
37. Lyklema, J., *Rec. Trav. Chim.* 81: 890-897 (1962).
38. Lyklema, J., Scholten, P.C. & Mysels, K.J., *J. Phys. Chem.* 69: 116-123 (1965).
39. Overbeek, J.Th.G., *J. Phys. Chem.* 64: 1178-1183 (1960).
40. Lyklema, J. & Mysels, K.J., *J. Am. Chem. Soc.* 87: 2539-2546 (1965).
41. Jones, M.N., Mysels, K.J. & Scholten, P.C., *Trans. Far. Soc.* 62: 1336-1348 (1966).
42. Duyvis, E.M. & Overbeek, J.Th.G., *Proc. Kon. Ned. Akad. Wetensch., Ser. B* 65: 26-30 (1962).
43. Clunie, J.S., Corkill, J.M. & Goodman, J.F., *Disc. Far. Soc.* 42: 34-41 (1966).
44. Clunie, J.S., Corkill, J.M., Goodman, J.F. & Ingram, B.T., *Spec. Disc. Far. Soc.* 1: 30-36 (1971).
45. Ingram, B.T., *J. Chem. Soc., Far. I* 68: 2230-2238 (1972).
46. Prins, A. & Van den Tempel, M., *Spec. Disc. Far. Soc.* 1: 20-29 (1971).
47. Bruil, H.G. & Lyklema, J., *J. Electroanal. Chem.* 37: 31-37 (1972).
48. Den Engelsens, D. & Frens, G., *J. Chem. Soc., Far. Trans. I* 70: 237-248 (1974).
49. Yamanaka, T., *Bull. Chem. Soc. Jap.* 48: 1755-1759 (1975).
50. Yamanaka, T., *Bull. Chem. Soc. Jap.* 48: 1760-1763 (1975).
51. Princen, H.M. & Mason, S.G., *J. Colloid Sci.* 29: 156-172 (1965).
52. Princen, H.M., Ph.D. Thesis, Utrecht, 1965.
53. Mysels, K.J., Huisman, H.F. & Razouk, R.I., *J. Phys. Chem.* 70: 1339-1340 (1966).
54. Princen, H.M., *J. Phys. Chem.* 72: 3342-3345 (1968).
55. Frankel, S. & Princen, H.M., *J. Phys. Chem.* 74: 2580-2581 (1970).
56. Princen, H.M. & Frankel, S., *J. Colloid Interface Sci.* 35: 386-394 (1971).
57. Prins, A., *J. Colloid Interface Sci.* 29: 177-178 (1969).
58. Mysels, K.J. & Buchanan, J.W., *J. Electroanal. Chem.* 37: 23-30 (1972).
59. Agterof, W.G.M., Ph.D. Thesis, Utrecht, 1977.

60. De Vries, A.J., *Rec. Trav. Chim.* 77: 383-399 (1958).
61. De Vries, A.J., *Rec. Trav. Chim.* 77: 441-461 (1958).
62. McEntee, W.R. & Mysels, K.J., *J. Phys. Chem.* 73: 3018-3028 (1969).
63. Frankel, S. & Mysels, K.J., *J. Phys. Chem.* 73: 3028-3038 (1969).
64. Mysels, K.J. & Stikeleather, J.A., *J. Colloid Interface Sci.* 35: 159-162 (1971).
65. Frens, G., Mysels, K.J. & Vijayendran, B.R., *Spec. Disc. Far. Soc.* 1: 12-19 (1971).
66. Scheludko, A., *Proc. Kon. Ned. Akad. Wetensch., Ser. B* 65: 87-96 (1962).
67. Vrij, A., *Disc. Far. Soc.* 42: 23-33 (1966).
68. Scheludko, A., *Proc. Kon. Ned. Akad. Wetensch., Ser. B* 65: 76-86 (1962).
69. Felderhof, B.U., *J. Chem. Phys.* 49: 44-51 (1968).
70. Lucassen, J., Van den Tempel, M., Vrij, A. & Hesselink, F.Th., *Proc. Kon. Ned. Akad. Wetensch., Ser. B* 73: 109-123 (1970).
71. Vrij, A., Hesselink, F.Th., Lucassen, J. & Van den Tempel, M., *Proc. Kon. Ned. Akad. Wetensch., Ser. B* 73: 109-123 (1970).
72. Joosten, J.G.H., Vrij, A. & Fijnaut, H.M., in: "Physicochemical Hydrodynamics, Vol II: V.G. Levich Festschrift" (D.B. Spalding, Ed.) Imp. Coll. Sci. Technol., London; Adv. Publ. Ltd., 1977.
73. Joosten, J.G.H., Ph.D. Thesis, Utrecht, 1982.
74. Miles, G.D., Ross, J. & Shedlovsky, L., *J. Amer. Oil Chem. Soc.* 27: 268-273 (1950).
75. Mysels, K.J., Cox, M.C. & Skewis, J.D., *J. Phys. Chem.* 65: 1107-1111 (1961).
76. Razouk, R.I. & Mysels, K.J., *J. Amer. Oil Chem. Soc.* 45: 381-384 (1968).
77. Roberts, K., Axberg, C., Oosterlund, R. & Saito, H., *Nature* 255: 53-54 (1975).
78. Koczó, K. & Rácz, G., *Colloids and Surfaces* 22: 97-110 (1987).
79. Highfield, R.R., Humes, R.P., Thomas, R.K., Cummins, P.G., Gregory, D.P., Mingins, J., Hayter, J.B. & Schaerpf, O., *J. Colloid Interface Sci.* 97: 367-373 (1984).
80. Von Wandruszka, R. & Winefordner, J.D., *Talanta* 33: 871-874 (1986).

CHAPTER II

PROFILE OF THE PLATEAU BORDER IN A VERTICAL FREE LIQUID FILM

ABSTRACT

Profiles of the Plateau border at a vertical film in a 0.02 M CTAB solution are measured by optical interference, in the part of the border near the film, at two heights above the bulk liquid surface.

The Laplace pressure in the border, calculated from these profiles, appears to be lower than the hydrostatic equilibrium pressure at a height close to the bulk liquid meniscus (6.2 mm); at a greater altitude (11.3 mm) the pressures are equal. An upward flow in the border close to the film is observed, while a downward flow takes place in the periphery of the border. Both effects can be explained by Marangoni flows.

INTRODUCTION

In the course of an investigation on the stability of foams in suspensions we came across the problem, that for mobile films the first stages of foam history, viz. the drainage, are not completely understood, in spite of the fundamental work by Mysels and collaborators on this

subject (1). These authors found that in a film drawn vertically in a foam, drainage to the Plateau border predominates over the vertical drainage directly to the bulk liquid. They started from the following assumptions:

- a. In the Plateau border, the pressure is equal to, or slightly larger than, the hydrostatic equilibrium pressure at the height concerned;
- b. If a film is drawn from a border, the surface tension in the film must surpass that in the border.

On the basis of these assumptions, Mysels c.s. predicted a dip in film thickness just before the junction with the border. This, however, was not found experimentally in mobile films. In addition, a limit was derived for the thickness of the film, which can be drawn out of a border with energy supplied by the falling in of film of a given thickness; but this prediction was contradicted by experiments.

Later studies of film thinning concentrated in most cases on contact angles at the transition film/Plateau border (2-17), and on the influence of surface waves on film drainage (18-23). Thus the paradoxes mentioned in the previous paragraph remained, to the knowledge of the present authors, unsolved. This lack of understanding of mobile film behaviour is the more to be regretted, since many foams formed either intentionally or unintentionally, consist of mobile films.

We therefore thought it profitable to learn more about pressure and flows in Plateau borders, by extending the optical interference method developed by Scheludko c.s. (2-5) and Haydon c.s. (9,10) for measuring contact angles in horizontal films, to vertical films, and to larger distances from the film into the Plateau border.

EXPERIMENTAL

Materials

CTAB (Cetyltrimethylammoniumbromide): ex Sigma Chemical Co. The surface tension vs. concentration graph had a distinct break near the c.m.c. (= $9 \cdot 10^{-4}$ M (24)) without a minimum; no further purification was applied. All experiments refer to 0.02 M CTAB solutions at 25°C. In this

solution, the surface tension measured by the Wilhelmy plate method at 25°C, was 37 mN/m. In this concentration range, there is only a slight concentration dependence. A 0.25 M solution at 25°C (supersaturated) had a surface tension of 33 mN/m.

Glass: ex Louwers Glass (Hapert, The Netherlands), consisting of spherical particles with diameter $< 10 \mu\text{m}$. The sample was divided into fractions with narrower size distributions, by sedimentation in deionized water. Particle size distributions were measured with a Coulter Counter; standard deviations varied from 0.2 μm for the fraction with the smallest particles ($< 1 \mu\text{m}$) to 2.7 μm for the one with the largest ($> 5 \mu\text{m}$). Before fractionation by sedimentation the density of the glass particles was determined with a Quantachrome Stereopyknometer to be 2.47 g/cm³.

Water employed in the Plateau border experiments: twice distilled.

Apparatus

A film was drawn in a vertical glass frame, which was held at fixed position. The frame consisted of a 2 mm thick, 10x21 mm glass plate with a rectangular, 4x10 mm indentation at one of the short ends; the two legs thus formed had rectangular cross sections. The observation point was fixed at 1.2 mm below the upper edge of the window; its height above the bulk liquid could be varied by changing the amount of sample in the glass vessel below the frame.

This height was determined by measuring the conductance of the liquid between two platinum wire ends connected parallel to and 4 mm in front of the frame legs (fig. II-1), which hung in the liquid. Care was taken not to create a film between the two wires or between a wire and a frame leg. The conductance of a 0.02 M CTAB-solution varied linearly with the depth in the liquid of the two wires, and thus with the measuring height, by an amount of 42.94 $\mu\text{mho/mm}$.

For the calibration line the height of the bulk liquid meniscus with respect to the observation height was changed manually and measured with a kathetometer. Because the bulk liquid surface in the small glass vessel, inner diameter 16.5 mm, containing the surfactant solution, was

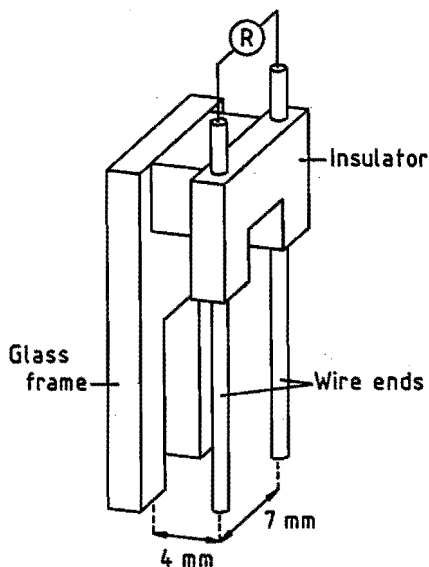


Fig. II-1. Schematic representation of the two wire ends, via an insulator block attached to the glass frame, used for obtaining the depth in the liquid through resistance measurements.

disturbed by the frame legs and the wire ends, we measured the height of the bulk liquid in a larger, external beaker, connected with the sample vessel by a very thin, sample filled hose.

Before an experiment the frame was surrounded by the sample vessel. Frame and glass vessel were contained in a double-walled stainless steel chamber of 30 mm inner diameter. Samples were left in this closed sample chamber at 25°C for several hours before experiments. A film was drawn by lowering the vessel pneumatically in less than 1 sec. at the start of an experiment.

The films were observed through a Leitz Metalloplan microscope placed on its backside in order to permit direct observation of a vertical film without intervention of mirrors. A 10 mm working distance, 20x objective with a numerical aperture of 0.4 was inserted in the sample chamber, and together with a 12.5x ocular resulted in a 250x magnification.

As light source a 50 W super pressure mercury lamp (Osram HBO 50 W) was used; the principal wavelengths of the light (in vacuo) were 440 and 554 nm. The microscope images of the transition region between film and Plateau border were photographed at predetermined times by a Minolta X-700 camera equipped with Autowinder and Multi-Function Back. We used Agfacolor 1000 ASA films. These photographs were converted into half film thickness vs. distance graphs, with Fizeau's formulas for plane parallel films (correction of curvature not necessary: see Appendix): distances were measured between the blue or, with the use of a 546 nm interference filter, black lines. In both cases these are subsequent interference orders of the 554 nm wavelength's minima.

The interference order p was determined by comparison of the photographs of one series starting from the last ones, on which the Plateau border adjoins the black film: the first blue or black line is of order $p = 1$, the second of order $p = 2$, etc. For these lines the local Plateau border thickness δ_f is then calculated from the wavelength $\lambda = 554$ nm in air and the index of refraction $n = 1.3342$ (25) according to Fizeau's equation of interference minima (26,27):

$$\delta_f = \frac{p\lambda}{2n} \quad \text{[II-1]}$$

The calibration scale for the horizontal distance was determined with an object micrometer. The origin in this distance was taken arbitrarily, but remained fixed during a series of experiments with one film.

For experiments with glass particles a magnetic stirrer was used to keep these particles in suspension; during an experiment stirring was ceased in order to minimize vibrations. Movements of the glass particles in the Plateau border were recorded with a Sony video camera and recorder.

The contact angle of the sample solution at the glass frame θ_g was measured by photographing a droplet of the surfactant solution on the glass surface in a closed chamber and manually fitting a circle section to the droplet surface on the photograph near its base. To match the conditions during an experiment, the hydrophobic monolayer of CTAB on

the glass was not removed, and the receding contact angle was determined by sucking away part of the liquid in the droplet after its deposition on the glass plate.

Surface tension measurements were performed with a Krüss Digital-Tensiometer K10T, using a Wilhelmy plate.

RESULTS

A typical series of experimental data is shown in fig. II-2. In this graph, the film is at the left side, and one frame leg is off the right side at a distance of about 460 μm . In this figure the Plateau border profiles at times $t = 169$ and 192 s start from a black film, while the thickness at the utmost left points of the curves at $t = 31, 49$ and 109 s is calculated for $p = 1$ and at $t = 7$ s for $p = 4$ [II-1], as determined from the photographs. The experiments are restricted to the part of the Plateau border near the film, since the optical arrangement did not permit collection of light rays

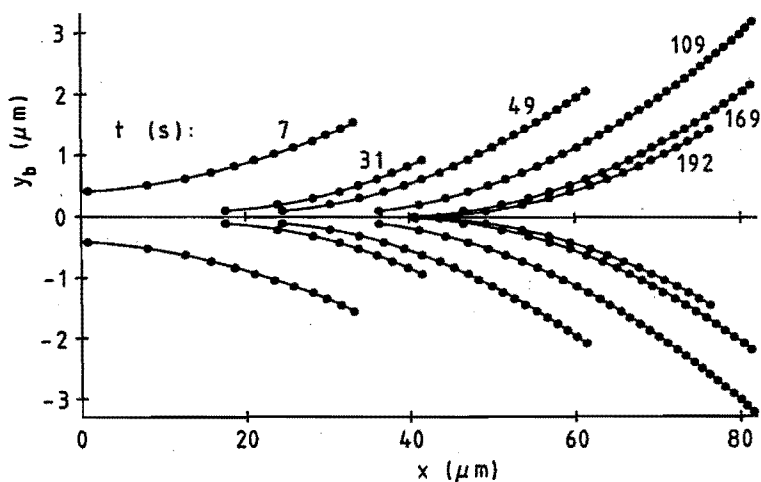


Fig. II-2. Profiles of the film-near region of the vertical Plateau border in a vertical free liquid film, drawn out of a 0.02 M CTAB-solution as a function of time t after film formation (Horizontal cross section). The x -axis, in the direction away from the film, is the symmetry axis of the profiles; y_b -axis perpendicular to the film, $y_b = 0$ in the mid of the film, origin otherwise arbitrarily.

reflected in the region of the Plateau border near the frame (see Appendix). Here typical marginal regeneration phenomena are observed analogous to those reported by Mysels c.s. (1,28). The turbulences gradually decrease in time and marginal regeneration is practically finished, when a black film is formed.

The obvious feature of fig. II-2 is the contraction of the Plateau border toward the leg of the frame (or, put differently, of the film to expand) with increasing time. No dip in film thickness, at the transition to the border, is seen, in agreement with Mysels' observations (1).

We have developed two methods for analyzing the data for surface curvature at the moment each set of data was obtained; the first one permits to detect changes in radius of curvature of the Plateau border in a horizontal section, but requires smoothing of data. The second one starts from the assumption of a constant radius of curvature in a horizontal section in that part of the border, in which measurements are possible; but no smoothing of data is required.

First method of calculating the radius of curvature of a horizontal section through the border

If we want to check whether the radius of curvature changes along the measured profile of the transition region between film and Plateau border, we must be able to calculate these radii at any arbitrary point P on the curve. For this, the relation for the radius of curvature

$$r_p = \frac{- \left[1 + \left(\frac{dy_b}{dx} \right)^2 \right]^{\frac{3}{2}}}{\frac{d^2y_b}{dx^2}} \quad \text{[II-2]}$$

is applied to the experimental data. The first and second derivatives have to be obtained from the experimental data.

Taking first and second derivatives of adjoining points causes large instabilities even when the scattering of the measured points is only small. Therefore a smoothed curve through these points is calculated by

performing a polynomial fit of maximum power 2 in each point using all points. Deviations of the measured points from the fitted curve were within the measuring error. On this fitted curve 105 points at the most are taken for calculating the radii of curvature.

Through linear interpolation a limited number of equidistant points is obtained for calculating the first and second derivatives using Lagrange's five-point interpolation formulas (29). The radii of curvature are calculated for different numbers of interpolated points.

As a test for this calculation we calculated the radius of curvature for a) points of a geometrical circle of radius 500 μm , and b) the curve derived from the interference pattern calculated for such a circle by the method described in the Appendix, in which the influence of the border curvature is taken into account. The results are shown in fig. II-3. Except for the first and last points of the curve, where numeric instability still causes large deviations, the radii of curvature for both curves are fairly constant.

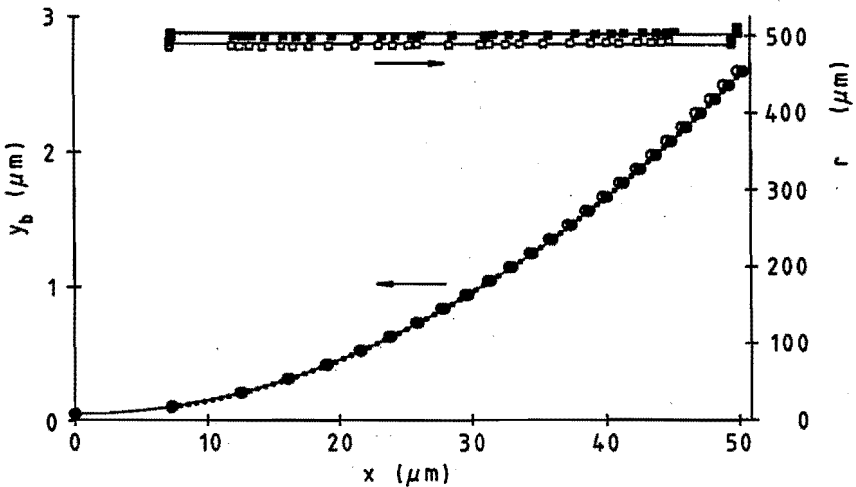


Fig. II-3. Radii of curvature r , calculated according to the first method, ■ for a circular profile (●) and □ for a profile, calculated according to the computed interference pattern for this circular profile (○). 5 to 10 interpolated values for double numeric differentiation. Also drawn are the two profiles of fig. II-11, together with the smoothed curve of the proper circle (•). See Appendix.

The profile derived sub b) has a slightly smaller radius ($488.0 \pm 2.3 \mu\text{m}$) than the profile from the geometrical circle ($500.3 \pm 2.2 \mu\text{m}$). This can be seen in fig. II-3, because one profile has a slightly larger radius than the other. These radii as well as those for the experimental data, are calculated as the mean of the radii for 5 to 15 interpolated points, omitting extreme values on the edges, which results in about 100 out of 110 values. The fact, that the radius of the derived curve deviates $12.3 \mu\text{m}$ or 2.5 % from the circle radius, is somewhat surprising, since the deviation in the x-values of the profiles amounts to only about 1 %.

It indicates that small deviations in the x-values have a large effect on the radius of curvature. Furthermore, both radius curves show a slightly ascending tendency, which is ascribed to the method of calculation. We conclude, that for curves smoothed by the described procedure this method works reasonably well.

A typical example is shown in fig. II-4 for experimental data. The smoothed curve follows the measured points quite well. The radii of curvature calculated from these smoothed curves are always constant with a standard deviation of $2.5 \mu\text{m}$ at the most. The radius increases

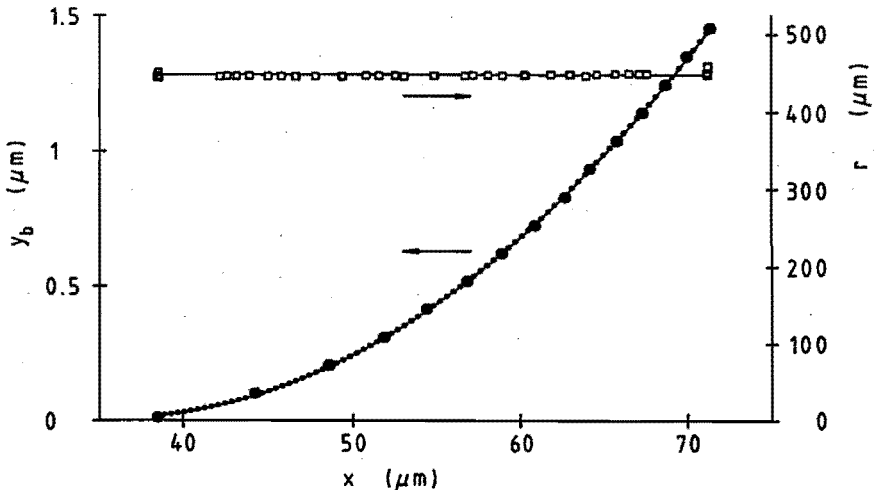


Fig. II-4. Measured (●) and smoothed (○) Plateau border profile and calculated local radii of curvature r (□). $z = 6.2 \text{ mm}$; $t = 192 \text{ s}$; 5 to 10 interpolated values for double numeric differentiation. See First Method.

slightly with the distance from the film, as already described for the circle; this is taken into account in the standard deviation.

In fig. II-5 the results of all the calculations according to the first method are plotted as a function of time from film formation for three experiments, two at a height of 6.2 ± 0.1 mm and one at a height of 11.3 ± 0.1 mm above the meniscus. In case of the 11.3 mm altitude the frame legs, having a length of 10 mm, are completely above the bulk liquid surface, but connected with it by a 1.3 mm high meniscus. This is clearly less than the maximum meniscus height, which for this aqueous solution with surface tension $\gamma = 37$ mN/m and glass contact angle $\theta_g = 10^\circ$ (see below) amounts to 3.87 mm (30,31), i.e. when the large glass plate is horizontal and above the level of liquid. It is also less than the meniscus height for this solution against a vertical glass plate, which amounts to 2.50 mm (1,30,31).

Also shown are two dashed lines representing the radii at the heights concerned according to hydrostatic equilibrium, when the Laplace

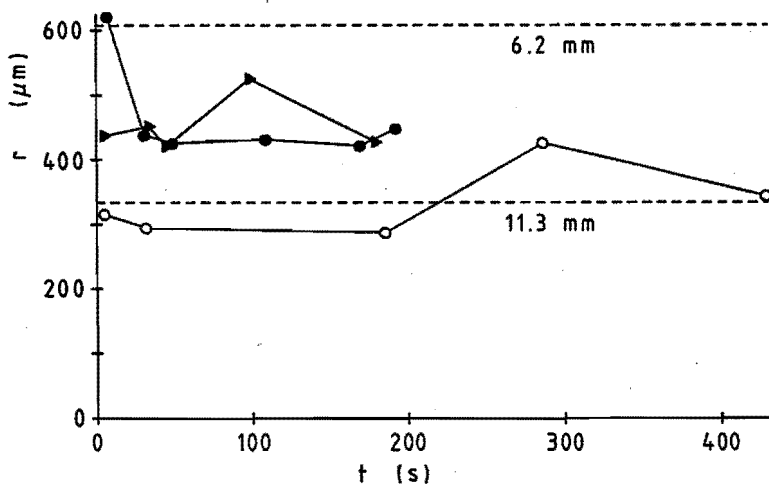


Fig. II-5. Calculated radii of curvature r vs. time t after film formation for 2 measuring heights (●, ▲: 6.2 mm; ○: 11.3 mm). Also drawn are the (time independent) radii of curvature for these heights, when the Laplace pressure equals the hydrostatic equilibrium pressure according to eqn. [II-3].

pressure equals the hydrostatic pressure:

$$\Delta\rho gz = \gamma \left(\frac{1}{R_1} + \frac{1}{R_2} \right) \approx \frac{\gamma}{r} \quad \text{[II-3]}$$

where $\Delta\rho$ is the difference in density between the solution and the surrounding air, g is the gravity acceleration, z is the height of the observation point above the bulk liquid meniscus, γ is the surface tension of the bulk solution (37 mN/m) and R_1 and R_2 are the principal radii of curvature (see Discussion, part b); if one of these radii becomes infinite, then the other radius approaches r , the Plateau border radius at hydrostatic equilibrium. We see, that the experimental radii do not show a distinct trend with time; except for two points at the height of 6.2 mm, the values cluster around a level. For the height of 6.2 mm this level amounts to $434 \pm 11 \mu\text{m}$, for the 11.3 mm height the values oscillate around an average value of $297 \pm 12 \mu\text{m}$, being less well defined than the former level.

Except for one value at shorter times of 6.2 mm height, all experimental radii are smaller than the radius for hydrostatic equilibrium at this height. For the high observation point range of 11.3 mm the calculated hydrostatic radius equals the level of the experimental points.

Second method of analyzing horizontal section data for surface curvature

This is based on the result of the first method, that the surface curvature is constant over the interval measured. Compared with the first method, it has the advantage that smoothing of experimental data, which might introduce systematic errors, is avoided. It is based on the assumptions that at a certain height above the bulk liquid meniscus, pressure and surface tension are constant (but not necessarily equal to the hydrostatic equilibrium pressure at that height, and the surface tension of the bulk solution, respectively).

In addition it is assumed that the surface curvature agrees with the Laplace equation:

$$\frac{1}{r} = \frac{\Delta p_L}{\gamma} \quad \text{[II-4]}$$

with Δp_L as the pressure difference according to the Laplace equation and again

$$\frac{1}{R_1} + \frac{1}{R_2} \approx \frac{1}{r} \quad \text{[II-5]}$$

This equation implies, that only one of the radii of curvature of the surface of the Plateau border is important for determining the pressure.

Deviations from the Laplace equation are improbable, because they imply a disturbance of force equilibrium, which would result in accelerated motion of the surfaces concerned to be expected, especially because of the pronounced mobility of the surface.

The surface curvature at the observation heights concerned is found from the experimental data as follows:

We calculate a $y_b(x)$ -curve (with x = distance in horizontal direction away from the film into the border; y_b = half thickness of the Plateau border) starting from the experimental point lying farthest away from the film, (i.e. most border-inwards). We assume a slope dy_b/dx at that point and a value for the surface curvature $1/r$, and calculate $y_b(x)$ numerically by a large number of step calculations:

$$\left(\frac{d^2y_b}{dx^2}\right)_{k+1} = \frac{\left[1 + \left(\frac{dy_b}{dx}\right)^2\right]^{\frac{3}{2}}}{r} \quad \text{[II-6]}$$

$$\left(\frac{dy_b}{dx}\right)_{k+1} = \left(\frac{dy_b}{dx}\right)_k + \left(\frac{d^2y_b}{dx^2}\right)_{k+1} dx \quad \text{[II-7]}$$

$$(y_b)_{k+1} = (y_b)_k + \left(\frac{dy_b}{dx}\right)_{k+1} dx \quad \text{[II-8]}$$

Equation [II-6] is derived from equation [II-2].

In the calculations, a step value $dx = 0.03 \mu\text{m}$ was taken, much smaller

than the distance between experimental points. The initial slope $(dy_b/dx)_{k=1}$, and the curvature $1/r$ were then fitted by a least squares method. Alternatively, only the initial slope was fitted while the curvature was assumed to be consistent with the hydrostatic equilibrium pressure and the surface tension of the bulk solution.

fig. II-6 compares the deviations from experimental values for a curve calculated with both surface curvature and initial slope fitted, with those for a curve calculated with only initial slope fitted. It is seen, that not only are the deviations in the latter case larger than in the former (which is to be expected, since there is one parameter only fitted in the latter case), but that there are systematic deviations of the curve calculated with only slope fitted, from the experimental data: the calculated values are in this case systematically too low near the film, and too high at the other end of the border.

The deviations are consistent with a radius of curvature smaller for the experimental points, than for the values calculated on the basis of $p = p_{\text{hydrostatic equilibrium}}$ and $\gamma = \gamma_{\text{bulk solution}}$. The radii of curvature as calculated according to this second method, both slope and curvature

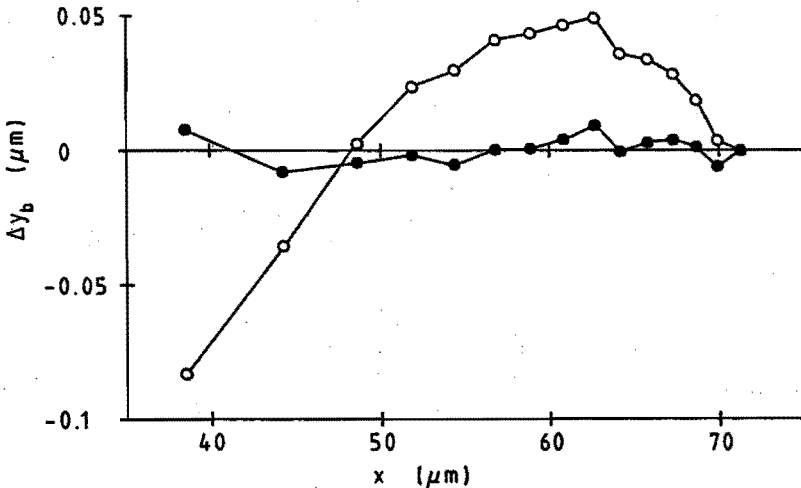


Fig. II-6. Deviations from experimental values $\Delta\gamma_b$ for a curve, calculated with both surface curvature and initial slope fitted (●), and with only initial slope fitted (○). $z = 6.2$ mm; $t = 192$ s. See Second Method.

being fitted, are roughly the same as those as a result of method 1, as expected.

Theory permits also to calculate the half film thickness ($y_f = \frac{1}{2}\delta_f$) and the pressure in the film from the experiments, as follows:

Starting from the last (i.e. most border-near) experimental value of the half border thickness y_b , the Plateau border surface is extrapolated on the assumption of a constant pressure (equal to the optimum fit value for the border surface) until (cf. [I-23])

$$1 - \cos\theta - \frac{p_i y_b}{\gamma} = 0 \quad \text{[II-9]}$$

Here, $\theta = \arctan(dy_b/dx)$, p_i is the pressure due to interaction between the film surfaces, and γ is the bulk surface tension. This requirement is based on the equality of pressure force and surface tension force, both per unit length in vertical direction along the film, at a point shortly before the border/film transition.

In the absence of significant interaction between the surfaces, the contact angle at the border/film transition (θ_f) is zero and (cf. [I-13])

$$\gamma_f = \gamma_b + (p_f - p_b) y_f \quad \text{[II-10]}$$

where now $p_f = p_a =$ atmospheric pressure; [I-8]

$$p_b = p_a - \gamma_b/r. \quad \text{[I-7]}$$

The values for γ_f thus calculated were larger than γ_b , in agreement with Mysels' observations, but did not differ more than 0.7 % from the bulk γ -value.

In using eqn. [II-9] during the extrapolation, the interaction pressure in the film is calculated as:

$$p_i = p_A + p_R \quad \text{[II-11]}$$

with p_A and p_R the Van der Waals attractive and double layer repulsive pressures, resp., mentioned in Ch. I (eqns. [I-14]-[I-20]). The main

Table II-i: Pressures in the film and film contact angles. [CTAB] = 0.02 M; frame width = 4 mm; height above bulk 6.2 mm.

t (s)	y_f (μm)	P_A (Pa)	P_R (Pa)	$\text{tg}\theta_f$
7	0.4001	0.0002	0	$0.44 \cdot 10^{-4}$
31	0.0969	0.0685	-0.000846	$5.48 \cdot 10^{-4}$
49	0.0681	0.377	-0.235	$7.05 \cdot 10^{-4}$
109	0.1075	-	-	-
169	0.0203	-	-	-
192	0.0209	-	-	-

difficulty in applying these equations is the uncertainty both in the Hamaker constant and in the osmotically active surfactant concentration. Above the c.m.c. the surfactant concentration weighed in can not be assumed to be osmotically active as single ions. In addition, the liquid in the film may have a lower surfactant concentration than that weighed in due to the pronounced surface excess of the surfactant combined with the large surface/volume ratio in the film. On the other hand, if we take the c.m.c. as active electrolyte concentration, then in the cases of small film thicknesses no value can be found on extrapolating the experimental y_f -values, for the distance x , at which eqn. [II-9] is obeyed, unless values for the Hamaker constant greatly exceeding $1 \cdot 10^{-19}$ J (32) are assumed.

In view of these uncertainties, we took the c.m.c. (24) as the value for the active electrolyte concentration (Table II-i). In those cases, where eqn. [II-9] did not reach zero, no $\text{tg}\theta_f$ can be calculated on the assumptions mentioned. The y_f -value mentioned in table II-i then is the value calculated from the best fitted $y_f(x)$ -curve through the experimental data, for the x -value, at which the film starts.

Flow visualization

Flow visualization in the border was effected by the addition of glass

particles. Clearly two distinct regions could be discerned: in the region near the film, an upward flow was observed, while near the frame a downward flow was seen. In between, the glass particles showed only little movement, in most cases circulating movements (downwards when more near the frame, upwards when more near the film). These flows fade away in the long run, approximately simultaneously with the marginal regeneration phenomena.

DISCUSSION

According to fig. II-5 the radius of curvature of the vertical Plateau border close to the bulk liquid meniscus is smaller than the radius calculated on the basis of hydrostatic equilibrium, while this discrepancy vanishes at greater heights. This means that at the lower height investigated the local underpressure in relation with the outside pressure is larger than one would expect from hydrostatic equilibrium pressure. Since this is quite unexpected (1), we must check, whether this result is really a physical phenomenon. For this, three questions need to be answered carefully:

a. Is the radius of curvature constant at a certain height?

The experiments show, that the radius of curvature of the Plateau border close to the transition region between film and border varies only slightly over the first $30 \pm 10 \mu\text{m}$ in horizontal direction. The total distance film/glass frame, i.e. the breadth of the Plateau border, at the heights concerned was taken from separate photographs of the glass frame with film as a whole. The Plateau border was found to be $460 \pm 25 \mu\text{m}$ in width at the height of 6.2 mm above the bulk meniscus and about $300 \mu\text{m}$ at 11.3 mm. This means, that we have established, that the radius is constant over 6, resp. 10 % of the Plateau border width.

The contact angle with the glass θ_g was separately measured to be 10° . If we assume a constant radius of curvature in the horizontal plane, then with the aid of this contact angle θ_g and the experimental radii of curvature in the transition region r the width of the Plateau border x_b is calculated according to:

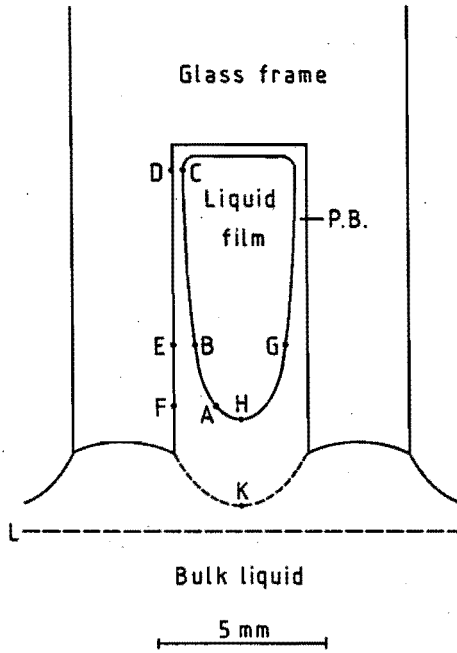


Fig. II-7. Macroscopic drawing of the glass frame with the liquid film suspended in it. Because of the curved Plateau borders, the film deviates substantially from a rectangle. P.B. = Plateau border; L = Bulk liquid meniscus. See the text for the remaining symbols.

$$x_b = r \cos\theta_g \quad \text{[II-12]}$$

As a result we found $x_b = 427 \pm 11 \mu\text{m}$ for the height of 6.2 mm and $x_b = 292 \pm 12 \mu\text{m}$ for the 11.3 mm altitude. These values appear to be lower than the directly measured widths mentioned above, but the differences are within the standard deviations. We conclude, that the radius of curvature may slightly increase in the direction toward the frame; however, this increase should be small.

- b. Is the radius of curvature in vertical direction large enough to neglect its reciprocal value?

Until now we have neglected other than horizontal curvatures. The macroscopic photographs, however, show, that in a film in a glass frame as small as used in our experiments vertical curvatures may be

significant; e.g. the actual thin film in the rectangular frame is not really rectangular, but its periphery shows an appreciable curvature because of a meniscus between the two frame legs and a decreasing Plateau border width in upward direction, as illustrated in fig. II-7. The meniscus between the legs, i.e. the transition between the film and the bottom Plateau border (H in fig. II-7), is pulled up about 2.5 mm by the film, compared with the situation in absence of the film (K in fig. II-7). This fluid bridge shows strong vertical curvatures not only in a plane parallel to the film, but also in a plane perpendicular to it.

Let us consider a pending drop or a bowl with a vertically oriented axis of rotation. Twice the mean surface curvature J at a certain point $P(r_p, z_p)$ on the outer, resp. inner surface of these objects is defined as (31):

$$J = \frac{1}{R_1} + \frac{1}{R_2} \quad \text{[II-13]}$$

where R_1 is the meridional (pertaining to the plane through the axis of an object with rotational symmetry and a point P on its surface) radius of curvature and R_2 is the azimuthal (pertaining to the plane through P normal to the surface and to the meridian) radius of curvature; the circles with these radii osculating to the surface at P lie in these planes. So R_1 can be derived from the equation describing the meridional circle by double differentiation:

$$R_1 = \frac{\left[1 + \left(\frac{dz}{dr} \right)^2 \right]^{\frac{3}{2}}}{\frac{d^2z}{dr^2}} \quad \text{[II-14]}$$

and R_2 , being the distance between P and the rotation axis perpendicularly to the tangent plane, can be calculated by:

$$R_2 = \frac{r_p \left[1 + \left(\frac{dz}{dr} \right)^2 \right]^{\frac{1}{2}}}{\frac{dr}{dz}} \quad \text{[II-15]}$$

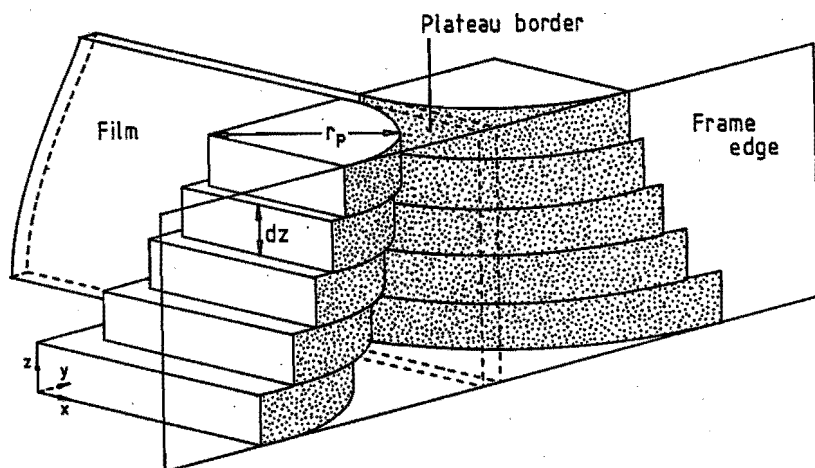


Fig. II-8. Schematic representation of the Plateau border, built up of cylinder segments with radius r_p and height dz .

In these equations the z -axis is the rotation axis and the r -axis runs horizontally, perpendicularly to the z -axis; r_p is the horizontal distance from P to the z -axis.

Application of these equations to our Plateau border is restricted to the first quadrant of the ground plane ($= xy$ -plane; $r^2 = x^2 + y^2$) and is justified only if a vertical rotation axis is present. However, the measured horizontal radius of curvature decreases with increasing height z , while dz/dr remains positive. This means that the centre of the circles describing the border gradually moves towards the border on ascending along the z -axis, which destroys the symmetry. If, however, we consider only small increases in height (dz), we may regard the border as rotation symmetrical and we may apply the above equations to height fractions dz . In this way the Plateau border surface can be regarded as being built up by cylinder segments in the first quadrant of height dz , each one with its axis shifted along the bisector of the x - and y -axis towards the border in such a way, that it leans slightly over its lower neighbour (fig. II-8).

The question is, whether the meridional curvature of the Plateau border $1/R_1$ is sufficiently strong at greater heights above the bulk liquid meniscus for J to differ considerably from the azimuthal curvature $1/R_2$. The macroscopic photographs tell us, that the strongest curvature of the

periphery appears just above the meniscus, although this is not one of the principal radii of curvature: the radius of this curvature is in the order of 1 mm (H in fig. II-7), while at larger altitude the radius increases very rapidly. At the heights concerned the meridional curvature is negligible and J approaches the azimuthal curvature $1/R_2$, which in turn approaches the measured horizontal curvature $1/r_p$ for dz/dr approaching infinity.

c. Does the surface tension in the Plateau border differ from the bulk liquid value?

Another possibility is, that the deviation of the experimental radii of curvature from the theoretical ones at hydrostatic equilibrium at the height of 6.2 mm is caused by a strong decrease in surface tension, which e.g. might be effected by evaporation. This is highly improbable for three reasons:

- a) the solution was left in the metal vessel long enough to saturate the environment;
- b) the bulk liquid's surface tension in a 0.02 M CTAB solution was measured to be 37 mN/m, while for a supersaturated solution of 0.25 M CTAB the surface tension did not reach a lower value than 33 mN/m. This decrease is not sharp enough, since for the experimental radii to agree with hydrostatic equilibrium the surface tension should be 26.4 mN/m [II-3];
- c) this mechanism does not explain, why the difference between the radius observed experimentally, and that agreeing with the hydrostatic equilibrium value vanishes at greater height.

On the other hand, both the anomalous radius of curvature of the border at low heights, and the complex flow patterns can be explained by a systematic variation of surface tension in the border in the direction:

$$\gamma < \gamma_A < \gamma_B < \gamma_C = \gamma_D = \gamma_E = \gamma_F \quad \text{[II-16]}$$

(for the meaning of the letters A, B, C, etc., see fig. II-7).

Proposed mechanism for flows and radii of curvature observed in the border.

The simultaneity of the gradual vanishing of the flows in the border and the marginal regeneration suggests a connection between both phenomena:

In the film there exists a surface tension gradient in vertical direction (Ch. I), because the weight of liquid in the film up to a certain level B must be supported by the surface tension along BC (fig. II-7, cf. fig. I-4) (33).

During film drainage there is an exchange of film volume elements with accompanying surfaces against Plateau border volume elements, in the process of marginal regeneration (1). A film volume element, after being exchanged with a border volume element, will occupy a position with a slightly larger thickness compared with its original film thickness, and consequently its surface in the border is smaller than in its original position. Part of the surface of the original film volume element has migrated to the bulk, when arriving in the border. This locally causes a surfactant concentration higher than the surrounding border bulk, while the surface tension at that instant is not changed compared with the film surface tension. Diffusion of surfactant molecules to the surface will lower this surface tension, until complete equilibrium has been established. In addition, the surfactant concentration at the surface may change because of expansion or contraction of the surface during the film/border element exchange. In view of the incompressibility of the liquid this also involves transport of water from the surface to the bulk. However, if molecular transport is assumed to be slow compared with the marginal regeneration exchange, then the new border element is expected to retain its original surface tension (i.e. that of the film at the height concerned), and thus to have a larger surface tension than the surrounding border.

Thus, marginal regeneration leads to a surface tension gradient $\gamma_A < \gamma_B < \gamma_C$ along the transition region film/border, if equal amounts of surface exchange would take place at all heights. However, drainage is less pronounced for thinner films than for thicker ones (1, 34). This effect reduces the surface tension gradient expected; it is assumed here, that

the latter is not quite suppressed.

This surface tension gradient causes a Marangoni flow. Initially, surface tension differences may be levelled off by horizontal flow (e.g., at level B in fig. II-7, by a flow from E to B). However, this will lead to a slightly increased surface tension at this level (compared with the surface tension of the bulk solution), because at E there is only a finite amount of liquid available for surface renewal.

At A, however, bulk liquid can be sucked up, and the amount of liquid available for surface renewal is much larger. This increases the driving force for a flow from A to C, viz. the surface tension difference between A and C, and makes the upward flow from A to C self-reinforcing. This self-reinforcement lets the flow along the border/film transition establish itself rather than flow in horizontal direction. A similar self-reinforcement is assumed in the establishment of for Marangoni instabilities due to temperature gradients (35).

The Marangoni flow becomes stationary, when it is counteracted sufficiently by a pressure gradient and viscous drag. The latter is not very pronounced (see later), and the pressure gradient corresponds with the Plateau border at C being too bulky, at A being too thin (as observed experimentally). The excess liquid at C is levelled off horizontally to D, and removed downward along E and F to the bulk liquid. This flow is then no more a Marangoni flow. Thus the experimentally observed flow pattern can be accounted for.

Liquid moving from C through D to E and F entrains a surface with a relatively large surface tension. This explains the absence of horizontal flow, e.g. from E to B, once the vertical upward flow from A to C has been established: The excess pressure at E (compared with the hydrostatic equilibrium pressure), which is shown by the downward flow there, can not level off the too low pressure at B, which is evidenced by the radius of curvature, because a flow from E to B would be an anti-Marangoni one.

Thus, at F a surface tension difference with the bulk liquid is generated, which counteracts (but not completely suppresses) the transport of liquid from the border to the bulk liquid. This is evidenced by

the gradual thinning of the border (fig. II-2).

The horizontal surface tension differences, between e.g. E and B, should be only small in view of the observed constancy of the radius of curvature both in the direct observation range (fig. II-4), and calculated from contact angle and total breadth of the Plateau border.

At first view, this process might seem unlikely, because of a large hydrodynamic resistance expected for the flow bulk \rightarrow A \rightarrow B \rightarrow C \rightarrow D \rightarrow E \rightarrow F \rightarrow bulk, especially, since the thinness of the border would make contributions to the hydrodynamic resistance pronounced, which are connected with velocity differences in the direction perpendicular to the midfilm plane. However, both front and back surfaces of the border are expected to have the same velocity. Consequently, there is no velocity gradient in the direction concerned. All hydrodynamic resistance experienced by this flow is then connected with the border/film transition, the upward/downward flow transition, and the border/glass frame boundary. Nevertheless, the hydrodynamic resistance of the observed flows is expected to be larger than that experienced by horizontal flows such as E \rightarrow B. The reason for the establishment of the experimentally observed flows (in preference to horizontal flows) therefore should be in the larger driving force of the bulk \rightarrow A \rightarrow B \rightarrow C \rightarrow D \rightarrow E \rightarrow F \rightarrow bulk flows rather than in their low resistance. This larger driving force is generated by their self-reinforcing character.

This mechanism is a tentative one, since the most important hypothesis, on which it is based, viz. the surface tension differences in the Plateau border, can not be checked independently. However, it can account for the experimental data.

CONCLUSIONS

In a foam film drawn from a surfactant solution by means of a glass frame with square legs, there exists a lower pressure than the hydrostatic equilibrium one, shortly above the bulk meniscus. At larger heights (\approx 10 mm) above the meniscus, the hydrostatic equilibrium pressure is observed.

The phenomena may be explained by a Marangoni flow caused by surface tension gradients in the border induced by surface tension differences in the film.

SUMMARY

The measured deviation of the local pressure in the vertical Plateau border from hydrostatic equilibrium pressure near the film base, which vanishes at higher altitude, indicates an extra suction in the lower part of the border. Flows in opposite directions in the border, are observed: an upward flow near the transition region with the film, a downward flow at some distance from the film. Both effects are explained by flows due to surface tension gradients.

ACKNOWLEDGEMENT

We wish to express our gratitude to A. Prins, J.Th.G. Overbeek, K.J. Mysels and A.K. Chesters for their valuable discussions. We also wish to thank J.A. Poulis for his fruitful discussion about the subject treated in the Appendix.

APPENDIX

Interference pattern of light reflected from front and back surfaces of a Plateau border viewed in a microscope.

Consider the microscope to be focused in the front surface of the film (to be distinguished from the front surface of the Plateau border, see fig. II-9a). The image seen in the microscope then corresponds to a real object as far as the film is concerned; in the Plateau border the object is a virtual one. Thus, in the image of a point like A (fig. II-9b) a number of rays such as GFEDC (reflected at the back surface of the border) and HDC (reflected at the front surface) are combined, which do not really pass through A.

For shortness' sake, rays reflected at the front surface are indicated as "primary" rays, and rays reflected at the back surface are called "secondary" rays. A minimum light intensity will be observed apparently

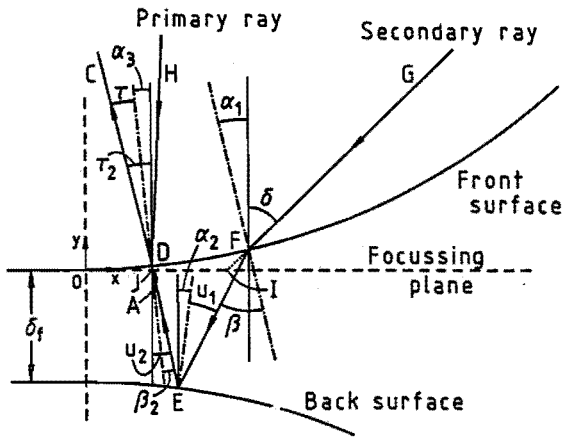


Fig. II-9a. Example of two rays reflected and refracted by a circular Plateau border, whereby the rays leaving the condensed phase coincide.

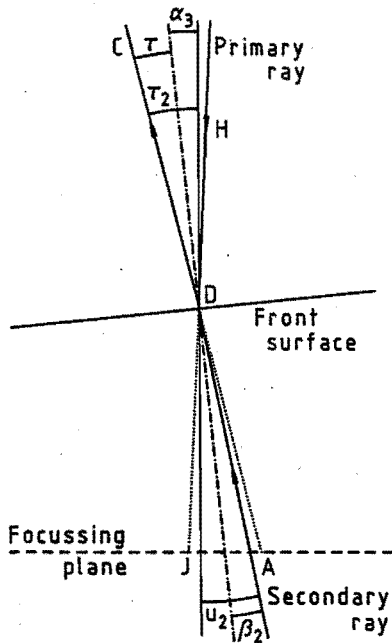


Fig. II-9b. Detail of fig. II-9a showing the construction of points A and J on the focussing plane.

coming from a point A in the focusing plane, when the majority of rays like HD and GFED interfere destructively at D.

The fact, that interference is observed, implies, that primary and secondary rays, having the same phase, when being generated at the light source, are within one coherence length, when interfering at D. This in turn implies, that they would have the same phase, when arriving at the focussing plane, when the border would be absent; differences in geometrical path length between light source and focussing plane are partially compensated by differences in lengths of paths through various media (air, different types of glass) such as to make the optical paths lengths, in terms of wavelengths, equal.

The phase difference between a primary and a secondary ray, interfering at a point like D (fig. II-9a), can then be calculated for a cylindrical Plateau border with radius r , as follows:

- a) Consider a secondary ray (DC), leaving the border while making an angle τ_2 with the normal to the focussing plane. It makes an angle $\tau = \tau_2 - \alpha_3$ with the normal to the front surface of the border at D (where $\alpha_3 = \arctg(dy_3/dx)$; $y_3 = r - \sqrt{(r^2 - x^2)}$ in the coordinate system described in fig. II-9a).

This secondary ray has traversed the Plateau border, after having been reflected at the back surface, along line ED. Line ED makes an angle $\beta_2 = \arcsin(\sin\tau/n)$ with the normal to the front surface, and an angle $u_2 = \beta_2 + \alpha_3$ with the normal to the focusing plane.

Thus, once point A and angle τ_2 being chosen, line AC is fixed and the coordinates of its intersection point D with the Plateau front surface can be calculated. With the angles mentioned in the preceding paragraph, line DE is known, and the coordinates of its intersection point E with the Plateau back surface ($y_2 = -r - \delta_f + \sqrt{(r^2 - x^2)}$) can be calculated; and also the angle, which line DE makes with the normal to the Plateau back surface ($u_2 - \alpha_2$, with $\alpha_2 = \arctg(dy_2/dx)$ at E, $\alpha_2 < 0$).

Then the angle, which the secondary ray makes, before reflection at the back surface, with the normal to the back surface at E is $u_1 =$

$-u_2 + \alpha_2$. Thus, the angle, which FE makes with the normal to the focussing plane, is known ($-u_2 + 2\alpha_2$), and therefore also the coordinates of point F, where the secondary ray enters the Plateau border. Then also the angle between the normal to the front surface at F and the normal to the focussing plane, is known ($\alpha_1 = \arctg(dy_1/dx)$ at F); the angle, which the secondary ray makes with the normal to the front surface, then is $\beta = u_1 + \alpha_2 - \alpha_1$, the angle, which it makes with the normal to the front surface, before it enters the border, is $\arcsin(n \sin\beta)$, and therefore the angle, which it makes with the normal to the focusing plane, will be:

$$\delta = \arcsin\{n \sin(u_1 + \alpha_2 - \alpha_1)\} - \alpha_1 \quad [\text{II-17}]$$

- b) The course of the primary ray is calculated straightforwardly from the condition, that it must, after reflection at point D, coincide with the secondary ray considered. Thus, its angle with the normal to the focusing plane after reflection is τ_2 , and its angle with the normal to the focusing plane before reflection is $-\tau_2 + 2\alpha_3$.
- c) Let the phase, which the secondary ray GF would have, when arriving in the absence of liquid, at point I in the focusing plane be ϕ_0 . Its phase when arriving at F,

$$\phi_{2F} = \phi_0 - (FI) 2\pi/\lambda \quad [\text{II-18}]$$

Therefore, its phase when arriving at D,

$$\phi_{2D} = \phi_0 - (FI) 2\pi/\lambda + (FE + ED) 2\pi n/\lambda \quad [\text{II-19}]$$

Similarly, the phase of the primary ray when arriving at D is:

$$\phi_{1D} = \phi_0 - (DJ) 2\pi/\lambda \quad [\text{II-20}]$$

which becomes after reflection:

$$\phi_{1D} = \phi_0 - (DJ) 2\pi/\lambda - \frac{1}{2}\pi \quad [\text{II-21}]$$

The phase difference between the rays is:

$$\Delta\phi = \phi_{2D} - \phi_{1D} = \{DJ - FI + n (FE + ED)\} 2\pi/\lambda + \frac{1}{2}\pi \quad [\text{II-22}]$$

The coordinates of the points I and J can be calculated from the coordinates of D and F, and the angles τ_2 and δ . With these coordinates and those of point E, $\Delta\phi$ can be calculated for any ray which appears to originate at point A, and makes an angle τ_2 with the normal to the focussing plane.

- d) The intensity of the light emerging at a time t at point D, making an angle τ_2 with the normal to the focussing plane, is then given by:

$$I_{\text{int}} = \{A_1 \sin(Kct) + A_2 \sin(Kct - \Delta\phi)\}^2 \quad [\text{II-23}]$$

A_1 and A_2 are the amplitudes of the electric field vector for the primary and secondary ray, respectively; $K = 2\pi/\lambda$, c is the velocity of light in vacuo. The average intensity reflected over one period from point D in the direction concerned is obtained by summing eq. [II-23] for various values (usually 100) of t ($t_0 < t < t_0 + T$), and the total intensity appearing to originate from point A is obtained by summing the values of the intensity thus obtained for different values of τ_2 .

The summations were performed by means of a program (INSIDE.PAS) written in Pascal, which can be run on any IBM compatible PC. In the calculations A_1 and A_2 have been taken to be equal. Any additional intensity due to e.g., the primary ray being more pronounced than the secondary one, would be superimposed on the interference pattern, but does not shift the latter's minima.

In the calculations, the restrictions were imposed that both incoming and outgoing primary and secondary rays had to be within the numerical aperture (N.A.) of the objective employed.

The result of such a calculation is shown in fig. II-10 for a Plateau border radius of 500 μm and a film thickness of 0.1 μm ; the step size amounts 0.05 μm , which means, that after each calculation the observation point D moves 0.05 μm in the x-direction. This theoretical interference pattern shows several discontinuities due to the fact, that for each point a summation is performed for 50 different values of τ_2 , which

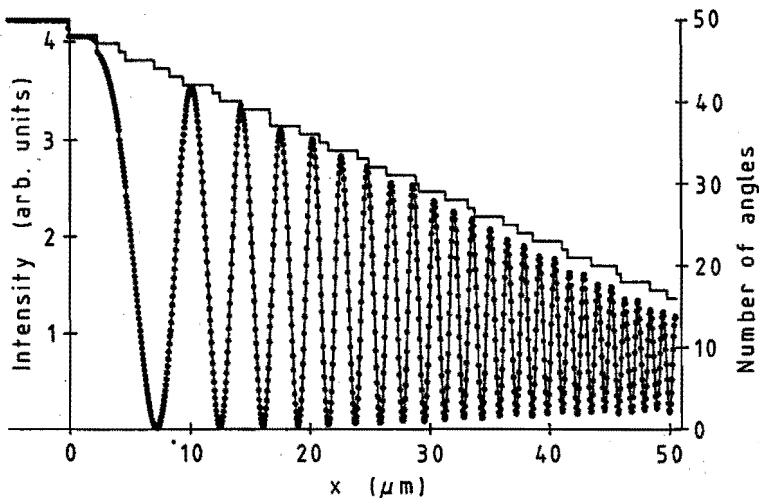


Fig. II-10. Computed interference pattern for the transition from a film, $\delta_F = 0.1 \mu\text{m}$, to a circular Plateau border with $r = 500 \mu\text{m}$. $x = 0$ at the start of the border. The computation is performed for 50 rays in a 2-dimensional cone of light, transmitted by an objective with $N.A. = 0.4$. The stepwise decreasing number of angles is due to the increasing number of emitted rays, which do not reach the objective after reflection/refraction on going to the steeper part of the border.

obey the condition

$$\tau_2 \leq \arcsin(N.A.) \quad [\text{II-24}]$$

where $N.A.$ is the numerical aperture of the objective used, i.e. $N.A. = 0.4$. Also the angles $-\tau_2 + 2\alpha_2$ and δ of the primary and secondary, resp., incoming rays must satisfy this condition. If one of them does not, there will be no interference, and the other ray will be added to the background light; if they both do not, then the outgoing ray with the τ_2 concerned cannot originate from any ray coming out of the objective. In both cases the outgoing ray is omitted in the summation.

On going to the steeper part of the Plateau border surface (the positive x -direction in fig. II-10) less and less rays will participate in the summation. Since the number of rays is limited (50), each time an outgoing ray is omitted, the intensity of the interference light decreases

abruptly. In fig. II-10, the steps in the number of rays used in the calculation correspond to the discontinuities in the interference curve. Although an integration over the angles, if possible, would make these discontinuities disappear and thus would result in a more accurate interference pattern, this would not change the locations of the minima.

After determination of the x -values of the minima, these data are treated the same way as experimental data, which means, that every x -value is provided with the proper thickness. These thicknesses are obtained by employing Fizeau's equation of interference minima [II-1] for which a plane parallel film is assumed. The order of interference is determined by the film thickness: the thickness for the first interference minimum should be calculated for the smallest p , for which δ_p is larger than the film thickness.

In this case, $p = 1$ and $\delta_p = 0.20775 \mu\text{m}$. The other thicknesses are calculated with successive p -values. Also, the original circular Plateau border profile, for which the interference pattern is computed, is calculated according to the proper circle equation with the thicknesses of the interference minima:

$$x_c^2 + (y_b - y_f - r)^2 = r^2 \quad \text{[II-25]}$$

where x_c is the x -value for the circle, y_b and y_f are the half thicknesses of the Plateau border, resp. the film, measured from the film's parallel symmetry plane, and r is the radius of the circular Plateau border.

fig. II-11 shows a plot of this circular profile (closed circles) and the profile, according to the calculated interference pattern (open circles). It is clear, that the deviation of the latter from the circle is only small: it varies from $0.09 \mu\text{m}$ for the first minimum to $0.39 \mu\text{m}$ for the 25th minimum, or in percentages, from 1.2 to 0.7 %. Considering the accuracy, with which the minima are measured on the photographs, this deviation is negligibly small. To see, what effect this deviation has on the radius of curvature, the reader is referred to METHOD 1 in the results.

We realize, that this is only a 2-dimensional analysis, while in reality we are dealing with a 3-dimensional cone of light. However, rays out of

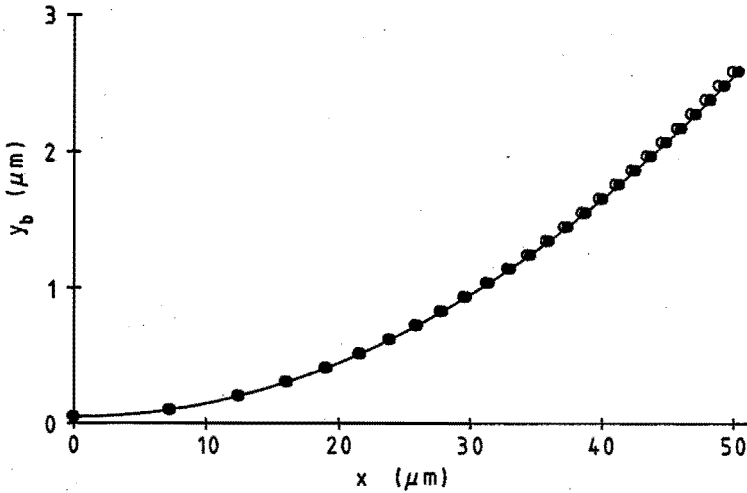


Fig. II-11. Profiles of a circular Plateau border (●, $\delta_F = 0.1 \mu\text{m}$; $r = 500 \mu\text{m}$) and a border, calculated according to the interference pattern in fig. II-10 (○); •: smoothed curve, computed for the circular profile. The utmost left point is only calculated for the circle, but is not derived from the interference pattern.

the horizontal plane and reflected/refracted by a circular Plateau border, upon refraction encounter an ellipsoidal border, which makes a computation rather complicated. Furthermore, 3-dimensional calculations for a wedge shaped border were compared with analogous 2-dimensional ones, showing no large deviations. Therefore, the assumption, that for determination of the local thickness of a Plateau border, measured interferometrically with a microscope with conical illumination, the surfaces are considered plane parallel, may be applied; in other words, Fizeau's equations for maxima and minima are valid and fig. II-3 does not need to be corrected.

REFERENCES

1. Mysels, K.J., Shinoda, K. & Frankel, S., "Soap films; studies of their thinning and a bibliography". Pergamon Press, 1959.
2. Scheludko, A., *Kolloid Z.* **155**: 39-44 (1957).
3. Scheludko, A., Platikanov, D. & Manev, E., *Disc. Far. Soc.* **40**: 253-265 (1965).

4. Scheludko, A., Radoev, B. & Kolarov, T., *Trans. Far. Soc.* **64**: 2213-2220 (1968).
5. Kolarov, T., Scheludko, A., & Exerowa, D., *Trans. Far. Soc.* **64**: 2864-2873 (1968).
6. Mysels, K.J., Huisman, H.F., & Razouk, R.I., *J. Phys. Chem.* **70**: 1339-1340 (1966).
7. Huisman, H.F., & Mysels, K.J., *J. Phys. Chem.* **73**: 489-497 (1969).
8. Mysels, K.J. & Buchanan, J.W., *J. Electroanal. Chem.* **37**: 23-30 (1972).
9. Haydon, D.A., & Taylor, J.L., *Nature* **217**: 739-740 (1968).
10. Requena, J.L., Billet, D.F., & Haydon, D.A., *Proc. Roy. Soc. London A-347*: 141-159 (1975).
11. Princen, H.M., *J. Phys. Chem.* **72**: 3342-3345 (1968).
12. Frankel, S., & Princen, H.M., *J. Phys. Chem.* **74**: 2580-2581 (1970).
13. Princen, H.M., & Frankel, S., *J. Coll. Interf. Sci.* **35**: 386-394 (1971).
14. Prins, A., *J. Coll. Interf. Sci.* **29**: 177-178 (1969).
15. de Feijter, J.A., & Vrij, A., *J. Electroanal. Chem.* **37**: 9-22 (1972).
16. de Feijter, J.A., Rijnbout, J.B., & Vrij, A., *J. Coll. Interf. Sci.* **64**: 258-268 (1978).
17. de Feijter J.A., & Vrij, A., *J. Coll. Interf. Sci.* **64**: 269-277 (1978).
18. Lucassen, J., van den Tempel, M., Vrij, A., & Hesselink, F.Th., *Proc., Kon. Ned. Akad. Wetensch., Ser. B* **73**: 109-123 (1970).
19. Vrij, A., Hesselink, F.Th., Lucassen, J., & van den Tempel, M., *Proc., Kon. Ned. Akad. Wetensch., Ser. B* **73**: 124-135 (1970).
20. Sharma, A. & Ruckenstein, E., *Langmuir* **2**: 480-494 (1986).
21. Ruckenstein, E., & Sharma, A., *J. Coll. Interf. Sci.* **119**: 1-13 (1987).
22. Ruckenstein, E., & Sharma, A., *J. Coll. Interf. Sci.* **119**: 14-29 (1987).
23. Ruckenstein, E., & Sharma, A., *Coll. Polym. Sci.* **266**: 60-69 (1988).
24. Vassiliades, A.E. in: "Cationic Surfactants" (E. Jungerman, ed.), Ch. 12. Dekker, New York, 1970.
25. Washburn, E.W., "International Critical Tables of Numerical Data, Physics, Chemistry and Technology", Vol. VII, p. 13. McGraw-Hill Book Company Inc., New York and London, 1930.
26. Longhurst, R.S., "Geometrical and Physical Optics", Ch. VIII (3rd edition). Longman Group Ltd., London, 1973.
27. Born, M. & Wolf, E., "Principles of Optics", pp. 286-288 (6th edition). Pergamon Press, 1980.
28. Mysels, K.J., *J. Phys. Chem.* **68**: 3441-3448 (1964).

29. Hoerl, A.E., Nashed, M.Z., McKetta, J.J., & Silberberg, J.H., in: "Perry's Chemical Engineer's Handbook" (D.W. Green & J.O. Maloney, Eds.), p. 2-65 (6th edition). McGraw Hill Book Co., 1984.
30. Isenberg, C., "The science of soap films and soap bubbles", Ch. 5. Woodspring Press Ltd., Somerset, 1978.
31. Levich, V.G. "Physicochemical Hydrodynamics", Ch. VII. Prentice Hall, Englewood Cliffs, N.J., 1962.
32. De Feijter, J.A., Ph.D. Thesis, Utrecht, 1969.
33. Lucassen, J., in: "Surfactant Series 11: Anionic Surfactants, Physical Chemistry of Surfactant Action" (E.H. Lucassen-Reijnders, Ed.), pp. 218-265. Marcel Dekker Inc., 1981.
34. Hudales, J.B.M. & Stein, H.N, paper submitted to *J. Colloid Interface Sci.*
35. Tritton, D.J., "Physical Fluid Dynamics", p. 47 (2nd ed.). Clarendon Press, Oxford, 1988.

CHAPTER III

MARGINAL REGENERATION OF A MOBILE VERTICAL FREE LIQUID FILM

ABSTRACT

Marginal regeneration is the main thinning mechanism of a mobile vertical free liquid film, whereby thicker film regions, including the surfaces, are sucked in by the Plateau border, in exchange of thinner regions in an immediately adjacent section. Its hydrodynamic theory is confirmed by calculations performed on profiles of films, drawn from a 0.02 M CTAB solution, where the net flow out of the film is described as a result of a surface flow combined with a bulk flow caused by a pressure gradient.

INTRODUCTION

Although vertical free liquid films have been investigated for a long time already (for an extended bibliography of early investigations, see ref. (1)), the principles of their drainage still are not fully understood. Drainage has been studied extensively in the case of horizontal films (2-4); however, investigations of vertical films were focused on Frankel's law for film formation (1,5-8), black films (9-21), bursting (22-25), film

contact angles (26-31) and surface waves (32-42), the last subject being treated mainly theoretically. Only few papers dealt with actual flow in free films (10,43-45) and Plateau borders (46), but the physics of the main drainage mechanism for mobile films, viz. marginal regeneration (1,7), remained unsolved. Recently, several new techniques for the measurement of film thickness were developed (45,47).

During marginal regeneration thicker parts of a film are withdrawn into the adjacent Plateau border and replaced by thinner parts generated from the same Plateau border at neighbouring spots (1), while the total surface area of the film does not change significantly. This exchange of thinner against thicker film parts results in an effective drainage of the film. Gravity influences these phenomena, because the thinner film elements formed by the marginal regeneration move to that part of the film, where thicknesses match; in a horizontal film there is no systematic variation of film thickness along the border, whereas such a systematic variation is present in a vertical film. Thus, vertical films are expected to show a drainage behaviour basically different from that found for horizontal films.

Frankel (1) derived an equation for describing the marginal regeneration, but to the knowledge of the present author this equation has never been experimentally verified in a quantitative sense. It will be seen, that a starting point for a quantitative elaboration of this theory is the pressure in the Plateau border at a certain height. It was shown in a previous paper (48, Ch. II), that this is equal to the hydrostatic equilibrium pressure at a height of 11 mm above the meniscus, while it is lower at smaller heights. Calculations in the present paper are restricted to heights equal to or larger than 10 mm, where the hydrostatic equilibrium pressure is assumed in the border.

EXPERIMENTAL

Materials

CTAB (= Cetyltrimethylammoniumbromide): ex Sigma Chemical Co. The surface tension vs. concentration graph had a distinct break near the

c.m.c. ($= 9 \cdot 10^{-4}$ M (49)) without a minimum; no further purification was applied.

Twice distilled water was used to make the surfactant solutions.

Apparatus

Single free liquid foam films suspended in a glass frame were studied with a Fizeau interferometer constructed analogously to the apparatus used by Mysels (1).

The glass frame consisted of an upper bar with a 40 mm long leg at either end; the glass was 2 mm thick. Cross sections of the legs and upper bar were either rectangular (2x5 mm) or sharp-angled by cutting the frame's inner sides at one side under an angle of 45°. Of the latter type frames with different distances between the legs were available, producing 107.7, 30.0, 30.1, 45.0 and 15.3 mm wide films, while the frame with rectangular legs had a width of 30.1 mm (measured between the inner sides of the legs).

The sample solution was contained in a glass beaker under the frame with 58 mm height and 56 mm inner diameter; only for the 107.7 mm frame a beaker with 47 mm inner height and 124 mm inner diameter was used.

Beaker and frame were positioned in a double walled metal chamber with 188 mm inner height and 133 mm inner diameter, which was closed airtightly by a P.V.C. lid. The frame was attached to a rod through the centre of this lid. This rod was supplied with a ball joint in the lid, by means of which the frame could be positioned properly (i.e. perpendicular to the light beam of the Fizeau interferometer). The beaker was placed on a platform, which was also thermostatted.

Before an experiment the beaker was filled up to the edge with the sample solution and after closing the chamber with the lid, to which the frame is attached, the system was left for at least 4 hours to allow the interior of the chamber to obtain the saturated water vapour pressure at the temperature concerned, i.e. 25°C.

A liquid film was created by first raising the platform with the beaker pneumatically, such as to immerse the glass frame in the sample solution, and then lowering the platform within 1 second, leaving the lower ends of the frame in the solution. In this way a film was drawn, suspended between the 3 frame sides and the bulk liquid.

The liquid film was observed with a home built Fizeau interferometer: it consists of a 25 cm long metal tube (diameter 40 mm) with a low pressure mercury vapour lamp (Mazda) at one end and a 25 cm focal distance lens at the other. The latter end is inserted horizontally into a hole in the vessel in such a way, that the frame containing the soap film is perpendicularly illuminated by the parallel light beam. This light is reflected from the film back into the tube and via a semi-reflecting mirror into a side tube, at an angle of 73° with the main tube, containing the ocular, to which a Minolta X-700 photo camera is connected. This camera is equipped with the standard 50 mm object lens, a Tokina conversion lens and a close-up lens (no. 1), an Autowinder and a programmable data back, all Minolta except for the converter. We used either 400 ASA Kodacolor or 1000 ASA Agfacolor films.

The lifetimes of foam films were measured visually with a stopwatch.

For an experiment the interference pattern of a whole film was photographed at several times: the first photograph was taken at the moment the beaker reached its lowest point after film formation ($t = 0$). We usually started with 6 exposures, taken at 6 s intervals, after which the intervals were elongated more and more up to 1 min., if the foam film was still intact. This interval elongation was applied, because drainage of the film takes place at a decreasing speed. The time, at which a certain photograph was taken, was imprinted on it by the Multi-Function Back.

The light source emitted bluish green light, with wavelengths 440 nm (violet blue) and 554 nm (yellowish green) predominating. These colours are recognized in the interference pattern reflected by the foam film. This interference pattern consisted of many, closely spaced, horizontal lines, which, however, did not extend quite up to the sides of the film. There the regular film thickness vs. height pattern is disturbed by marginal regeneration. Between new film elements introduced in the film by

marginal regeneration the film thickness was generally found to be thicker than far away from the border at the same height.

The interference lines became broader in time and moved downwards, when the film became thinner approaching a plane parallel film, whereas turbulences at the periphery of the film decreased. Because of the difference in wavelength the green lines outnumbered the blue lines. At certain thicknesses the minima of the two wavelengths nearly coincided resulting in a dark line. Together with the appearance of the black film at very small thickness, this phenomenon is used to determine the order of interference of all the lines observed and thus the film thickness at various heights above the bulk meniscus.

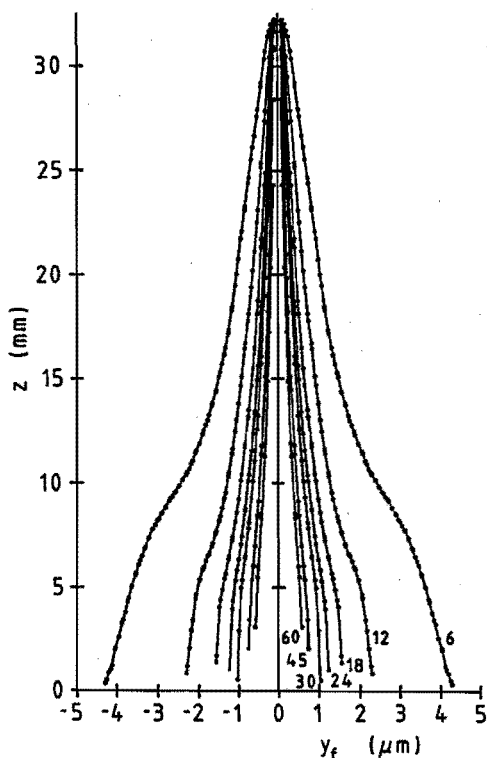


Fig. III-1. Profiles of vertical liquid films in 0.02 M CTAB solution. Frame width, 30,1 mm, rectangular frame legs. Figures close to the curves are times from film formation in s.

RESULTS

A typical series of profiles of one experiment is shown in fig. III-1 for a film in a 30.1 mm frame, which had legs with rectangular cross sections. Compared with the coordinate axis for the height the ordinate axis for the thickness is scaled up by a factor of about 2450. We clearly notice a bell shape for the early profiles, which more and more approaches a wedge shaped film. Marginal regeneration was observed at the bottom of the film and along the frame legs, turbulent at first, but gradually decreasing. The film, in its lower parts, is seen to deviate from the parabolic shape expected for rigid films, in accordance with Mysels' observations (1).

These authors studied long-living films lasting for days, although thickness measurements were performed up to 2500 s, while our films never lived longer than 250 s. Mysels (50) suggested, that the glass frame becomes de-wetted more easily in case of a cationic, strongly adsorbed surfactant than in an anionic one, because of the finite contact angle (10° (48, Ch. II)). Mysels et al. used a 0.7% (~ 0.02 M) solution of "Santomerse No. 1", which consisted of mixed sodium alkyl benzene sulfonates (predominantly monododecyl) containing 60% Na_2SO_4 , to produce mobile films 10 cm high. This difference makes it difficult to treat our data in the same way as they did to calculate the descent constant. Indeed, they stated, that the agreement of a semi-logarithmic relation of height with time for a certain thickness, on which their descent constants are based, is best for relatively quiescent films, in which turbulence is moderate.

For our films, however, we found in an important respect the same as has been observed by Mysels c.s. (1) for films formed from SodiumDodecylBenzeneSulfonate + Na_2SO_4 solutions: the thinning rate at given values of film thickness and height is in good approximation inversely proportional to the frame width (fig. III-2). Here the thinning rate (v_t) is defined as the velocity of film surface movement in the direction perpendicular to the film midplane (see below). Thus, horizontal drainage to the Plateau border predominates over vertical drainage to the bulk liquid.

In order to verify another aspect of the theories mentioned in (1),

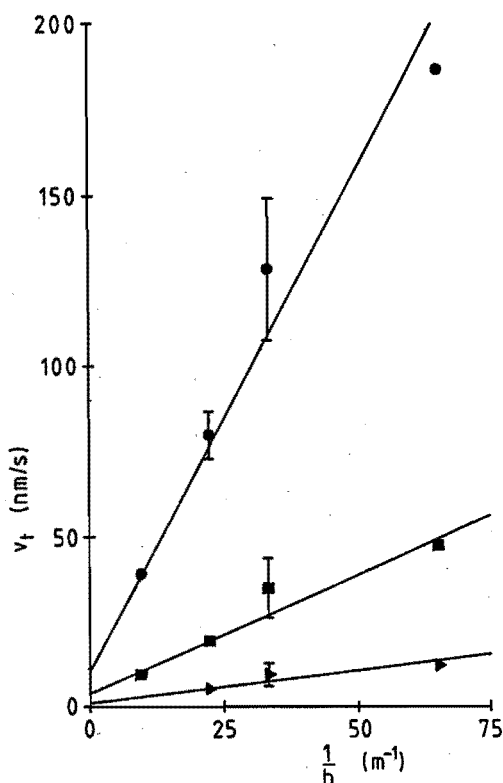


Fig. III-2. Thinning rate v_t (in direction perpendicular to film surface) vs. reciprocal frame width $1/b$. Sharp-angled frame legs. Height: 10 mm. Film thickness: \blacktriangleright : $0.5 \mu m$; \blacksquare : $1 \mu m$; \bullet : $2 \mu m$.

namely Frankel's hydrodynamic theory of marginal regeneration, we treated our data in the following way: from our profiles we linearly interpolated film thicknesses at certain heights above the bulk liquid meniscus for the times, at which the photographs were taken. Through the reciprocal half film thickness vs. time curves at constant height, a smoothed curve is calculated by performing a polynomial fit of maximum power 4 through the points. A typical result is shown in fig. III-3. (The reciprocal half thickness versus time curves were close to straight lines and therefore easier to handle in the smoothing procedure than half thickness versus time curves).

For the many points of the smoothed curve (usually between 70 and 90, compared to 16 at most for experimental data points), the thickness is

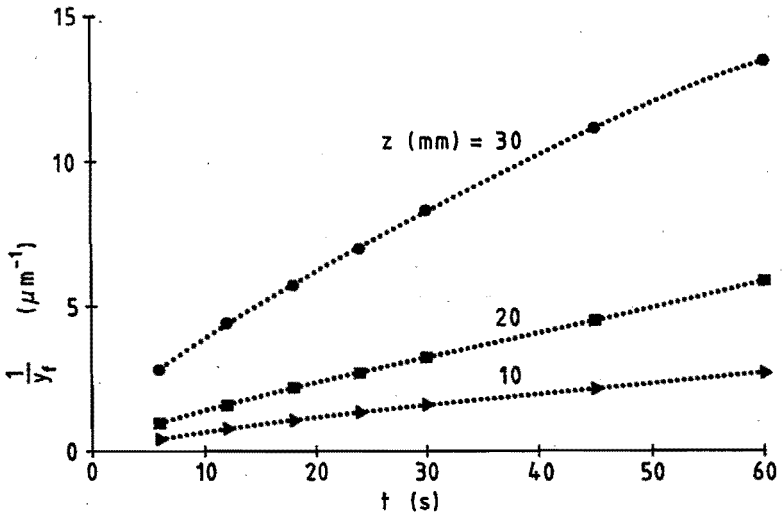


Fig. III-3. Typical reciprocal film thickness y_f vs. time t curves, employed for numerical differentiation. Rectangular frame legs.

recovered and the thinning velocity v_t is calculated by computing the first derivative using Lagrange's five-point interpolation formulas (51). A double-logarithmic plot of the thinning velocity v_t versus film thickness usually shows a fairly straight line deviating mostly at lower thicknesses.

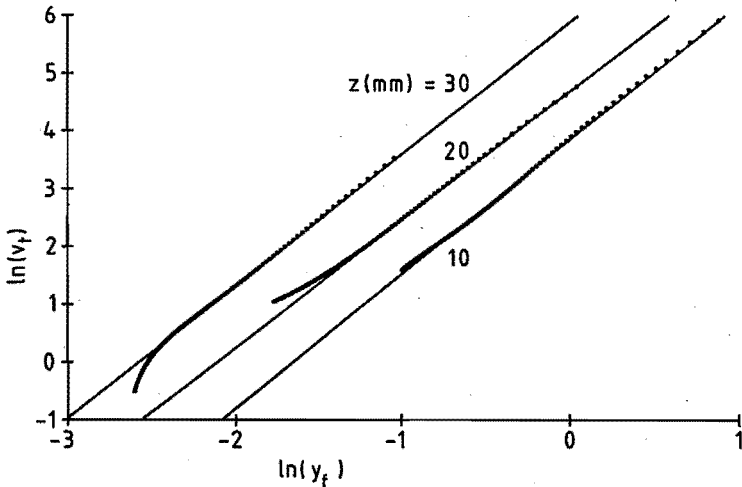


Fig. III-4. Calculation of power law index n (eqn. [III-1]) from experimental data. Same experiment as shown in fig. III-3.

Table III-i: Values of exponent in power law $Q = k\delta_f^n$ (eqn. [III-1]), derived from experimental data, for a sharp-angled frame.

Frame width	107.7 mm				45.0 mm		30.1 mm		30.0 mm		15.3 mm	
Height (mm)	n											
30	1.85	1.82	1.71	1.83	1.65	1.6	1.5	1.3	1.7	1.70	1.85	2.00
20	1.95	1.88	1.80	1.82	1.74	1.7	1.54	1.81	2.1	1.80	1.98	2.06
10	2.08	2.3	2.13	2.08	1.85	1.99	1.70	1.90	2.1	1.95	2.08	2.00
Average	2.0	2.0	1.9	1.9	1.7	1.7	1.6	1.7	2.0	1.8	2.0	2.0
Stand. Dev.	0.1	0.2	0.2	0.1	0.1	0.2	0.1	0.3	0.2	0.1	0.1	0.0
Tot. average	1.9 ± 0.2											

table III-ii: Values of exponent in power law $Q = k\delta_f^n$ (eqn. [III-1]), derived from experimental data, for a rectangular frame (width 30.1 mm)

Height (mm)	B			
	30	2.32	2.2	2.28
20	2.24	2.3	2.23	2.12
10	2.43	2.36	2.33	2.19
Average	2.3	2.3	2.3	2.1
Stand. Dev.	0.1	0.1	0.1	0.1
Tot. average	2.3 ± 0.1			

In fig. III-4 an example is shown of such a plot. Thus, for a particular film thickness δ_f , the drainage rate Q agrees reasonably with the equation

$$Q = k\delta_f^n \quad \text{[III-1]}$$

where k is a constant with dimension $m^3\text{-}n/s$. From the slope of such curves, the exponent n can be calculated.

The results are summarized in table III-i for sharp-angled and in table III-ii for rectangular frame types. Calculations were performed for three heights above the bulk liquid meniscus; a mean n -value for each frame is also given. We notice a clear decrease in n with increasing height for frame legs with sharp-angled cross sections, which is absent in case of the frame with legs with rectangular cross sections. Furthermore the frame width seems to have little or no influence on n : the mean n -value for all the frame widths with sharp-angled legs amounts to 1.9 ± 0.2 , while for the frame with legs with rectangular cross sections it amounts to 2.3 ± 0.1 .

DISCUSSION

The form of the frame legs appears to have an influence on the value of n in eq. [III-1]. Fig. III-5 shows, that for sharp-angled frame legs at

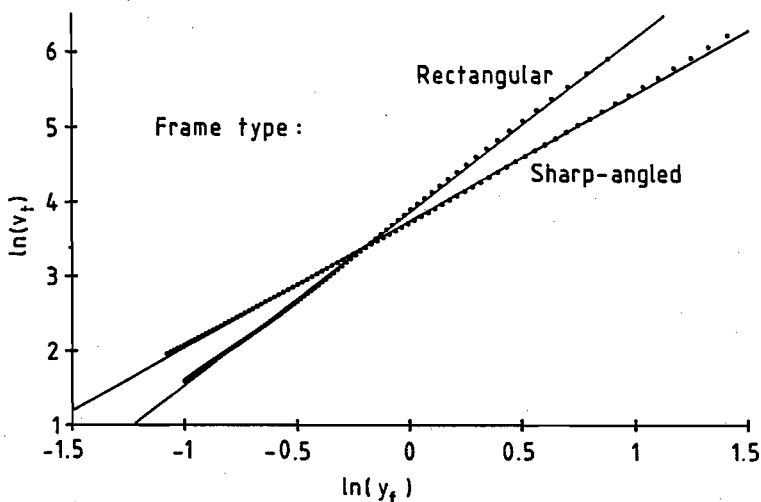


Fig. III-5. The logarithm of the thinning rate v_t as a function of the logarithm of the half film thickness y_f at a height of 10 mm for frames, respectively with sharp-angled and with rectangular legs.

large film thickness the thinning velocity v_t is smaller than for rectangular frame legs at the same thickness, while at small thicknesses the reverse holds true. A possible explanation is that the pressure gradient in the Plateau border is different for sharp-angled frame legs and for rectangular frame legs: deviations from the hydrostatic equilibrium pressure at a certain height are shown by measurements of the Plateau border surface curvature (48, Ch. II). These pressure differences have been ascribed to Marangoni flows in the border at the border/film transition and it is probable, that these flows depend on the frame leg angle, because of its influence on the shape of the Plateau border and consequently of the surface to volume ratio at a certain height.

The following calculations refer to rectangular frame legs at 10 mm height above the bulk liquid, where in the border far from the border/film transition, hydrostatic equilibrium may be assumed, in agreement with the data reported in (48, Ch. II).

In drainage caused by marginal regeneration, in the border/film boundary inflow regions alternate with outflow regions (1). We propose the following mechanism:

Small fluctuations in film thickness, e.g. induced by surface waves in vertical direction, are self-reinforcing. At a stationary border, with neither inflow into nor outflow from the film, a certain film thickness and border shape are mutually connected. A local smaller film thickness, with an unchanged border shape at some distance from the border/film transition, leads to inflow into the film, entailing a lower surface tension at this "primary inflow" spot compared with the surface tension in the surrounding film. The new film element therefore expands, the material being supplemented by further inflow from the border; in addition it rises because of hydrostatic forces. It pushes aside adjacent film elements, enlarging in first instance their thickness. Such slightly larger thicknesses in between new film elements have indeed been observed (see Experimental). This leads to outflow from these slightly thicker film elements into the border, which in turn facilitates entrance of new film elements from the border into the film at the primary inflow spot.

This mechanism can be quantified by an equation originally proposed by Frankel (1):

$$Q = 2v_s y_b + \frac{2y_b^3}{3\eta} \frac{dp}{dx} \quad \text{[III-2]}$$

where Q = the volume flow out of or into the film, per unit length (the latter taken in the z -direction, see fig. III-6)

x = distance in the direction from some arbitrary point in the Plateau border, in the film direction

y_b = half thickness of Plateau border

v_s = surface velocity in the border, parallel to the surface

η = viscosity

p = pressure

The first term corresponds to the flow within the border per unit length, if the flow in the border would be independent of y . The second term in [III-2] expresses the flow caused by the pressure gradient dp/dx . For the latter, Frankel substituted the Laplace pressure:

$$\Delta p_L = \frac{\gamma}{r} \approx \gamma \frac{d^2 y_b}{dx^2} \quad \text{[III-3]}$$

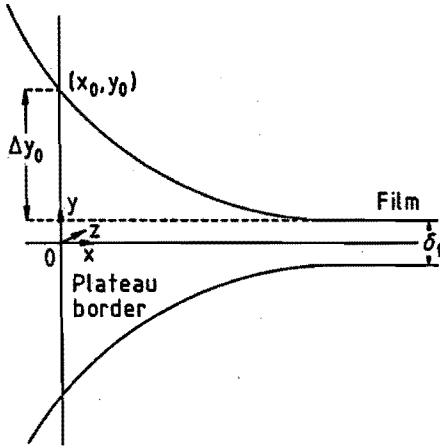


Fig. III-6. Parameters in the theoretical description of flow by marginal regeneration (eqn. [III-2] - [III-16]).

with Δp the pressure difference between the Plateau border and environment, γ the surface tension and r the radius of curvature, which is given by:

$$r = \frac{\left[1 + \left(\frac{dy_b}{dx} \right)^2 \right]^{\frac{3}{2}}}{\frac{d^2 y_b}{dx^2}} \quad \text{[III-4]}$$

Frankel arrived at eqn. [III-3] by assuming $|dy_b/dx| \ll 1$ in eqn. [III-4]. For the pressure gradient, he arrived at:

$$\frac{dp}{dx} = \gamma \frac{d^3 y_b}{dx^3} \quad \text{[III-5]}$$

which involves the approximations, that γ is independent of x (i.e. $\gamma = \gamma_{\text{bulk liquid}}$).

For stationary films, Q and v_s were assumed by Frankel to be independent of x ; thus:

$$Q = v_s \delta_f \quad \text{[III-6]}$$

In this theory the surface tension is assumed to be constant. In view of our previous results this is improbable (48, Ch. II) and can be true only as a first approximation. However, no distinct horizontal transport causing such γ -differences was found. Apparently, these surface tension differences are compensated by pressure differences. In the analysis to follow, γ again will be assumed to be constant as well as the pressure, as a first approximation to a presumably much more complex situation.

We avoided the restriction, that $|dy_b/dx| \ll 1$, and obtained the relation:

$$\frac{d^3 y_b}{dx^3} = \frac{3\eta}{2\gamma y_b^3} \left[v_s (\delta_f - 2y_b) + \frac{2\gamma y_b^3}{\eta} \frac{\frac{dy_b}{dx} \left(\frac{d^2 y_b}{dx^2} \right)^2}{\left[1 + \left(\frac{dy_b}{dx} \right)^2 \right]^{\frac{3}{2}}} \right] \left[1 + \left(\frac{dy_b}{dx} \right)^2 \right]^{\frac{3}{2}} \quad \text{[III-7]}$$

Equation [III-7] can be used for checking, whether the mechanism proposed agrees with the experimental dependency of thinning velocity on δ_f , as follows:

1. At some point (x_0, y_0) in the Plateau border (fig. III-6), the influence of the outflow of liquid from the film will have (practically) died away. We take $x_0 = 0$. The value of y_0 is one of the parameters, which have to be chosen.

At this point, dy_b/dx and $d^2 y_b/dx^2$ have values, which are independent of Q . For $d^2 y_b/dx^2$ at this point, we take the value corresponding to the hydrostatic equilibrium curvature at the height concerned:

$$\left(\frac{d^2 y_b}{dx^2} \right)_{x=0} = \frac{\rho g z}{\gamma} \left[1 + \left(\frac{dy_b}{dx} \right)_{x=0}^2 \right]^{\frac{3}{2}} \quad \text{[III-8]}$$

where ρ is the density, g is the gravitational acceleration and z is the height above the bulk liquid meniscus; the results mentioned below are for a height of 10 mm.

We first determine the profile of the Plateau border for $Q = 0$: assume a step dx (e.g. 0.01 μm) and a value for $(dy/dx)_{x=0}$ (which must

be smaller than 0 in the situation chosen, see fig. III-6). Then $(d^2y/dx^2)_{x=0}$ is known, which gives $(d^3y/dx^3)_{x=0}$ according to eqn. [III-7]. We proceed by calculating the situation at $x = dx$:

$$\left(\frac{d^2y_b}{dx^2}\right)_{x=dx} = \left(\frac{d^2y_b}{dx^2}\right)_{x=0} + \left(\frac{d^3y_b}{dx^3}\right)_{x=0} dx \quad \text{[III-9]}$$

$$\left(\frac{dy_b}{dx}\right)_{x=dx} = \left(\frac{dy_b}{dx}\right)_{x=0} + \left(\frac{d^2y_b}{dx^2}\right)_{x=dx} dx \quad \text{[III-10]}$$

$$(y_b)_{x=dx} = (y_b)_{x=0} + \left(\frac{dy_b}{dx}\right)_{x=dx} dx \quad \text{[III-11]}$$

This is repeated until $dy_b/dx = 0$; the value of y_b at this point is indicated by y_{\min} . The initial value of $(dy_b/dx)_{x=0}$ is then adjusted until $y_{\min} = y_f = \frac{1}{2}\delta_f$.

2. Next we calculate the border profile for $q > 0$ (i.e. where there is inflow from the border into the film). This will lead to a smaller value of the film thickness $(\delta_f - 2\Delta y_{in})$ at those points. It may come as a surprise, that positive values of q and v_s lead to a smaller film thickness. This is a consequence of eqn. [III-7]: for $q = 0$, $v_s = 0$ (eqn. [III-6]), therefore d^3y_b/dx^3 is smaller than zero, according to eqn. [III-7], while d^2y_b/dx^2 is larger than zero. A positive value for v_s in eqn. [III-7] increases the absolute value of d^3y_b/dx^3 (because $\delta_f - 2y_b < 0$). It therefore decreases d^2y_b/dx^2 (eqn. [III-9]), which means a less increasing dy_b/dx , and thus leads to smaller y -values at given x -values, resulting finally in a smaller film thickness.

Assume a value for Δy_{in} (e.g. 0.1 or 0.01 μm), and adjust v_s in eqn. [III-6] such to make $y_{\min} = \frac{1}{2}\delta_f - \Delta y_{in}$. This gives a value for q_{pos} , the inflow rate (per unit length in the z -direction) at those points of the border/film boundary.

3. We finally calculate the border profile for $q < 0$, i.e. for points at the border/film boundary, where there is outflow from the film into the border. Here there is a local increase in the film thickness $\frac{1}{2}\delta_f + \Delta y_{out}$, where Δy_{out} is connected with Δy_{in} , e.g. by the conditions:

$$\Delta y_{out} dz_{out} - \Delta y_{in} dz_{in} = 0$$

[III-12]

$$\frac{dz_{out}}{dz_{in}} = 1$$

dz_{out} and dz_{in} are fractions of unit lengths in the z -direction, in which outflow or inflow occurs. Application of eqns. [III-12] is equivalent to the assumption, that marginal regeneration is caused by thickness fluctuations in the film, in which there is no net flow in the x -direction; once formed, these thickness fluctuations persist although they cause movements in the x -direction (liquid flow out of, or into the film). This persistence of thickness fluctuations is suggested by the interference colours of the film (see also ref. 7), which show near the film/Plateau border transition regions of lower thickness alternating with regions of larger thickness than the normal thickness at a certain height; the latter remain for some time.

The assumption underlying eqns. [III-12] implies, that the necessary adjustments of the adjoining Plateau border are accompanied by net liquid transport in the z -direction. (Otherwise, $\int y dx$ should have been assumed to be constant instead of relations [III-12].) The assumption underlying eqns. [III-12] can, however, easily be defended, because in the Plateau border there is a pronounced transport in the z -direction (48, Ch. II).

On a reasonable assumption for dz_{out}/dz_{in} , e.g. taken to be 1, Δy_{out} can then be found and a value for Q_{neg} , the outflow rate (per unit length in the z -direction) in outflow regions of the border/film boundary.

The net outflow rate can then be found by:

$$Q_{net} = Q_{pos} dz_{in} + Q_{neg} dz_{out} \quad \text{[III-13]}$$

If we neglect the vertical drainage, as proposed by Mysels et al. (1), conversion of the net outflow rate to the surface velocity v_t in the direction perpendicular to the median plane of the film, as calculated from the experimental film profiles, is performed by:

$$Q_{\text{net}} = v_t b \quad \text{[III-14]}$$

where b is the total width of the glass frame, and the factor 2 for the two surfaces is compensated by the factor $\frac{1}{2}$ for the half frame width, from which the draining liquid originates.

This gives the outflow of liquid for various film thicknesses with parameters $\Delta y_0 (= y_0 - \frac{1}{2}\delta_f)$, Δy_{in} and $dz_{\text{out}}/dz_{\text{in}}$. It appears that variations in $dz_{\text{out}}/dz_{\text{in}}$ do not greatly influence the results. The value of Δy_{in} determines the absolute value of the net liquid flow, but does not influence the dependence of the liquid flow on film thickness. The latter is, however, distinctly influenced by Δy_0 : n in equation [III-1], derived from the logarithmic thinning rate vs. logarithmic film thickness curves by differentiation, at a given film thickness decreases with increasing Δy_0 .

The data, on which these conclusions are based, have been calculated on the assumptions:

$$v_s = v_{s,f} \exp[-\alpha (x_{\text{min}} - x)] \quad \text{[III-15]}$$

$$Q = Q_f \exp[-\alpha (x_{\text{min}} - x)] \quad \text{[III-16]}$$

i.e. with an exponentially decaying surface velocity and volume drainage rate decaying with the same constant α ; $v_{s,f}$ is the surface velocity at the border/film transition, Q_f the volume flow at this point. This was thought to be more realistic than Frankel's assumption, that v_s and Q are constant. In the context of the present paper, this comes down to the assumption, that v_s and Q are independent of x for $0 < x < x_{\text{min}}$ (where x_{min} is the x -value at the border/film transition), but suddenly drop to zero at $x = 0$. The decay constant α was calculated on the assumption, that $v_s = v_{s,f}/12,000$ at $x = 0$.

This leads to:

$$\frac{d^3 y_b}{dx^3} = \frac{3\eta}{2\gamma y_b^3} \left[v_{s,f} (\delta_f - 2y_b) \exp[-\alpha (x_{\min} - x)] + \frac{2\gamma y_b^3}{\eta} \frac{\frac{dy_b}{dx} \left(\frac{d^2 y_b}{dx^2} \right)^2}{\left[1 + \left(\frac{dy_b}{dx} \right)^2 \right]^{\frac{5}{2}}} \right] \left[1 + \left(\frac{dy_b}{dx} \right)^2 \right]^{\frac{3}{2}} \quad \text{[III-17]}$$

instead of eq. [III-7]. This can be derived directly by introducing eqns. [III-15] and [III-16] into eqn. [III-2]. It was found, that the assumption of a constant v_s (according to Frankel's original view) leads to similar values of the exponent n as the exponential decay assumed here, although Δy_0 has to be chosen at larger values on the assumption of exponentially decaying v_s and Q , in order to lead to n -values agreeing with those calculated from the experimental data. Fig. III-7 shows the exponent n as a function of the film thickness for various values of Δy_0 and Δy_{in} . The values for n are derived from the double-logarithmic plots of the thinning rate v_t as a

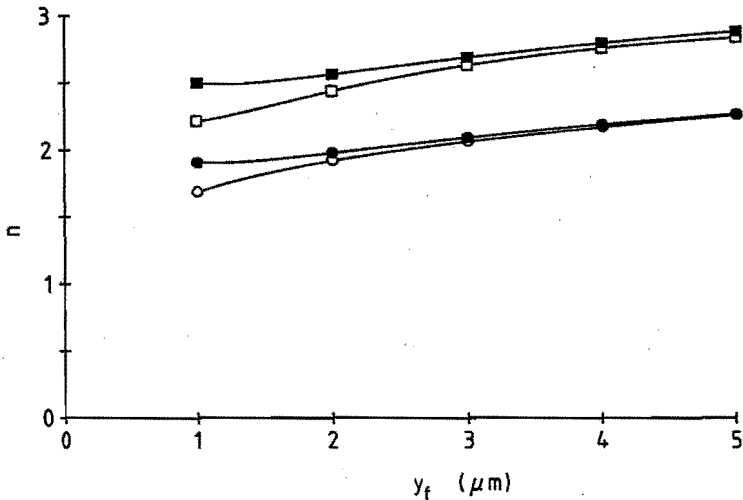


Fig. III-7. Power law index (n -) values (eqn. [III-1]) calculated by theory as a function of half thickness of the film (y_f). Open symbols: $\Delta y_{in} = 0.01 \mu\text{m}$; closed symbols: $\Delta y_{in} = 0.1 \mu\text{m}$; \circ, \bullet : $\Delta y_0 = 24 \mu\text{m}$; \square, \blacksquare : $\Delta y_0 = 6 \mu\text{m}$.

function of film thickness by differentiation. The experimental results are well described with $6 \mu\text{m} < \Delta y_0 < 12 \mu\text{m}$ for the rectangular frame, while for the sharp-angled frames a Δy_0 larger than $12 \mu\text{m}$ has to be assumed. The calculated values of n do not strongly depend on Δy_{in} , as long as Δy_{in} is taken to be independent of film thickness (fig. III-7). On the other hand, the assumption of a thickness fluctuation, which is proportional to film thickness (e.g. $\Delta y_{in} = 0.1 \cdot \delta_f$) leads to n -values which are substantially larger (≈ 4) than those found experimentally.

In this analysis it is assumed that all drainage is due to horizontal transport. Fig. III-2 shows, that such is in good approximation the case but not exactly. This might introduce an error into the n -values found by differentiating curves like those in fig. III-3. However, this is a small effect only; in addition, the v_t -values extrapolated to $1/b \rightarrow 0$ (corresponding to infinite film width, thus absence of horizontal transport) have about the same n -values (between 1.5 and 3) as those found for the v_t -values. Therefore no significant error is introduced.

On comparison with the experimental data (fig. III-4 and table III-i and III-ii), we find:

- a. n -Values calculated through eqn. [III-16] tend to increase with increasing film thickness for constant Δy_0 . The experimental data do not permit to confirm or reject such an increase of n with film thickness. In table III-i and III-ii constant (= thickness independent) average n -values are mentioned, which are best compared with average theoretical n -values.
- b. For a frame with rectangular legs, agreement between experiment and theory is good, if Δy_0 is between 6 and $12 \mu\text{m}$. For the frame with the sharp-angled legs, larger values of Δy_0 have to be assumed.
- c. The computed thinning velocities v_t for a glass frame 30 mm in width and at an altitude of 10 mm above the bulk meniscus, are in the same range as those calculated from the experiments. The exact values, however, depend on the value of Δy_0 .

CONCLUSIONS

Drainage of vertical mobile free liquid films can be described satisfactorily on the following assumptions:

- a. horizontal drainage predominates;
- b. the net flow out of the film is the result of a surface flow combined with a bulk flow caused by a pressure gradient;
- c. at some place, at which the half thickness of the Plateau border is about $9 \mu\text{m}$ larger than that of the film, surface flow and volume flow both have died away;
- d. marginal regeneration is caused by thickness fluctuations in the film with little or no flow in the x-direction; these thickness fluctuations persist once marginal regeneration leads to flow in the x-direction;
- e. The fluctuations are of the order of $0.1 \mu\text{m}$, independent of film thickness.

SUMMARY

Results of calculations on the profiles of vertical mobile free liquid films measured interferometrically, in which the net flow out of the film is a combination of surface flow with bulk flow caused by a pressure gradient, confirmed the existing hydrodynamic theory on marginal regeneration. Qualitatively, this theory comprises the thinning of a mobile film by the exchange of thicker film parts, including the surfaces, for thinner parts in the immediate vicinity of each other, by the Plateau border.

REFERENCES

1. Mysels, K.J., Shinoda, K. & Frankel, S., "Soap films; studies of their thinning and a bibliography". Pergamon Press, 1959.
2. Scheludko, A., *Kolloid-Z.* 155: 39-44 (1957).
3. Scheludko, A., *Adv. Colloid Interface Sci.* 1: 391-464 (1967).
4. Radoev, B.P., Scheludko, A.D. & Manev, E.D., *J. Colloid Interface Sci.* 95: 254-265 (1983).
5. Mysels, K.J. & Cox, M.C., *J. Colloid Sci.* 17: 136-145 (1962).
6. Lyklema, J., *Rec. Trav. Chim.* 81: 890-897 (1962).
7. Mysels, K.J., *J. Phys. Chem.* 68: 3441-3448 (1964).
8. Lyklema, J., Scholten, P.C. & Mysels, K.J., *J. Phys. Chem.* 69: 116-123 (1965).
9. Duyvis, E.M. & Overbeek, J.Th.G., *Proc. Kon. Akad. Wetensch., Ser. B* 65: 26-30 (1962).
10. Duyvis, E.M., Thesis, Utrecht, 1962.

11. Lyklema, J. & Mysels, K.J., *J. Am. Chem. Soc.* 87: 2539-2546 (1965).
12. Jones, M.N., Mysels, K.J. & Scholten, P.C., *Trans. Faraday Soc.* 62: 1336-1348 (1966).
13. Clunie, J.S., Corkill, J.M. & Goodman, J.F., *Disc. Faraday Soc.* 42: 34-41 (1966).
14. Prins, A. & Van den Tempel, M., *Spec. Disc. Faraday Soc.* 1: 20-29 (1971).
15. Clunie, J.S., Corkill, J.M., Goodman, J.F. & Ingram, B.T., *Spec. Disc. Faraday Soc.* 1: 30-36 (1971).
16. Bruil, H.G. & Lyklema, J., *J. Electroanal. Chem.* 37: 31-37 (1972).
17. Ingram, B.T., *J. Chem. Soc., Far. I* 68: 2230-2238 (1972).
18. Yamanaka, T., *Bull. Chem. Soc. Jap.* 48: 1755-1759 (1975).
19. Yamanaka, T., *Bull. Chem. Soc. Jap.* 48: 1760-1763 (1975).
20. Donners, W.A.B., Thesis, Utrecht, 1976.
21. Agterof, W.G.M., Thesis, Utrecht, 1977.
22. McEntee, W.R. & Mysels, K.J., *J. Phys. Chem.* 73: 3018-3028 (1969).
23. Frankel, S. & Mysels, K.J., *J. Phys. Chem.* 73: 3028-3038 (1969).
24. Mysels, K.J. & Stikeleather, J.A., *J. Colloid Interface Sci.* 35: 159-162 (1971).
25. Frens, G., Mysels, K.J. & Vijayendran, B.R., *Spec. Disc. Faraday Soc.* 1: 12-19 (1971).
26. Princen, H.M., *J. Phys. Chem.* 72: 3342-3345 (1968).
27. Prins, A., *J. Colloid Interface Sci.* 29: 177-178 (1969).
28. Frankel, S. & Princen, H.M., *J. Phys. Chem.* 74: 2580-2581 (1970).
29. Princen, H.M. & Frankel, S., *J. Colloid Interface Sci.* 35: 386-394 (1971).
30. Mysels, K.J. & Buchanan, J.W., *J. Electroanal. Chem.* 37: 23-30 (1972).
31. De Feijter, J.A. & Vrij, A., *J. Colloid Interface Sci.* 64: 269-277 (1978).
32. Vrij, A., *Disc. Faraday Soc.* 42: 23-33 (1966).
33. Vrij, A. & Overbeek, J.Th.G., *J. Am. Chem. Soc.* 90: 3074-3078 (1968).
34. Felderhof, B.U., *J. Chem. Phys.* 49: 44-51 (1968).
35. Lucassen, J., Van den Tempel, M., Vrij, A. & Hesselink, F.Th., *Proc. Kon. Ned. Akad. Wetensch., Ser. B* 73: 109-123 (1970).
36. Vrij, A., Hesselink, F.Th., Lucassen, J. & Van den Tempel, M., *Proc. Kon. Ned. Akad. Wetensch., Ser. B* 73: 124-135 (1970).

37. Joosten, J.G.H., Vrij, A. & Fijnaut, H.M., in: "Physicochemical Hydrodynamics, Vol. II: V.G. Levich Festschrift" (D.B. Spalding, Ed.). Imp. Coll. Sci. Technol., London; Advance Publications Ltd., 1977.
38. Joosten, J.G.H., Thesis, Utrecht, 1982.
39. Sharma, A. & Ruckenstein, E., *Langmuir* **2**: 480-494 (1986).
40. Ruckenstein, E. & Sharma, A., *J. Colloid Interface Sci.* **119**: 1-13 (1987).
41. Sharma, A. & Ruckenstein, E., *J. Colloid Interface Sci.* **119**: 14-29 (1987).
42. Sharma, A. & Ruckenstein, E., *Colloid Polymer Sci.* **266**: 60-69 (1988).
43. Mysels, K.J., Cox, M.C. & Skewis, J.D., *J. Phys. Chem.* **65**: 1107-1111 (1961).
44. Roberts, K., Axberg, C., Osterlund, R. & Saito, H., *Nature* **255**: 53-54 (1975).
45. Von Wandruszka, R. & Winefordner, J.D., *Talanta* **33**: 871-874 (1986).
46. Koczó, K. & Rácz, G., *Colloids and Surfaces* **22**: 97-110 (1987)
47. Highfield, R.R., Humes, R.P., Thomas, R.K., Cummins, P.G., Gregory, D.P., Mingins, J., Hayter, J.B. & Schaerpf, O., *J. Colloid Interface Sci.* **97**: 367-373 (1984).
48. Hudales, J.B.M. & Stein, H.N., submitted for publication in *J. Colloid Interface Sci.*
49. Vassiliades, A.E., in: "Cationic Surfactants" (E. Jungerman, Ed.), Ch. 12. Dekker, New York, 1970.
50. Mysels, K.J., personal communication, 1989.
51. Hoerl, A.E., Nashed, M.Z., McKetta, J.J. & Silberberg, J.H., in: "Perry's Chemical Engineer's Handbook" (D.W. Green & J.O. Maloney, Eds.), p. 2-65 (6th edition). McGraw Hill Book Co., 1984.

CHAPTER IV

THE INFLUENCE OF SOLID PARTICLES ON FOAM AND FILM DRAINAGE

ABSTRACT

The effect of hydrophilic glass particles in a CTAB-solution on the drainage and stability of foam and of single vertical free liquid films (0.02 M CTAB) in a glass frame was investigated. Large particles ($< 10 \mu\text{m}$), being present in the coloured films, retard both foam and film drainage and increase film stability. This is ascribed to quenching of surface waves by particles extending through the film surfaces. Smaller particles ($< 1 \mu\text{m}$) lack this property: they shorten film lifetime in foams, although they have no influence on foam drainage.

INTRODUCTION

The stability of foams has been investigated (1-15) for a long time. However, a simple and universally accepted measure for foam stability has never been introduced, although there have been several attempts (2-4,6,14). In a way, this is understandable, because a foam is a very complicated colloidal system. The present authors investigated foam stability by a method permitting distinction between influences on film

rupture and film drainage. This method is applied in the present paper to the influence of suspended solid particles on foam.

When surveying the existing literature, we were struck by the lack of information about the influence of hydrophilic solid particles with densities comparable to those encountered in practical situations (e.g. flotation, foamed concrete) with a cationic surfactant as foam stabilizer.

Hydrophobic solid particles, such as finely dispersed silica with polysiloxanes (16,17), teflon (18,19) and hydrophobized glass (19), were discovered to destabilize a foam, and therefore these substances may be used as anti-foaming agents, e.g. in lubricating oil and washing powder.

The effect of hydrophilic particles, i.c. powdered quartz (20), finely dispersed silica, sulfite cellulose, carbon black (21) and chalk (22-24), on foams stabilized by anionic surfactants has also been investigated previously. However, the results reported by Sazanov & Taube (20) on the one hand, and those reported by Kruglyakov & Taube (21) and by Portnaya c.s. (22-24) on the other, are not mutually comparable, because of the use of solid particles of different densities and porosities.

In this work, measurements of the effect of hydrophilic glass particles in CTAB-solutions on foam stability were supplemented by data on the stability of a single vertical free liquid film in a glass frame, and by data obtained on microscopic observations in the latter case.

EXPERIMENTAL

Materials

CTAB (Cetyltrimethylammoniumbromide): ex Sigma Chemical Co. The surface tension vs. concentration graph had a distinct break near the c.m.c. ($= 9 \cdot 10^{-4}$ M (25)) without a minimum; no further purification was applied.

Glass: ex Louwers Glass (Hapert, The Netherlands), consisting of spherical particles with diameter $< 10 \mu\text{m}$. The sample was divided into fractions with narrower size distributions, by sedimentation in deionized

water. Particle size distributions were measured with a Coulter Counter; standard deviations amounted from 0.2 μm for the fraction with the smallest particles ($< 1 \mu\text{m}$) to 2.7 μm for the one with the largest ($> 5 \mu\text{m}$). Before fractionation by sedimentation the density of the glass particles was determined with a Quantachrome Stereopyknometer to be 2.47 g/cm^3 .

Water employed in the experiments other than sedimentation: twice distilled.

Apparatus

Microscope and Fizeau interferometer

The influence of solid particles on the drainage and stability of a single vertical free liquid film was investigated with a Fizeau interferometer and a microscope set-up, both described earlier (26,27, see Ch. II and III). Both set-ups were equipped with a magnetic stirrer to keep the glass particles in suspension between experiments. In the case of the Fizeau interferometer a fan containing the magnet was driven by a jet of thermostatted water; for the microscope a tiny electric motor was built in in the platform under the sample beaker. During an experiment, from film formation until film rupture, stirring was ceased.

Foam meter

The influence of solid particles on foam stability was investigated with a foam meter (fig. IV-1), analogous to the apparatus used by Brady & Ross (4) and Bikerman (6). It consists of a graduated measuring cylinder [9] 50 cm high and 39 mm inner diameter, surrounded by a water jacket, through which water at 25°C from a thermostatted tank [10] was circulated. Air was blown into the cylinder through a Schott G4 sintered glass filter at the bottom.

Before entering the measuring cylinder [9], the air was passed through two washing-bottles containing 10% KOH [1] and a trace of H_2SO_4 [2], respectively, to remove CO_2 and traces of KOH, which might have come with the air out of the first washing-bottle. In addition, these washing-bottles saturated the air with water vapour, which minimized

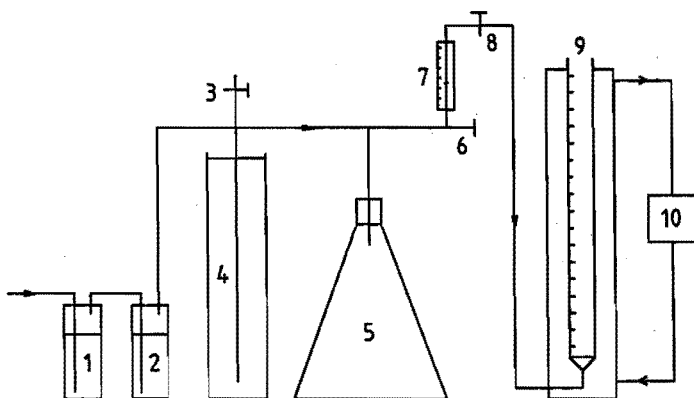


Fig. IV-1. Schematic representation of the foam meter set-up: 1. washing bottle with 10 % KOH; 2. washing bottle with some H_2SO_4 ; 3. de-aeration stopcock; 4. water column; 5. buffer vessel; 6. valve; 7. flow meter; 8. stopcock; 9. measuring cylinder; 10. thermostat.

evaporation inside the foam bubbles. An air outlet in the water column [4] created a constant pressure in the system and prevents the system from possible overpressure (e.g. after terminating the dynamic experiment). A de-aeration stopcock [3] over this water column was opened after an experiment to prevent liquid in the second washing-bottle from being pressed into the first by the rise of water in the hose in the column [4], after the air pump had been stopped. Small pressure differences in the system were levelled by a buffer vessel [5]. The gas flow, measured by means of a floating-ball flow meter [7], was kept at 50 ml/min. This flow was first established with the valve [6] preceding the flow meter, with 100 ml water in the measuring cylinder, after which the final stopcock [8] was closed. After exchanging the 100 ml water with 100 ml of the surfactant solution, approximately the same flow was reached when opening the final stopcock [8] again. The surfactant solution was pipetted into the measuring cylinder [9]; in doing so, the latter's walls were carefully wetted. Care was taken to prevent the liquid from draining through the glass filter by keeping the pressure under the latter at such values, that just no foam was created, until the experiment was started.

A complete foam meter experiment consisted of a dynamic and a static part: during the dynamic part air was blown through the sample for 5

minutes. Time started running at the moment the first air bubbles reached the surface and the liquid height was at its maximum; this height, which was about 2 mm above the original level, was read (h_0). This 2 mm rise corresponds to 2.4 ml air bubbles in the 100 ml solution and depends on the liquid density and viscosity and the air velocity. From the time $t = 0$ the height of the foam column (h_2) and of the liquid/foam interface (h_1) were read alternatively every 15 s. There was no need to take any action in keeping the particles in suspension, since the rising air bubbles stirred the liquid sufficiently to do so.

The static experiment was started by closing the final stopcock. Now time started running at the moment the last bubbles reached the liquid/foam interface and this interface height was at its minimum. The final values for the dynamic experiment during this lag time of about 10 s were obtained by extrapolation. The same readings of h_1 and h_2 were continued, gradually changing to longer time intervals, as the liquid and foam column approached their asymptotic heights. During this part of the experiment the particles were allowed to sediment.

From these readings the height of the foam column ($f = h_2 - h_1$) and its liquid ($l = h_0 - h_1$) and gas contents ($g = h_2 - h_0 = f - l$) were calculated as a function of time; heights at a certain time were obtained through linear interpolation, permitting the fraction of liquid in the foam (l/f) to be calculated.

RESULTS

Most samples used in this work yielded, after stirring, suspensions, which sedimented in a certain time, dependent of the particle size. However, some combinations of surfactant and glass particles in certain concentrations, i.e. low surfactant concentration, high glass amount and small particles size, cause the glass in the suspension to coagulate. This was the case for the $3.5 \cdot 10^{-5}$ M CTAB-solution with 0.27 % (m/m) of the original glass ($< 10 \mu\text{m}$) and for 0.01 M CTAB with 10 % glass particles of size 2-3 μm . Although these samples sedimented much faster than the not-coagulated suspensions, the same experiments were performed with them.

Microscope

Observation of a free liquid film drawn from a suspension with 10 % m/m solid particles sized between 4 and 5 μm , with a microscope showed, that some particles are present in the coloured film, but could be observed in the film only at a late stage of film history, shortly before the black film arrived at their position. In that stage, no movement of particles in the film toward the vertical Plateau borders is observed, but it should be noted, that then transport in the film towards the border is considerably reduced. Instead, at least at small thicknesses, the particles descend vertically along with the film thickness, in which they are embedded; in the black film absolutely no particles are observed.

Because of the small film thickness just below the black film, the presence of fairly large particles deforms the film surfaces by protuberation. This makes it very likely, that particles influence the lifetime of a foam film by their strong quenching effect on the surface waves (28, see also below).

In case of coagulated glass suspensions, coagulation in the Plateau border took place against the vertical frame legs, where the amount of coagulated glass increased in time, blocking flow in the border; this retarded drainage, especially at later times.

Fizeau interferometer: Lifetimes

Lifetimes of single foam films as measured in the Fizeau interferometer showed appreciable scatter; in Fig. IV-2, presenting some data, therefore not only average values, but also maximum lifetimes are plotted. As in a previous paper (27, Ch. III), a different behaviour is observed between frames with legs having sharp-angled and rectangular cross-sectional areas: in general, lifetimes of films in a sharp-angled frame are larger than those in a rectangular frame. Furthermore, lifetimes increase with the addition of glass particles, the effect being larger in case of the sharp-angled frame.

In order to investigate, whether some contaminant on the particles, which dissolves in the surfactant solution, causes the lifetimes to

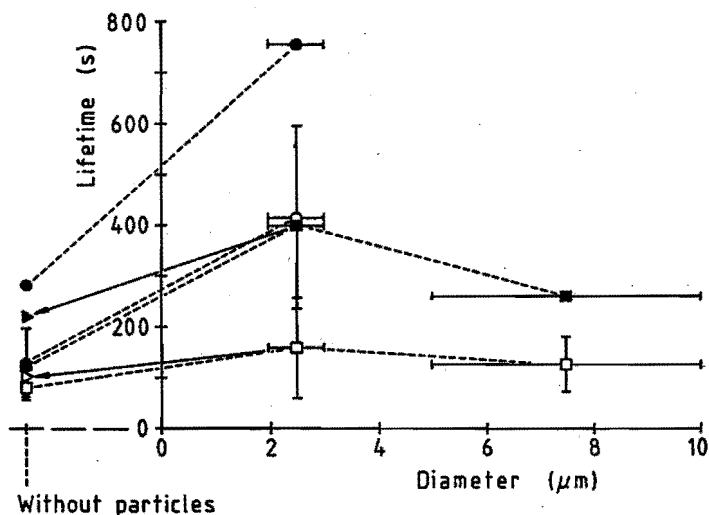


Fig. IV-2. Lifetimes of vertical free liquid films in a circa 3x3 cm glass frame; 0.02 M CTAB without particles or with 10 % (mlm) glass particles of the indicated average diameter. Open labels: average lifetimes; closed labels: maximum lifetimes. ○, ●: sharp-angled frame; □, ■, ▷, ►: rectangular frame; ▷, ►: supernatant after centrifuging; vertical and horizontal bars: standard deviations.

increase, after the usual lifetime measurements with a suspension, the particles were sedimented in a centrifuge and lifetime measurements were repeated with the supernatant: the average lifetime is indeed shortened about 50 % (Fig. IV-2).

Fizeau Interferometer: Drainage

The effect of solid particles on the drainage of a single free liquid film was investigated with the Fizeau interferometer, with which film profiles were obtained as described in (27, Ch. III). From the profiles thicknesses are calculated through linear interpolation at a certain height, i.c. 20 mm (27). Graphs of the reciprocal half thickness as a function of time are smoothed by performing a polynomial fit of maximum power 4 through the points obtained. This results in a larger number of points than the original reciprocal half thickness versus time plot. Horizontal velocities, perpendicular to the film midplane, are then computed by numerical

differentiation of the recovered half thickness versus time graphs, using Lagrange's five-point interpolation formulas (29). Velocities at a certain thickness, i.e. $1 \mu\text{m}$, are obtained by linear interpolation.

The results are shown in fig. IV-3. Except for the suspension with particles sized $3-4 \mu\text{m}$ in the sharp-angled frame, the drainage rate decreases with increasing diameter of the glass particles added. Drainage velocities for the frame with rectangular legs are larger than for the frame with legs with sharp-angled cross sections.

Foam meter

A typical result of a foam meter experiment is shown in fig. IV-4 for a 0.02 M CTAB solution without particles: during the first 5 minutes air was blown into the solution at constant flow, leading to a linear increase of the gas content (g) in the foam in time. The liquid content (l) in the foam column also rises in time, but with much lower velocity, since the volume fraction of liquid in the foam (l/f) is much lower than the fraction

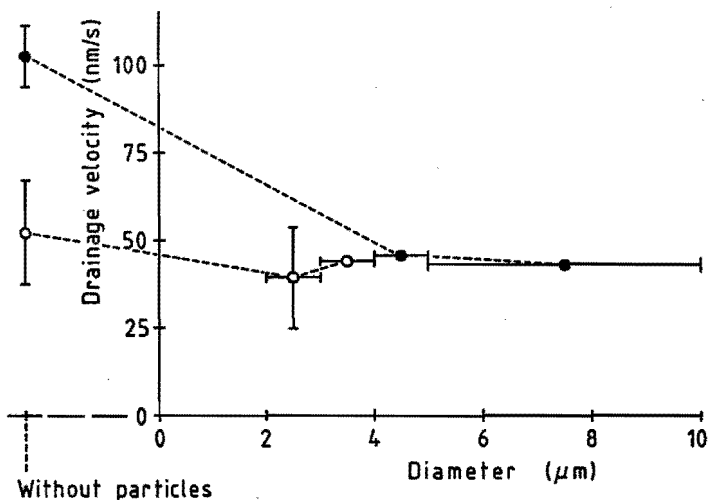


Fig. IV-3. Drainage velocities in the direction perpendicular to the film midplane at film thickness $1 \mu\text{m}$ and height 20 mm in the film. 0.02 M CTAB with or without 10% (m/m) glass particles of the indicated average diameter. O: sharp-angled frame; ●: rectangular frame; horizontal and vertical bars: standard deviations.

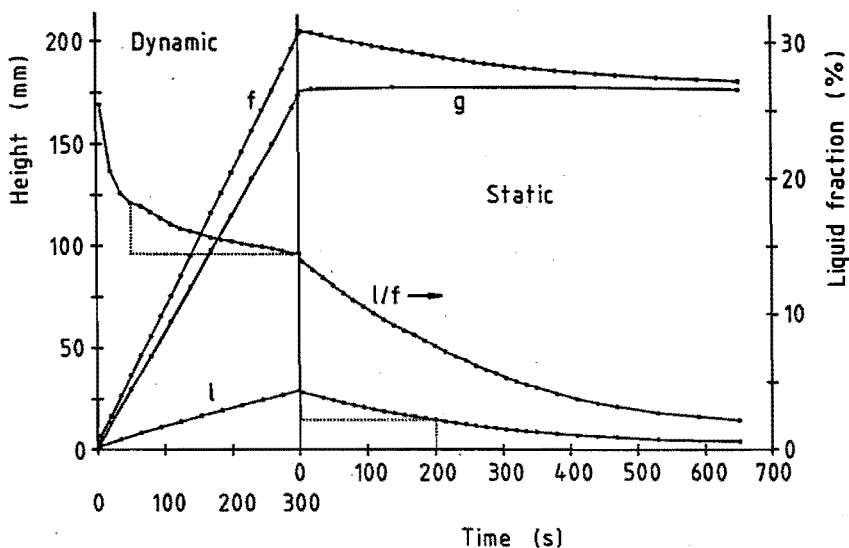


Fig. IV-4. Result of a dynamic and static foam meter experiment with 0.02 M CTAB without particles. Indicated are the column heights for the liquid content (l), gas content (g) and foam (f), as well as the liquid fraction (l/f) in %. Dotted lines: determination of the DDR and SDT in the dynamic and static part of the experiment, respectively; TGC is determined by the slope of g during the dynamic experiment.

of air. The liquid fraction usually decreases gradually in time.

Some time after the air supply was stopped, the rise of the foam/air interface also ceased. At the surfactant concentration used a very stable foam was obtained. However, drainage of liquid from the foam does take place; this is illustrated by the decrease of the liquid content and liquid fraction of the foam. They both should approach zero in the end, when all the foam has collapsed, but the accuracy of the readings ($0.1 \text{ mm} \sim 119.5 \text{ mm}^3$) did not permit to detect the amount of liquid in the foam, when most films have become black.

From the dynamic experiments the, in most cases constant, rising velocity of the foam was calculated by linear regression of the $g(t)$ -values. This velocity is compared with the linear air velocity: if it equals 0.70 mm/s ($\approx 50 \text{ ml/min}$) then all the air blown through the suspension is encysted in the stable foam. Poor foamability results in a large deviation

from this value. The percentage air retained in the foam is referred to as Transient Gas Capture (TGC), which is determined by film rupture of the bubbles at the top of the foam.

The rate of the liquid fraction decrease is predominantly a measure of the drainage during foam formation: the difference in liquid fractions at two arbitrarily chosen times, 50 and 290 s, was divided by the time interval covered (4 min), yielding the procentual decay rate of the liquid fraction in the film during formation (Dynamical Decay Rate = DDR). The decay time, as used for the static experiment (see below), appeared not to be very practical in this case, since the intake of liquid during foam formation usually prevented the liquid fraction from reaching half its original value during the time the dynamic experiment lasted.

The static experiment supplies us with decay times for the amount of liquid (l) and the liquid fraction (l/f) (and in case of poor foamability for the amount of gas (g) and foam (f)). Time intervals are obtained, in which the maximum at the start of the static experiment reduces to half of this

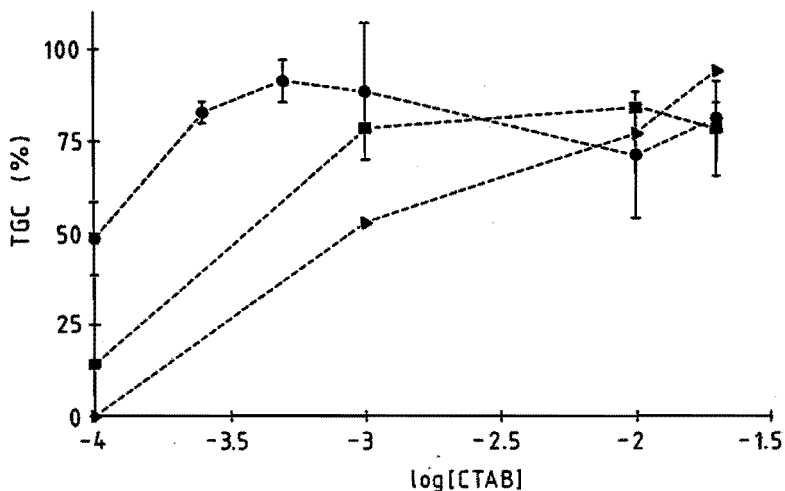


Fig. IV-5. TGC (the percentage of air encysted in the foam, compared with the total amount of air blown in) as a function of the logarithm of the CTAB-concentration without particles (●) or with 0.25 % (■) or 0.5 % (▴) (ml/m) of glass particles smaller than 1 μm ; vertical bars: standard deviations.

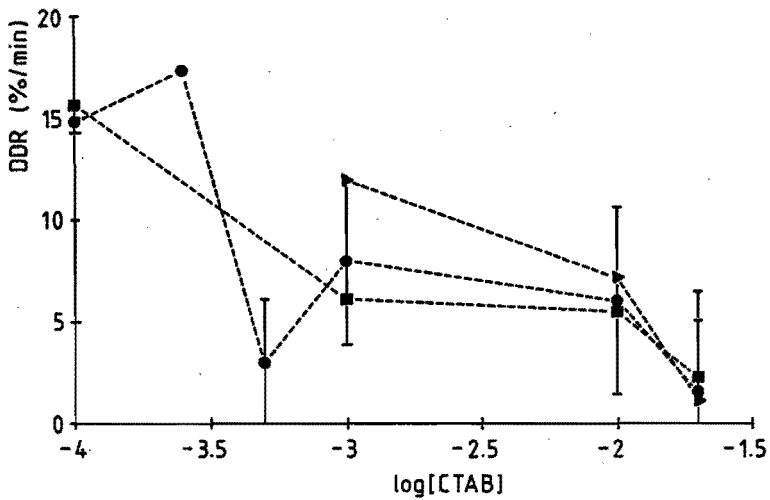


Fig. IV-6. *DDR (the relative liquid fraction decay rate during a 4 minutes interval of the dynamic experiment) as a function of the logarithm of the CTAB-concentration. For an explanation of the labels see legend of fig. IV-5.*

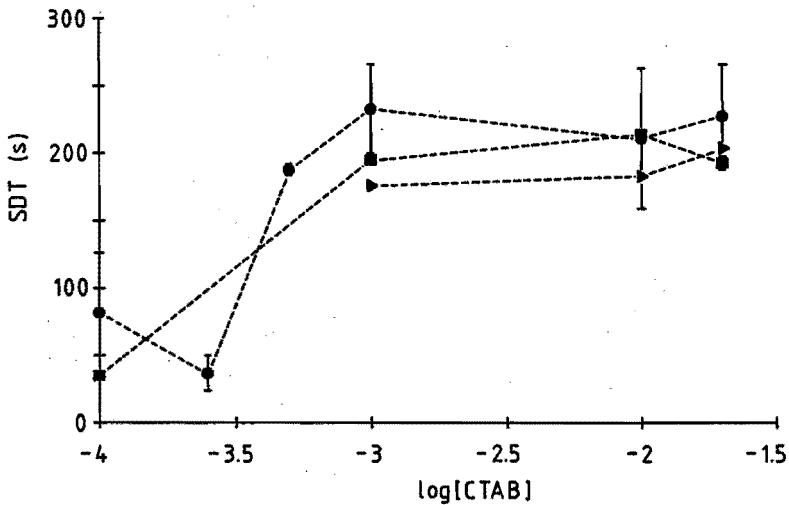


Fig. IV-7. *SDT (the time, during which the liquid content of the foam is halved) as a function of the logarithm of the CTAB-concentration. For an explanation of the labels see legend of fig. IV-5.*

maximum (21). The decay time of the liquid fraction always appears to be somewhat larger than that of the liquid content. Both showed the same trends and therefore we mention only the latter magnitude, which is indicated as Static Decay Time (SDT).

In the absence of glass, TGC increases (fig. IV-5), DDR decreases (fig. IV-6) and SDT increases (fig. IV-7) with increasing surfactant concentration. Addition of small amounts ($< 0.5\%$) of small glass particles ($< 1\ \mu\text{m}$) has no significant effect on DDR (fig. IV-6) and SDT (fig. IV-7), but decreases TGC at low CTAB-concentration (fig. IV-5).

Increase of the amount of these particles up to 2.5% in 10^{-4} or 10^{-3} M CTAB decreases TGC (fig. IV-8) and SDT (fig. IV-9). However, for larger particles ($< 10\ \mu\text{m}$) in an intermediate CTAB-concentration ($5.4 \cdot 10^{-4}$ M) the theoretical TGC was found over the range of glass amounts added, while SDT increased at high (2.5%) glass content. Similar, though less distinct effects were found for DDR (not shown).

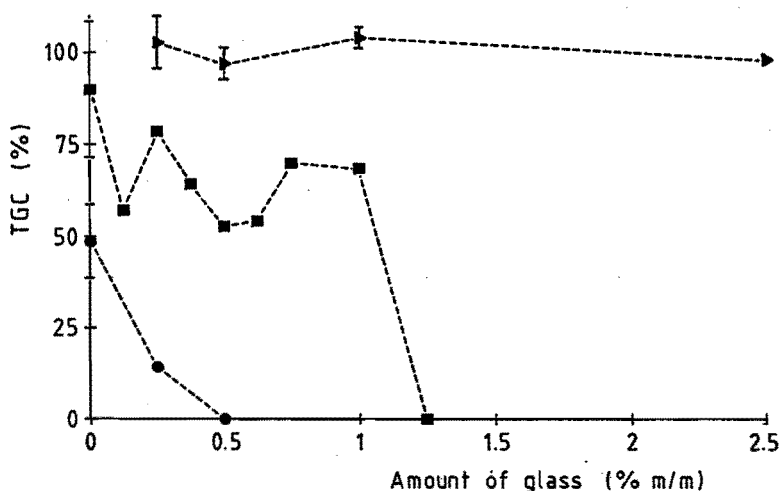


Fig. IV-8. TGC as a function of the amount of glass added to the sample. ●: 10^{-4} M CTAB + particles $< 1\ \mu\text{m}$; ■: 10^{-3} M CTAB + particles $< 1\ \mu\text{m}$; ▴: $5.4 \cdot 10^{-4}$ M CTAB + particles $< 10\ \mu\text{m}$; vertical bars: standard deviations.

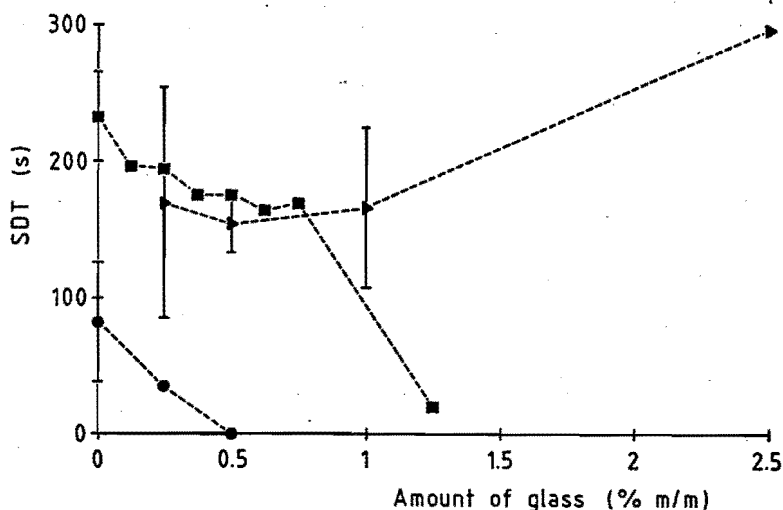


Fig. IV-9. SDT as a function of the amount of glass added to the sample. For an explanation of the labels see legend of fig. IV-8.

DISCUSSION

Fizeau interferometer ([CTAB] = 0.02 M)

The difference between a sharp-angled and a rectangular frame has already been discussed in (27, Ch. III). The larger drainage rate for the rectangular frame (fig. IV-3) is explained by the larger cross-sectional area of the Plateau border for the rectangular frame as compared with the sharp-angled frame, permitting more liquid to flow through. This drainage increase is accompanied by a shorter lifetime of the film (fig. IV-2).

Drainage of separate films is retarded by glass particles (fig. IV-3), at least if they are larger than the average film thickness (27, Ch. III). This effect can be ascribed to a quenching of surface waves, which cause marginal regeneration (27, Ch. III), by diffraction. In agreement with this statement is the increase in lifetime of separate films (fig. IV-2): film rupture is connected with the occurrence of surface waves as well (28). It is true, that surface waves leading to film rupture occur in black films, in which no solid particles are observed. However, surface waves in the black film will continue in the coloured film (and vice versa), thus

quenching of surface waves in the coloured film is expected to lead to a smaller amplitude of surface waves in the black film.

Foam meter

Of the three criteria on the stability of foams in the foam meter, the TGC is determined by the lifetimes of films on top of the foam, while the DDR and SDT are determined by both drainage and rupture. Film rupture, taking place equally spread over the centre of the foam, causes larger bubbles and drainage of the excess liquid from the ruptured film, but the amount of gas in the foam remains constant; film rupture on top of the foam only means loss of gas, which, however, is accompanied by a negligible increase in the drainage.

According to fig. IV-5, -6 and -7, foam stability increases with increasing CTAB-concentration in the absence of glass. Indeed, at low CTAB-concentration the film lifetime is short, as observed when trying to form separate films in the Fizeau interferometer. However, at such CTAB-concentrations a slower drainage might be expected, because the films then have a more or less rigid surface. A possible explanation of the high DDR- and low SDT-values found is, that short film lifetimes prevent accumulation of liquid in the films.

At first sight, this appears to be contradicted by the influence of glass particles in the same figures. This, however, may be due to small particles indeed promoting film rupture to a limited extent at low CTAB-concentration (fig. IV-5): per Plateau border there is then more liquid, but there are less borders, when the number of foam bubbles decreases. A total mutual compensation of both effects might be fortuitous, but the influence of particles on lifetimes may be masked such as to leave no distinct effect at the conditions of fig. IV-6 and -7. Larger amounts of glass indeed lead to smaller SDT-values (fig. IV-9).

Large particles act differently: the SDT increases rather than decreases (fig. IV-9). This difference is ascribed to part of the glass particles having diameters exceeding the average film thickness. When present in a film, as observed with the microscope, they will diffract surface waves and counteract both drainage and rupture. Even at a

CTAB-concentration of $5.4 \cdot 10^{-4}$ M, the TGC may approach the value for total gas capture (fig. IV-8).

Sazanov & Taube (20) explain the destabilizing action of quartz on foams formed in sulfonol solutions by adsorption of the surfactant on the quartz, leading to depletion of the liquid with regard to the sulfonol. In our case, this explanation is not convincing. Indeed, it is known, that CTAB is adsorbed on glass surfaces, which leads to coagulation of the glass particles in the case of small CTAB-concentrations and large amounts of small glass particles; however, at the higher CTAB-concentrations used, the total glass surface area is too low to lead to any surfactant depletion of the solution. The destabilizing action found by Sazanov & Taube in the case of small surfactant concentration is found in the present investigation also, for glass particles smaller than $1 \mu\text{m}$. For larger particles we found a stabilizing effect; comparison with the results mentioned by Sazanov & Taube (20) is not possible, because of lack of data on the size of the quartz particles employed by them.

CONCLUSIONS

Hydrophilic suspended particles smaller than $1 \mu\text{m}$ shorten the lifetime of films in foams. Larger particles (up to $10 \mu\text{m}$) stabilize films in foams against rupture and decrease their drainage. This is confirmed by measurements on drainage and lifetime of separate films. This difference is explained by quenching of surface waves by particles protuberating into the film surfaces.

SUMMARY

Drainage and lifetimes of foams and single vertical free liquid films were measured as criteria for the foam stability in the absence and presence of solid particles. Glass beads with a diameter smaller than $1 \mu\text{m}$ destabilize foam slightly, although drainage is not affected. Larger particles, which are observed to be present in the coloured films, retard drainage and increase lifetime; the explanation for this is the quenching of the surface waves, which introduce film rupture, by the particles protuberating into the film surfaces.

REFERENCES

1. Foulk, C.W. & Miller, J.N., *Ind. Eng. Chem.* **23**: 1283-1288 (1931).
2. Bikerman, J.J., *Trans. Far. Soc.* **34**: 634-638 (1938).
3. Clark, G.L. & Ross, S., *Ind. Eng. Chem.* **32**: 1594-1598 (1940).
4. Brady, A.P. & Ross, S., *J. Am. Chem. Soc.* **66**: 1348-1356 (1944).
5. Ross, S., *J. Phys. Chem.* **50**: 391-401 (1946).
6. Bikerman, J.J., "Foams: Theory and Industrial Applications", Ch. 2. Reinhold Publ. Corp., 1953.
7. De Vries, A.J., Dissertation, Utrecht, 1957.
8. Kitchener, J.A. & Cooper, C.F., *Quart. Rev.* **13**: 71-97 (1959).
9. Kruglyakov, P.M. & Taube, P.R., *J. Appl. Chem. USSR* **38**: 1483-1488 (1965) (Translation from: *Zh. Prikl. Khim.* **38**: 1514-1519 (1965)).
10. Kruglyakov, P.M. & Taube, P.R., *J. Appl. Chem. USSR* **39**: 1403-1407 (1966) (Translation from: *Zh. Prikl. Khim.* **39**: 1499-1503 (1966)).
11. Exerowa, D., Khristov, Khr. & Penev, I., in: "Foams, Proc. Symp. Brussel Univ. 1975" (R.J. Akers, Ed.), pp. 109-123. Academic Press, 1976.
12. Khristov, Khr., Krugljakov, P. & Exerowa, D., *Colloid & Polymer Sci.* **257**: 506-511 (1979).
13. Khristov, Kh.I., Ekserova, D.R. & Kruglyakov, P.M., *Colloid J.* **43**: 80-84 (1981) (Translation from: *Kolloidn. Zh.* **43**: 101-106 (1981)).
14. Khristov, Kh.I., Ekserova, D.R. & Kruglyakov, P.M., *Colloid J.* **43**: 166-168 (1981) (Translation from: *Kolloidn. Zh.* **43**: 195-197 (1981)).
15. Khristov, Khr.I., Exerowa, D.R. & Krugljakov, P.M., *Colloid & Polymer Sci.* **261**: 265-270 (1983).
16. Taube, P.R., Kotova, T.T & Sazanov, V.A., *Sb. Nauch. Rab., Penz. Inzh.-Stroit. Inst.* **7**: 119-127 (1970).
17. Ross, S. & Nishioka, G., in: "Emulsions, Latices and Dispersions" (P. Becher & M.N. Yudenfreund, Eds.), pp. 237-256. M. Dekker Inc., 1978.
18. Garrett, P.R., *J. Colloid Interface Sci.* **69**: 107-121 (1979).
19. Frye, G.C. & Berg, J.C., *J. Colloid Interface Sci.* **127**: 222-238 (1989).
20. Sazanov, V.A. & Taube, P.R., *Sb. Nauch. Rab., Penz. Inzh.-Stroit. Inst.* **7**: 128-131 (1970).
21. Kruglyakov, P.M. & Taube, P.R., *Colloid J.* **34**: 194-196 (1972) (Translation from: *Kolloidn. Zh.* **34**: 228-230 (1972)).
22. Portnaya, I.B., Deposited Doc., VINITI 858-862 (1981).

23. Portnaya, I.B., Mazina, G.R., Polukhina, T.I. & Panich, R.M., *Colloid J.* **43**: 482-484 (1981) (Translation from: *Kolloidn. Zh.* **43**: 592-594 (1981)).
24. Portnaya, I.B., Suchkova, L.N., Novgorodova, S.N. & Panich, R.M., *Colloid J.* **43**: 718-723 (1982) (Translation from: *Kolloidn. Zh.* **43**: 883-889 (1981)).
25. Vassiliades, A.E., in: "Cationic Surfactants" (E. Jungerman, Ed.), Ch. 12. M. Dekker, New York, 1970.
26. Hudales, J.B.M. & Stein, H.N., submitted for publication in *J. Colloid Interface Sci.*
27. Hudales, J.B.M. & Stein, H.N., submitted for publication in *J. Colloid Interface Sci.*
28. Vrij, A. & Overbeek, J.Th.G., *J. Am. Chem. Soc.* **90**: 3074-3078 (1968).
29. Hoerl, A.E., Nashed, M.Z., McKetta, J.J. & Silberberg, J.H., in: "Perry's Chemical Engineer's Handbook" (D.W. Green & J.O. Maloney, Eds.), p. 2-65 (6th ed.). McGraw Hill Book Co., 1984.

CHAPTER V

CONCLUSIONS

This investigation has shown, that it is possible to explain a number of phenomena concerning foam stability by the occurrence of surface waves in thin liquid films.

1. A mechanism for film drainage based on surface waves in films is consistent with the experimentally observed relations between drainage and film thickness found for separate films (Ch. III). Such surface waves lead to inflow from the border into the film at places of lower thickness, and to outflow at places of higher thickness at the border/film transition. This leads to a lower surface tension in the film near inflow places, which induces the new film elements to expand, pushing aside other film elements enlarging the latter's thickness and consequently enhancing outflow. This leads to exchange of film volume elements against border volume elements (marginal regeneration) (1).
2. Consistent with this view is the influence of suspended hydrophilic particles on the drainage of films in foams (Ch. IV): this drainage is retarded, but only when a substantial portion of the suspended solid particles is large enough ($< 10 \mu\text{m}$) to penetrate the film surface, when

incorporated into a film. This effect can be explained by quenching of surface waves through diffraction.

3. Also consistent with this view is the retarding influence of such relatively large suspended particles on film rupture. Again, the quenching of surface waves through diffraction by hydrophilic particles protruding through the film surfaces can be held responsible for the observed retardation.
4. Smaller particles ($< 1 \mu\text{m}$), however, decrease foam stability. The role of surface waves in film drainage postulated in the present investigation is consistent with Ruckenstein and Sharma's theory (2-5) on the drainage of films, developed for the special case of films not subject to a hydrostatic pressure gradient. Film rupture in general is thought to be connected with surface waves (6,7). Though waves leading to film rupture occur in black films, where no solid particles have been observed, such waves will be connected with surface waves in the nearby coloured films. Quenching of surface waves in the film is therefore expected to decrease the chance on film rupture.

In separate films drawn in a frame, pronounced flows in the Plateau border have been observed (Ch. II). These flows are directed upwards near the border/film transition, and directed downwards near the border/glass frame boundary. The flows can best be accounted for as Marangoni flows caused by a surface tension gradient, induced in the Plateau border by the marginal regeneration process. By this process, the surface tension at large heights becomes larger than just above the bulk meniscus, but also at a certain height a surface tension gradient is expected: near the border/film transition the surface tension is larger than near the border/glass frame boundary. Initially, this may indeed occur. Nevertheless, only a vertical flow is established, because this is self-reinforcing: once started it leads to sucking up of bulk liquid at the lower part of the border/film transition, which decreases the surface tension there and increases the surface tension differences in vertical direction. The surface tension near the border/frame boundary consequently is increased, because there pronounced downward transport occurs. This prevents further horizontal transport, except at the top of the border.

In such films, an anomalous pressure is found at low heights above the bulk liquid near the border/film transition. The phenomenon also is ascribed to the Marangoni flows mentioned: because of low viscous friction, the surface tension gradient must be balanced by a pressure gradient.

REFERENCES

1. Mysels, K.J., Shinoda, K. and Frankel, S., "Soap films; studies of their thinning and a bibliography". Pergamon Press, 1959.
2. Sharma, A. & Ruckenstein, E., *Langmuir* **2**: 480-494 (1986).
3. Ruckenstein, E. & Sharma, A., *J. Colloid Interface Sci.* **119**: 1-13 (1987).
4. Sharma, A. & Ruckenstein, E., *J. Colloid Interface Sci.* **119**: 14-29 (1987).
5. Sharma, A. & Ruckenstein, E., *Colloid & Polymer Sci.* **266**: 60-69 (1988).
6. Vrij, A., *Disc. Far. Soc.* **42**: 23-33 (1966).
7. Vrij, A. & Overbeek, J.Th.G., *J. Am. Chem. Soc.* **90**: 3074-3078 (1968).

LIST OF SYMBOLS

- A : Hamaker constant
- $A_{1,2}$: amplitude of the electric field vector of the primary (1) or secondary ray (2)
- F_{P_b} : pressure force exerted by the Plateau border
- F_{P_f} : pressure force exerted by the film
- F_{Y_b} : surface tension force exerted by the Plateau border
- F_{Y_f} : surface tension force exerted by the film
- G : Gibbs free energy
- J : twice the mean surface curvature
- K : wave number
- R_1 : meridional radius of curvature
- R_2 : azimuthal radius of curvature
- T : absolute temperature (Ch. I)
- T : reciprocal wave frequency (Ch. II)
- Q : drainage rate
- Q_f : volume flow at the Plateau border/film transition
- Q_{neg} : outflow rate per unit length in z-direction
- Q_{net} : net drainage rate due to marginal regeneration
- Q_{pos} : inflow rate per unit length in z-direction
- Q_v : total flow rate downward
- V : volume
- V_A : attraction energy
- b : film width
- c : velocity of light in vacuo
- dz_{in} : fraction of unit length in z-direction, where inflow occurs
- dz_{out} : fraction of unit length in z-direction, where outflow occurs
- f : correction factor for retardation effect
- g : acceleration of gravity
- k : Boltzmann constant (Ch. I)
- k : step counter for numerical calculations (Ch. II)
- k : proportionality constant (Ch. III)
- $n(i)$: electrolyte concentration (Ch. I)
- n : index of refraction (Ch. II)

- n : exponent in power law (Ch. III)
 p : $2\pi\delta_f/\lambda$ (Ch. I)
 p : order of interference (Ch. II)
 p : pressure (Ch. III)
 P_A : London-Van der Waals attractive pressure
 P_R : double layer repulsive pressure
 P_a : pressure in the surrounding atmosphere
 P_b : pressure in the Plateau border
 P_f : pressure in the film
 P_f' : pressure in the film in the absence of interaction
 P_i : pressure due to attractive and repulsive interaction
 $r(P)$: radius of curvature (in an arbitrary point P on a surface)
 t : time from film/foam formation
 t_0 : starting time
 u : potential midway between the film surfaces
 u_1 : angle between the secondary ray before reflection against the back surface of the Plateau border and the normal to the back surface at the point of reflection
 u_2 : angle between the secondary ray after reflection against the back surface of the Plateau border and the normal to the film midplane
 v_s : surface velocity in the Plateau border, parallel to the surface
 $v_{s,f}$: surface velocity at the Plateau border/film transition
 v_t : thinning velocity in the direction perpendicular to the film midplane
 v_v : vertical liquid velocity
 w : surface area
 x : distance parallel to the film midplane in horizontal direction
 x_b : Plateau border width in the x -direction
 x_c : x -value of an arbitrary point on a circle
 x_{\min} : x -value of the point of the Plateau border surface, where $dy_b/dx = 0$
 x_0 : x -value of the point of the Plateau border surface, where first and second derivatives are independent of Q
 y : distance from the film midplane
 y_b : half Plateau border thickness ($= \frac{1}{2}\delta_b$)
 y_f : half film thickness ($= \frac{1}{2}\delta_f$)

- y_{\min} : y-value of the point on the Plateau border surface, where $dy_b/dx = 0$
 y_0 : y-value at the point of the Plateau border surface, where first and second derivatives are independent of Q
 $y_{1,2,3}$: y-values of the points of the Plateau border surface, where the secondary ray is refracted by the front surface (1), is reflected by the back surface (2), and is refracted by the front surface again (3)
 z : distance from the bulk liquid surface
 Δp_L : Laplace pressure difference across a curved surface
 Δy_b : difference between measured and calculated half Plateau border thickness
 Δy_{in} : decrease in half film thickness due to liquid inflow
 Δy_{out} : increase in half film thickness due to liquid outflow
 Δy_0 : Plateau border width in y-direction, in which inflow into and outflow from the film occurs, minus half the film thickness
 $\Delta \gamma$: excess surface tension
 $\Delta \rho$: difference in density between liquid and air
 $\Delta \phi$: phase difference between primary and secondary ray
 θ : angle between the tangent to the Plateau border surface and the film midplane
 θ_f : contact angle at the transition film/Plateau border
 θ_g : receding contact angle between the liquid and the glass
 α : decay constant
 $\alpha_{1,2,3}$: angle between the normal to the Plateau border surface and the normal to the film midplane at the points, where the secondary ray is refracted by the front surface (1), is reflected by the back surface (2), and is refracted by the front surface again (3)
 β : angle between the secondary ray after entering the Plateau border and the normal to the front surface at the point of refraction
 β_2 : angle between the secondary ray after reflection against the back surface of the Plateau border and the normal to the front surface at the point, where it leaves the border
 γ : surface tension of the bulk solution
 γ_b : surface tension in the Plateau border
 γ_f : surface tension in the film
 γ_f' : surface tension in the film in the absence of interaction

- δ : angle between the secondary ray before entering the Plateau border and the normal to the film midplane
- δ_b : Plateau border thickness
- δ_f : film thickness
- κ : Debye-Hückel parameter
- λ : wave length connected with the motion of electrons in atoms (Ch. I)
- λ : wave length of the light (Ch. II)
- η : viscosity
- ρ : liquid density
- τ : angle between the secondary ray leaving the Plateau border and the normal to the front surface at the point, where it leaves the border
- τ_2 : angle between the primary or secondary ray leaving the Plateau border and the normal to the film midplane
- ϕ_0 : phase of the secondary ray at the focusing plane in the absence of the Plateau border
- ϕ_{1X} : phase of the primary ray at point X
- ϕ_{2X} : phase of the secondary ray at point X

SUMMARY

Experiments were performed on foam and single vertical free liquid films in a glass frame on a macroscopic and microscopic scale. In Chapter I a general introduction is given, together with an elaboration of some aspects treated in the following chapters.

In Chapter II it was established, that on the ground of the measured curvature of the Plateau border of a liquid film at a height of 6.2 mm over the bulk liquid surface, in which the frame with film is hanging, the Laplace pressure in the border is lower than the hydrostatic equilibrium pressure at that height; at a height of 11.3 mm these pressures were equal. The border curvatures were measured interferometrically with a microscope, and it was demonstrated, that Fizeau's equations for the film thickness at the interference maxima and minima are applicable to the system, despite the conical illumination and the curved surfaces.

Furthermore, flows in opposite directions were observed in the vertical Plateau borders with the aid of suspended small glass particles: upward near the border/film transition and downward along the frame leg. Both phenomena (anomalous border curvature and bidirectional flows) were explained by Marangoni flows, originating from a surface tension gradient in the film and in the border near the film in upward direction, while close to the frame legs a gradient is absent.

Thickness profiles of vertical free liquid films in glass frames with different widths, measured as a function of time with the aid of a (macroscopic) Fizeau interferometer, agree with drainage via the vertical Plateau borders predominating over direct vertical drainage, as demonstrated in Chapter III. The former drainage mechanism is believed to take place through marginal regeneration: thicker film regions, including their surfaces, are sucked in by the Plateau border, in exchange of thinner regions in an immediately adjacent section. Its existing hydrodynamic theory is confirmed by calculations on the measured film thickness profiles, where the net flow out of the film is described as a result of a surface flow combined with a bulk flow caused by a pressure gradient.

Chapter IV deals with the influence of hydrophilic solid particles on the foam stability and the drainage of a vertical soap film, which was investigated with the two techniques mentioned above and with a foam meter. Glass particles were observed to be present in the coloured film, but not in the black film. Large particles (diameter $< 10 \mu\text{m}$) slowed down film and foam drainage and increased foam stability; this is ascribed to a quenching of the surface waves, which precede film rupture, by particles protuberating into the film surfaces. Smaller particles ($< 1 \mu\text{m}$) lack this property and destabilize the foam slightly, although drainage is not affected.

SAMENVATTING

Experimenten werden uitgevoerd aan schuim en aan verticale zeepvliësjes in een glazen raampje op macro- en microscopische schaal. In Hoofdstuk I is een algemene introductie gegeven, samen met de uitwerking van enige aspecten behandeld in de volgende hoofdstukken.

In Hoofdstuk II werd vastgesteld, dat op grond van de kromming van de Plateau rand van een vloeistof film op een hoogte van 6,2 mm boven het oppervlak van de bulk vloeistof, waarin de uiteinden van het raampje met film hangen, de Laplace druk in de Plateau rand lager is dan de hydrostatische evenwichtsdruk op die hoogte; op een hoogte van 11,3 mm zijn deze drukken gelijk. De kromming van de Plateau rand werd interferometrisch gemeten met een microscoop, en aangetoond werd, dat de formules van Fizeau voor de filmdikte van de interferentiemaxima en -minima toepasbaar zijn op dit systeem, ondanks de conische belichting en de gekromde oppervlakken.

Verder werden stromingen in tegengestelde richtingen waargenomen in de verticale Plateau randen met behulp van gesuspendeerde kleine glasbolletjes: naar boven bij de overgang van de Plateau rand naar de film en naar beneden langs de poten van het raampje. Beide verschijnselen (de afwijkende kromming van de Plateau rand en de tegengestelde stromingen) worden verklaard door Marangoni stromingen, die stammen van een oppervlaktespanningsgradiënt in de film en in de Plateau rand vlak bij de film in opwaartse richting, terwijl er geen gradiënt aanwezig is vlak langs de pootjes.

Dikteprofielen van een verticale zeepfilm in een glazen raampje met verschillende breedtes, gemeten als functie van de tijd met behulp van een (macroscopische) Fizeau interferometer, stemmen overeen met het feit, dat voor mobiele films rechtstreekse verticale drainage sterk wordt overheersd door drainage via de verticale Plateau randen. Dit wordt aangetoond in Hoofdstuk III. Van laatstgenoemd drainage mechanisme wordt algemeen aangenomen, dat het plaatsvindt door marginale regeneratie: dikkere film delen worden met oppervlak en al opgezogen door de Plateau rand, in ruil voor dünnere delen in de onmiddellijke nabijheid ervan. De bestaande hydrodynamische theorie wordt bevestigd

door berekeningen aan gemeten filmdikteprofielen, waarbij de netto vloeistofstroom uit de film wordt beschreven als de resultante van een oppervlaktestroming gecombineerd met een bulkstroming veroorzaakt door een drukgradiënt.

Hoofdstuk IV behandelt de invloed van hydrofiele vaste deeltjes op de schuimstabiliteit en op de drainage van een verticaal zeepvliesje, hetgeen onderzocht werd met de twee hierboven genoemde technieken en met een schuimmeter. Glas deeltjes werden waargenomen in de gekleurde film, doch niet in de zwarte film. Relatief grote deeltjes (diameter $< 10 \mu\text{m}$) vertragen de film- en schuimdrainage en verhogen de schuimstabiliteit; dit wordt toegeschreven aan het doven van de oppervlaktegolven, die de filmbreuk inleiden, door de deeltjes, die in de filmoppervlakken uitpuilen. Kleinere deeltjes ($< 1 \mu\text{m}$) missen deze eigenschap en destabiliseren het schuim enigszins, hoewel de drainage niet werd beïnvloed.

CURRICULUM VITAE

Hans Hudales werd op 30 juli 1957 geboren in Geleen. Aldaar behaalde hij in 1975 het diploma Gymnasium B aan de Scholengemeenschap St. Michiel. In augustus van dat jaar begon hij zijn studie Moleculaire Wetenschappen aan de Landbouwhogeschool te Wageningen. Hij behaalde in maart 1985 het doctoraalexamen, met als hoofdvak Moleculaire Fysica en bijvakken Natuurkunde en Plantenfysiologie. Onderdeel van bovengenoemd hoofdvak was een stage van zeven maanden aan de Royal Institution of Great Britain in Londen. Van 15 mei 1985 tot 15 mei 1989 is hij in dienst geweest van de Technische Universiteit Eindhoven, alwaar hij bij de vakgroep Colloidchemie en Thermodynamica van de afdeling Scheikundige Technologie het in dit proefschrift beschreven onderzoek verricht heeft.

STELLINGEN

1. De formules van Fizeau voor de dikte van een dunne, transparante film als functie van de golflengte van het gebruikte licht, de interferentie-orde en de brekingsindex, zijn toepasbaar op het interferentiepatroon van een systeem, waarbij conische i.p.v. parallelle belichting wordt gebruikt (microscop) en waarbij het voor- en/of achtervlak een bepaalde kromming vertoont.

Dit proefschrift, Ch. 2 (Appendix).

2. Gezien het belang van het mechanisme van marginale regeneratie voor de drainage van een mobiele verticale vrije vloeistoffilm, is het verwonderlijk, dat er sinds de introductie ervan in 1959 zeer weinig onderzoek is verricht om deze hypothese experimenteel te verifiëren.

Mysels, K.J., Shinoda, K. & Frankel, S., "Soap Films; Studies of their Thinning and a Bibliography", Chs. II, IV and V. Pergamon Press, London, 1959.
Dit proefschrift, Ch. 3.

3. Kruglyakov & Taube (1972) hebben nagelaten hun systeem van vaste deeltjes voldoende te karakteriseren qua grootteverdeling, dichtheid, intern oppervlak, e.d.

Kruglyakov, P.M. & Taube, P.R., *Colloid J.* **34**: 194-196 (1972) (Translation from: *Kolloidn. Zh.* **34**: 228-230 (1972)).

4. Hartland (1981) verwaarloost door het toepassen van de Reynolds relatie bij het beschrijven van de drainage van de dunne film tussen twee coalescerende vloeistofdruppels of gasbellen ten onrechte het duidelijke verschil in drainage mechanismes tussen mobiele en starre films.

Hartland, S., *Tenside Detergents* **18**: 178-189 (1981).

5. In de statistisch-thermodynamische theorie van Simha & Somcynsky (1969) over polymeermengsels wordt een aanname omtrent het vrije volume geïntroduceerd, die na sommatie met het bezette volume niet tot het totale volume leidt.

Simha, R. & Somcynsky, T., *Macromolecules* **2**: 342-350 (1969).

6. Hunter (1976-1985) gaat er bij de bepaling van de intrinsieke viscositeit en van de maximale volumefractie aan vaste stof, waarbij nog stroming mogelijk is, van uit, dat een toename van de volume fractie vaste stof resulteert in een toename van de viscositeit, ter grootte

$$d\eta_{PL} = 2.5 \eta_{PL} \frac{d\phi}{1 - \phi/\phi_{max}}$$

hetgeen met name voor coagulerende suspensies onjuist is.

Firth, B.A. & Hunter, R.J., *J. Colloid Interface Sci.* **57**: 266 (1976).
Van de Ven, T.G.M. & Hunter, R.J., *Rheol. Acta* **16**: 534 (1977).
Hunter, R.J. & Frayne, J., *J. Colloid Interface Sci.* **71**: 30 (1979).
Hunter, R.J., *Adv. Coll. Interface Sci.* **17**: 197 (1982).
Ekdawi, N. & Hunter, R.J., *J. Colloid Interface Sci.* **94**: 355 (1983).

7. Skalny & Young (1980) laten na te verklaren, waarom de inhibitie van $\text{Ca}(\text{OH})_2$ kristallen in hun functie van nuclei bij de hydratatie van tricalcium silicaat, waarbij silicaationen worden beschouwd als inhibitor, duidelijker is in aanwezigheid van toegevoegd $\text{Ca}(\text{OH})_2$ dan in afwezigheid ervan.

Skalny, J. & Young, J.F., in: "Proceedings of the 7th International Congress on the Chemistry of Cement", Vol. I: Ch. II-1. Principal Reports, Editions Septima, 1980.

8. Okuda & Ikeda (1989) gaan er bij de toepassing van de Gibbs adsorptie isotherm ter bepaling van de aan het oppervlak geadsorbeerde ionen ten onrechte van uit, dat de activiteitscoëfficiënt onafhankelijk is van de electrolyt concentratie.

Okuda, H. & Ikeda, S., *J. Colloid Interface Sci.* **131**: 333-348 (1989).

9. Het heeft weinig nut in nieuwbouwwijken met een onregelmatig stratenpatroon vast te houden aan de traditie om huizenrijen te voorzien van opeenvolgende even of oneven nummers.